

NASA CONTRACTOR REPORT

NASA CR-1858
C.1

NASA CR-1858

LOAN COPY: RETURN TO
AFWL (DOGL)
KIRTLAND AFB, N. M.

ATMOSPHERIC EFFECTS ON INFRARED MULTISPECTRAL SENSING OF SEA-SURFACE TEMPERATURE FROM SPACE

by D. Anding, R. Kauth, and R. Turner

Prepared by
UNIVERSITY OF MICHIGAN
Ann Arbor, Mich.

for Ames Research Center

NATIONAL AERONAUTICS AND SPACE ADMINISTRATION • WASHINGTON, D. C. • JULY 1971



0061041

1. Report No. NASA CR-1858		2. Government Accession No.		3. Recipient's Catalog No.	
4. Title and Subtitle Atmospheric Effects on Infrared Multispectral Sensing of Sea-Surface Temperature From Space				5. Report Date July 1971	
				6. Performing Organization Code	
7. Author(s) D. Anding, R. Kauth and R. Turner				8. Performing Organization Report No.	
				10. Work Unit No.	
9. Performing Organization Name and Address University of Michigan				11. Contract or Grant No. NAS 12-2117	
				13. Type of Report and Period Covered Contractor Report	
12. Sponsoring Agency Name and Address National Aeronautics & Space Administration Washington, D.C. 20546				14. Sponsoring Agency Code	
				15. Supplementary Notes	
16. Abstract This report defines the effect of the atmosphere on the infrared spectral radiance emanating from the sea surface and discusses the application of multichannel infrared remote sensing as a means of compensating for these atmospheric effects to obtain improved estimates of the sea temperature from high-altitude or space platforms. It is demonstrated that by performing simultaneous radiometric measurements in three narrow spectral intervals centered at 4.9, 9.1, and 11.0 μm , the effects of noncloudy atmospheres on the observed radiance can be nearly completely compensated for and estimates of sea temperature to an accuracy of 0.15°K can be obtained. For fields of view which contain clouds, the three-channel radiometric data also provide the necessary information to indicate the presence of semitransparent or opaque clouds within the field of view and, if opaque, the fractional amount of cloud obscuration to an accuracy of approximately 10% for any field-of-view size. The analysis is concerned only with the effects of the atmosphere on the ability to estimate accurately the sea temperature; therefore, the effects of system noise and system calibration are not considered.					
17. Key Words (Suggested by Author(s)) atmospheric model, infrared, remote-sensing, sea-surface temperature, multispectral, infrared radiation			18. Distribution Statement UNCLASSIFIED-UNLIMITED		
19. Security Classif. (of this report) UNCLASSIFIED		20. Security Classif. (of this page) UNCLASSIFIED		21. No. of Pages 98	22. Price* 3.00

FOREWORD

The research described herein, which was conducted by Willow Run Laboratories, a unit of The University of Michigan's Institute of Science and Technology, was performed under NASA contract NAS 12-2117. This final report under the contract covers the period 1 April 1969 to 30 June 1970. The work was done under the management of NASA Project Managers, Mr. A. Holland, Electronics Research Center, and Mr. J. Arvesen, Ames Research Center. The Willow Run Laboratories' number for this report is 2676-6-F.

ABSTRACT

This report defines the effect of the atmosphere on the infrared spectral radiance emanating from the sea surface and discusses the application of multichannel infrared remote sensing as a means of compensating for these atmospheric effects to obtain improved estimates of the sea temperature from high-altitude or space platforms. It is demonstrated that by performing simultaneous radiometric measurements in three narrow spectral intervals centered at 4.9, 9.1, and 11.0 μm , the effects of noncloudy atmospheres on the observed radiance can be nearly completely compensated for and estimates of sea temperature to an accuracy of 0.15^oK can be obtained. For fields of view which contain clouds, the three-channel radiometric data also provide the necessary information to indicate the presence of semitransparent or opaque clouds within the field of view and, if opaque, the fractional amount of cloud obscuration to an accuracy of approximately 10% for any field-of-view size. The analysis is concerned only with the effects of the atmosphere on the ability to estimate accurately the sea temperature; therefore, the effects of system noise and system calibration are not considered.

CONTENTS

Foreword	iii
Abstract	v
List of Figures	viii
List of Tables	ix
Summary	1
1. Introduction	2
2. Theoretical Basis of Remote Sea-Temperature Measurement at Thermal Infrared Wavelengths	2
3. Procedure for Calculating Spectral Radiance	4
3.1. Methods for Estimating Molecular Absorption and Haze Extinction	10
3.2. Method for Estimating Cloud Radiance and Cloud Extinction	12
4. Calculations of Spectral Radiance	18
4.1. Definition of Atmospheric States	18
4.2. Synthesis of Spectra	21
4.3. Discussion of Representative Spectra	23
4.4. Comparison of Calculated Spectra to Measured Spectra	32
5. Development of Multispectral Systems	32
5.1. Maximum Likelihood Estimate of h for Covariance Matrices Identical	35
5.2. Maximum Likelihood Estimate of h for Covariance Matrices Slightly Different	39
6. Applications of Remote-Sensing Procedure	41
6.1. Estimate of Sea Temperature for Clear Atmospheres	42
6.2. Estimation of Fractional Cloud Cover	45
6.3. Detection of Semitransparent Clouds	53
6.4. Critique of Three-Band System	54
Appendix I: Solution of the Equation of Transfer for Homogeneous Clouds	57
Appendix II: Band Models for Calculating Atmospheric Transmittance	68
Appendix III: Presentation of Spectral Radiance for Clear Atmospheres for Various Model Atmospheres, Zenith Observation Angles, and Sea Temperatures	81
References	97
Distribution List	98

FIGURES

1. Schematic of Atmospheric Model	5
2. Spectral Index of Refraction of Water	13
3. Maritime Haze Droplet Distribution	14
4. Scattering and Extinction Coefficients for H ₂ O, 100 Particles/cm ³	15
5. Aerosol Number Density Versus Altitude.	16
6. Spectral Emittance of an Opaque Water-Drop Cloud	16
7. Particle Size Distribution of Water-Drop Cloud	17
8. Spectral Transmittance and Emittance of Semitransparent Clouds	19
9. Temperature Profiles for La Jolla Area	21
10. Water Vapor Profiles for La Jolla Area	22
11. Liquid Water Reflection 60° and 80° Angle of Incidence	23
12. Upwelling Spectral Radiance at 100 km for a Noncloudy Atmosphere with Sea Temperature as a Parameter	24
13. Upwelling Spectral Radiance at 100 km for a Noncloudy Atmosphere with Zenith Angle as a Parameter	26
14. Upwelling Spectral Radiance at 100 km for Noncloudy Atmospheres with Model Atmosphere as a Parameter.	27
15. Upwelling Spectral Radiance at 100 km with Opaque Clouds at Four Altitudes	28
16. Upwelling Spectral Radiance at 100 km with a Semitransparent Cloud at Four Altitudes	29
17. Upwelling Spectral Radiance at 100 km for Semitransparent Clouds with Cloud Thickness as a Parameter	30
18. Upwelling Spectral Radiance at 100 km for Opaque Clouds with Percent Cloud Cover as a Parameter.	31
19. Comparison of Calculated Spectral Radiance with Measurements for a Clear Atmosphere	33
20. Comparison of Calculated Spectral Radiance with Measurements for a Clear Atmosphere	34
21. Sketch Showing the Effect of a Coordinate Transformation on Each of Two Collections of Output Vectors	37
22. Two-Dimensional Geometrical Interpretation of Interpolation Procedures Given by Eqs. (51) and (53)	39
23. Two-Dimensional Geometrical Interpretation of Interpolation Procedures Given by Eqs. (54) and (55)	40
24. Schematic of Hyperlines for a Two-Dimensional Vector Representation of Output Spectra	43
25. Spectral Radiance in Band 1 Versus That in Band 2 as a Function of Atmospheric State	44

26. Spectral Emittance of Liquid Water and Opaque Water-Drop Cloud	46
27. Schematic Representation of Hyperplanes for Fractional Cloud Cover Determination	49
28. Error in Estimate of Fractional Cloud Cover	51
29. Spectral Radiance in Band 1 Versus That in Band 2 as a Function of Atmospheric State	54

TABLES

1(a). Description of the Data Point Distribution for Each Hyperplane	48
1(b). Eigenvectors Corresponding to Least Eigenvalue (Vector Normal to Hyperplane)	48
2. Comparison Between the Temperature Estimated by the 4.9, 9.1- μm Band Pair and the Temperature Estimated by the 9.1, 11.0- μm Band Pair as a Function of Cloud Thickness, Cloud Altitude, and Sea Temperature	55
3. Spectral Absorption Coefficients for H_2O	70
4. Transmission Vs. the Product $W' \cdot K(\Delta\lambda)$ for CO_2	72
5. Spectral Absorption Coefficients for CO_2	73
6. Spectral Absorption Coefficients for the 4.3- μm CO_2 Band	75
7. Spectral Absorption Coefficients for the 15.0- μm CO_2 Band.	76
8. Empirical Constants for Ozone	78
9. Spectral Absorption Coefficients for CH_4	79
10. Spectral Absorption Coefficients for N_2O	80

ATMOSPHERIC EFFECTS ON INFRARED MULTISPECTRAL SENSING OF SEA-SURFACE TEMPERATURE FROM SPACE

Final Report

SUMMARY

Through the use of a radiative transfer computer program, the effect of the atmosphere on the upwelling spectral radiance emanating from the sea surface is investigated. The atmospheric constituents whose effects are included in the analysis are: the infrared active molecules H_2O , CO_2 , O_3 , N_2O , and CH_4 ; atmospheric haze; and water clouds. The procedures used to perform these radiative transfer calculations are discussed in detail, and it is demonstrated that the effects of the infrared active molecules and atmospheric haze are accurately represented. The procedures used to account for the effects of water clouds were based on empirical models which have not been thoroughly verified and, hence, are considered less accurate.

By the use of the computer program, the upwelling spectral radiance at 100 km altitude was calculated for the spectral range 4.0 to 30.0 μm for a broad range of sea temperatures, atmospheric water vapor and temperature distributions, cloud altitudes, cloud temperatures, cloud thicknesses, and fractional amounts of cloud cover. These spectral-radiance data were considered the results of a simulated spaceborne experiment and were used to define potentially useful, infrared, multichannel, remote-sensing systems capable of compensating for the effects of the atmosphere, thereby obtaining estimates of sea temperature that are approximately equal to those estimates which would be obtained in the absence of an intervening atmosphere. The analysis completed thus far indicates that, by performing simultaneous radiometric measurements in three narrow spectral intervals centered at 4.9, 9.1, and 11.0 μm , the effects of non-cloudy atmospheres on the observed radiance can be nearly completely compensated for and estimates of sea temperature to an accuracy of 0.15°K can be obtained. For fields of view which contain clouds, the three channel radiometric data also provide the necessary information to indicate the presence of semitransparent or opaque clouds within the field of view and, if opaque, the fractional amount of cloud obscuration to an accuracy of approximately 10% for any field-of-view size.

Work is in progress to develop accurate models for calculating the radiative-transfer characteristics of water clouds and to incorporate these models into the computer code. This improved code will then be used to define multichannel systems capable of estimating the sea temperature when the field of view is partially obscured by clouds.

1 INTRODUCTION

The long-range purpose of the present study is to investigate the effects of the atmosphere on the multispectral, infrared remote sensing of the earth's resources from space. The specific remote-sensing application studied is the measurement of sea-surface temperature.

Estimating the sea-surface temperature from spacecraft has been achieved with reasonable success from Nimbus with the MRIR (medium-resolution infrared radiometer) and the THIR (temperature-humidity infrared radiometer). These systems measure the radiance in the atmospheric-window region near $11 \mu\text{m}$ and convert the measured radiance values into equivalent blackbody temperatures which are used to estimate the sea-surface temperature. In general, the presence of opaque clouds within the field of view are easily discernible in the measured data because of the inordinately low values of radiance. The presence of semitransparent clouds, or opaque clouds near the surface, are not discernible from a single-band measurement, and large errors in the estimate of the sea-surface temperature can result. Even for noncloudy atmospheres, because of the effects of atmospheric water vapor and haze on the measured values of radiance, the estimated temperatures could be on the order of $\pm 2.0^\circ\text{C}$ different from those which would be obtained in the absence of an intervening atmosphere.

The present study specifically defines the nature of each of these atmospheric effects and investigates the use of multiband radiometric sensing as a means of observing and compensating for these effects to obtain improved estimates of the sea-surface temperature.

2 THEORETICAL BASIS OF REMOTE SEA-TEMPERATURE MEASUREMENT AT THERMAL INFRARED WAVELENGTHS

The spectral radiance emitted by an opaque body at wavelength λ is given by

$$L_{\lambda}^g = \epsilon(\lambda)L_{\lambda}^b(T) \quad (1)$$

where $\epsilon(\lambda)$ is the spectral emittance of the opaque body and $L_{\lambda}^b(T)$ is the spectral radiance emitted by a blackbody. The latter is represented as

$$L_{\lambda}^b(T) = \frac{2hc^2}{\lambda^5 (e^{hc/\lambda kT} - 1)} \quad (2)$$

where T = the temperature of the blackbody

c = the velocity of light

h = Planck's constant

λ = wavelength

k = Boltzmann's constant

It is clear from these expressions that if the emittance is known, the temperature can be determined by measuring the emitted spectral radiance and inverting Eq. (1). The application of such a measurement procedure to determine the temperature of a water surface exposed to the atmosphere is more complex. The spectral emittance of a sea surface has a maximum value of approximately 0.98, which occurs near 11 μm . Consequently, as one attempts to measure the emitted radiation, some sky radiation will be reflected from the water surface and collected by the infrared sensor. Also, since water does not become opaque to infrared radiation at thermal wavelengths until a depth of approximately 0.10 mm, some of the measured radiation emanates from below the surface, which generally has a slightly different temperature. Therefore, the temperature derived from a measurement of the radiance at the surface will be the temperature of a blackbody which yields an equivalent value of radiance (i.e., the "equivalent radiometric temperature"). It will be different from the actual surface temperature; the degree of difference will depend upon the magnitude of the reflected radiation and the temperature gradient near the surface.

The present analysis is not concerned with the relationship between the equivalent radiometric temperature and the actual surface temperature, but only with the effect of the atmosphere on the equivalent radiometric temperature derived from a radiometric measurement performed at satellite altitudes. Therefore, all future references to sea-surface temperature will refer to the equivalent radiometric temperature that would be derived from a radiance measurement at the surface.

Before reaching a spaceborne sensor, the spectral radiance emanating from the sea surface will be attenuated by atmospheric constituents, such as clouds, haze, and absorbing gases. These atmospheric constituents also emit and scatter radiant energy, which contributes to the total signal received by the sensor. The central problem in accurately measuring the water temperature from space lies in determining the extent to which such effects can be observed and compensated. To demonstrate more clearly the nature of the problem of measuring the sea temperature from space, consider the spectral radiance leaving the top of the atmosphere, L_λ , which can be represented by:

$$L_\lambda = L_\lambda^G(T)\tilde{T}(\lambda) + L_\lambda^A \quad (3)$$

where $L_\lambda^G(T)$ = the radiance at the water surface

$\tilde{T}(\lambda)$ = the atmospheric spectral transmittance

L_λ^A = the spectral radiance emitted by the atmosphere

If a measurement of the spectral radiance at wavelength λ were performed and the values of atmospheric spectral transmittance, $\tilde{T}(\lambda)$, and atmospheric spectral emission, L_λ^A , were accurately known at the wavelength of the measurement, Eq. (3) could be inverted and an accurate tempera-

ture estimate could be made. Hence, remotely measuring the sea temperature accurately requires the ability to estimate $\tilde{T}(\lambda)$ and L_{λ}^A accurately for any atmospheric condition. A potentially useful procedure capable of achieving this objective is multispectral pattern recognition. A requirement for the successful application of this procedure is that the radiance spectrum at the top of the atmosphere for any atmospheric condition be different for each different sea temperature. This will, in general, be true if the field of view is not obscured by an opaque cloud. Then, by performing measurements at a sufficient number of wavelengths to indentify this unique spectrum, the values of $\tilde{T}(\lambda)$ and L_{λ}^A will be determinable, and the sea temperature can be estimated. From the standpoint of practicality, measurements cannot be performed at each wavelength throughout the thermal-infrared wavelength region, but only at a discrete number of wavelengths. The problem, therefore, is to determine the number of wavelengths, their spectral location and how the measurement at each wavelength should be weighted (i.e., the spectral-filter definition) in order to restrict the possible values of $\tilde{T}(\lambda)$ and L_{λ}^A sufficiently to obtain a satisfactory estimate of temperature for any atmospheric condition. The present study was not designed to necessarily specify an n-band system capable of solving the entire problem, but only to investigate the effects of the atmosphere on the remote measurement of the sea temperature and to define potentially useful spectral-band systems. Therefore, the specific objectives were restricted to define an n-band system capable of: (1) providing accurate estimates of sea temperature for noncloudy atmospheres, and (2) conclusively indicating the presence of clouds within the field of view and, if opaque, the fractional amount of cloud cover. In order to perform this spectral-band selection, it was first necessary to define the relationship between the spectral radiance leaving the top of the atmosphere and the sea temperature and atmospheric conditions. Since spaceborne-measured data for a broad range of known atmospheric conditions did not exist, this relationship was obtained analytically. The procedures used to calculate the radiance spectra for atmospheres which contain the normal infrared active gases H_2O , CO_2 , O_3 , CH_4 , and N_2O , atmospheric haze, semi-transparent clouds, and opaque clouds are given in the next section.

3

PROCEDURE FOR CALCULATING SPECTRAL RADIANCE

Consider a plane-parallel atmosphere, shown in Fig. 1, which is divided into n-layers, each layer composed of a homogeneous atmosphere (i.e., constant temperature, pressure, and density) which contains molecular absorbers and a haze-scattering medium. Between the j-th and j-th + 1 layer, there is a homogeneous cloud layer (constant density and temperature) of total optical depth τ_0 and geometric thickness z_0 . The optical depth τ at an arbitrary distance z from the cloud top is given by

$$\tau = Kz; \quad \tau_0 = Kz_0 \quad (4)$$

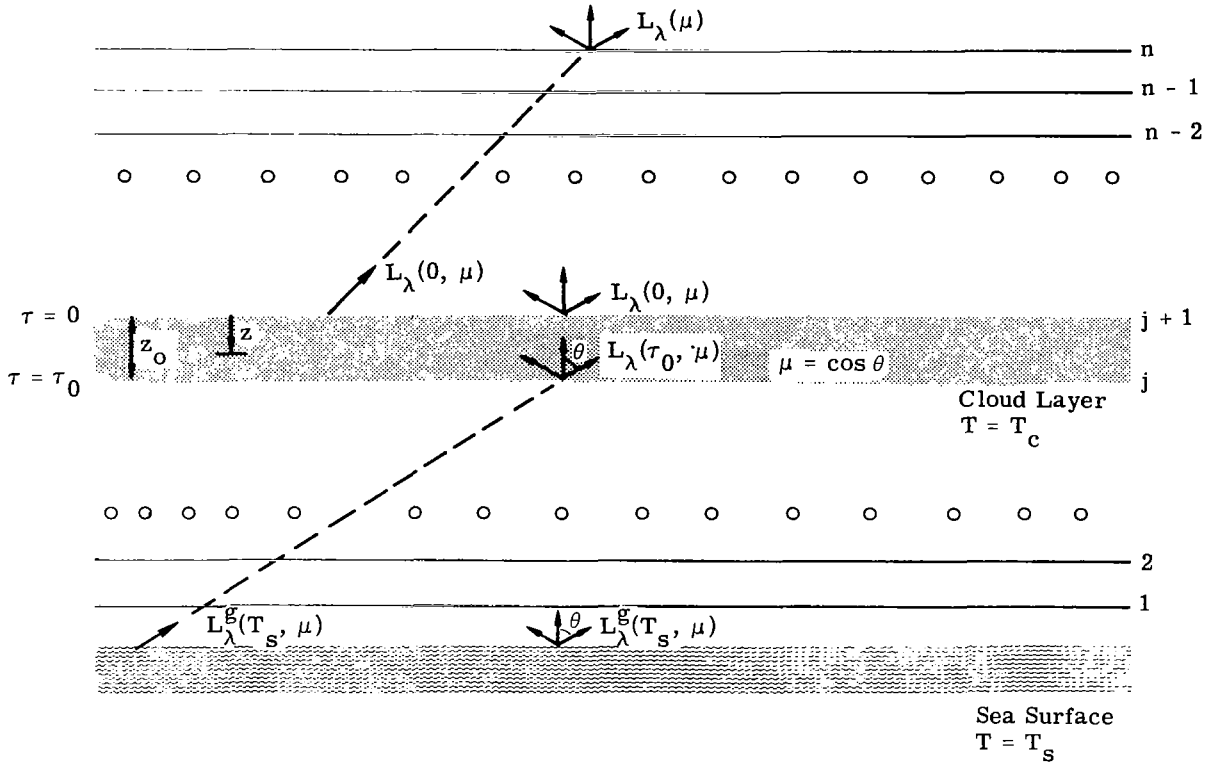


FIGURE 1. SCHEMATIC OF ATMOSPHERIC MODEL

where κ is the cloud extinction coefficient. The spectral radiance emanating from the sea surface at temperature T_s and direction μ ($\mu = \cos \theta$) is denoted by $L_\lambda^g(T_s, \mu)$ and is given by Eq. (1) with $\epsilon(\lambda)$ being the emittance at the direction μ . The spectral radiance at the base of the cloud in the direction μ is denoted by $L_\lambda(\tau_0, \mu)$ and is determined by the spectral radiance emanating from the sea surface and the temperature, pressure, haze, and molecular absorbing constituent distributions in the atmosphere below the cloud. Assuming that the amount of radiation scattered in the direction μ , which emanates from the sea surface in a different direction, is negligible (this is a good approximation at thermal infrared wavelengths), the spectral radiance at the base of the cloud is given by

$$L_\lambda(\tau_0, \mu) = L_\lambda^g(T_s, \mu) \tilde{T}_{0-j}^A(\lambda, \mu) + L_\lambda^A(\mu) \quad (5)$$

where $\tilde{T}_{0-j}^A(\lambda, \mu)$ is the atmospheric spectral transmission between the sea surface and the cloud base and L_λ^A is the spectral radiance emitted by the atmosphere below the cloud. For the layered atmosphere, $L_\lambda^A(\mu)$ is represented by a sum of the contributions of each layer

$$L_\lambda^A(\mu) = \sum_{i=1}^j L_\lambda^b(T_i, \mu) \epsilon_i(\lambda, \mu) \tilde{T}_{i-j}^A(\lambda, \mu) \quad (6)$$

where $\epsilon_i(\lambda, \mu)$ = the spectral emittance of the i-th layer

$\tilde{T}_{i-j}(\lambda, \mu)$ = the atmospheric spectral transmission between the i-th layer and the cloud base

T_i = the temperature of the i-th layer

The total extinction between the i-th layer and the cloud base is caused by molecular absorption, haze absorption, and haze scattering. The total transmission is given by:

$$\tilde{T}_{i-j}(\lambda, \mu) = \tilde{T}_{m_{i-j}}(\lambda, \mu) \tilde{T}_{a_{i-j}}(\lambda, \mu) \tilde{T}_{s_{i-j}}(\lambda, \mu) \quad (7)$$

where $\tilde{T}_{m_{i-j}}(\lambda, \mu)$ = the molecular transmittance

$\tilde{T}_{a_{i-j}}(\lambda, \mu)$ = the haze-absorption transmittance

$\tilde{T}_{s_{i-j}}(\lambda, \mu)$ = the haze-scattered transmittance

Now the emittance of the i-th layer for thermal infrared wavelengths is, to a good approximation, equal to the absorption of the i-th layer; or:

$$\epsilon_i(\lambda, \mu) = 1 - t_{m_i}(\lambda, \mu) t_{a_i}(\lambda, \mu) \quad (8)$$

where $t_{m_i}(\lambda, \mu)$ and $t_{a_i}(\lambda, \mu)$ are respectively the molecular and haze-absorption transmittance of the i-th layer.

In order to express the emittance of the i-th layer in terms of more easily calculable variables, the transmittance from the cloud base to the i-th + 1 layer is expressed as:

$$\tilde{T}_{(i+1)-j}(\lambda, \mu) = \tilde{T}_{i-j}(\lambda, \mu) t_i(\lambda, \mu) \quad (9)$$

where t_i is the transmittance of the i-th layer and is given by:

$$t_i(\lambda, \mu) = t_{m_i}(\lambda, \mu) t_{a_i}(\lambda, \mu) t_{s_i}(\lambda, \mu) \quad (10)$$

where $t_{s_i}(\lambda, \mu)$ is the haze-scattered transmittance of the i-th layer. Combining (8), (9), and (10) we have:

$$\epsilon_i(\lambda, \mu) \tilde{T}_{i-j}(\lambda, \mu) = \left[\tilde{T}_{i-j}(\lambda, \mu) - \frac{\tilde{T}_{(i+1)-j}(\lambda, \mu)}{t_{s_{i-j}}(\lambda, \mu)} \right] \quad (11)$$

Substituting (6) and (11) into (5), the spectral radiance at the cloud base is

$$L_\lambda(\tau_0, \mu) = L_\lambda^g(T_s, \mu) \tilde{T}_{0-j}(\lambda, \mu) + \sum_{i=1}^j L_\lambda^b(T_i, \mu) \left[\tilde{T}_{i-j}(\lambda, \mu) - \frac{\tilde{T}_{(i+1)-j}(\lambda, \mu)}{t_{s_{i-j}}(\lambda, \mu)} \right] \quad (12)$$

By a similar development, the spectral radiance leaving the top of the atmosphere, $L_\lambda(\mu)$, can be expressed in terms of the upwelling radiance at the top of the cloud, $L_\lambda(0, \mu)$:

$$L_\lambda(\mu) = L_\lambda(0, \mu) \tilde{T}_{(j+1)-n}(\lambda, \mu) + \sum_{i=j+1}^n L_\lambda^b(T_i, \mu) \left[\tilde{T}_{i-n}(\lambda, \mu) - \frac{\tilde{T}_{(i+1)-n}(\lambda, \mu)}{t_{s_{i-n}}} \right] \quad (13)$$

where $\tilde{T}_{i-n}(\lambda, \mu)$ is the transmission between the top of the atmosphere ($i = n$) and the i -th layer.

The upwelling radiance at the top of the cloud results from two sources: (1) the thermal radiation generated within the cloud, and (2) the thermal radiation which results from the external source at the cloud base, $L_\lambda(\tau_0, \mu)$. The internal thermal radiation source is represented by Planck's function at the uniform cloud temperature T_c ,

$$L_\lambda^b(T_c) = \frac{2hc^2}{\lambda^5 \left(e^{\frac{hc}{\lambda k T_c}} - 1 \right)} \quad (14)$$

which is an isotropic source of radiation and is independent of optical depth since T_c is assumed constant.

The radiation field at optical depth τ and direction μ , $L_\lambda(\tau, \mu)$ can be described by the following radiative transfer equation:

$$\mu \frac{dL_\lambda(\tau, \mu)}{d\tau} = L_\lambda(\tau, \mu) - \frac{\omega_0}{2} \int_{-1}^1 \rho(\mu, \mu') L_\lambda(\tau, \mu') d\mu' - (1 - \omega_0) L_\lambda^b(T_c) \quad (15)$$

where ω_0 is the single-scattering albedo and is given by:

$$\omega_0 = \frac{\beta}{\kappa}; \quad \kappa = \alpha + \beta \quad (16)$$

where α and β are respectively the spectral absorption and scattering coefficients and $\rho(\mu, \mu')$ is the scattering phase function. It is convenient to separate the radiance field into its two components

$$L_\lambda(\tau, \mu) = L_\lambda^{(o)}(\tau, \mu) + L_\lambda^s(\tau, \mu) \quad (17)$$

where $L_\lambda^{(o)}(\tau, \mu)$ is the spectral radiance which results from the internal thermal radiation, and $L_\lambda^s(\tau, \mu)$ is the spectral radiance which results from the external source at the cloud base. For a radiance field represented in this manner, the complete solution to Eq. (15) is given by the sum of the two solutions resulting from $L_\lambda(\tau, \mu)$ being sequentially replaced by $L_\lambda^{(o)}(\tau, \mu)$ and $L_\lambda^s(\tau, \mu)$. The spectral radiance at the cloud top in the downward direction and the spectral radiance at the cloud base in the upward direction resulting from the internal source, are both zero. Also, assuming there is no external source at the cloud top, the boundary conditions for the solution of Eq. (15) are

$$\begin{aligned} L_{\lambda}^{(o)}(0, -\mu) &= 0; & L_{\lambda}^S(0, -\mu) &= 0 \\ L_{\lambda}^{(o)}(\tau_o, \mu) &= 0; & L_{\lambda}^S(\tau_o, \mu) &= L_{\lambda}(\tau_o, \mu) \end{aligned}$$

where the minus signs represent radiance in the downward direction. With these boundary conditions, the two formal solutions to (15) for the radiance at the top of the cloud are

$$L_{\lambda}^{(o)}(0, \mu) = \frac{\omega_o}{2\mu} \int_{-1}^1 \rho(\mu, \mu') \int_0^{\tau_o} e^{-\tau'/\mu} L_{\lambda}^{(o)}(\tau', \mu') d\tau' d\mu' + (1 - \omega_o) L_{\lambda}^b(T_c) \left(1 - e^{-\tau_o/\mu}\right) \quad (18)$$

and

$$L_{\lambda}^S(0, \mu) = L_{\lambda}(\tau_o, \mu) e^{-\tau_o/\mu} + \frac{\omega_o}{2\mu} \int_{-1}^1 \rho(\mu, \mu') \int_0^{\tau_o} e^{-\tau'/\mu} L_{\lambda}^S(\tau', \mu') d\tau' d\mu' \quad (19)$$

The total radiance is the sum: i.e.,

$$L_{\lambda}(0, \mu) = L_{\lambda}^{(o)}(0, \mu) + L_{\lambda}^S(0, \mu)$$

The details of a procedure which can be used to evaluate (18) and (19) are given in Appendix I.

Since the procedures used to calculate atmospheric transmission are only applicable to finite spectral intervals, it is necessary to average $L_{\lambda}(\mu)$ over a wavelength interval $\Delta\lambda$. From Eq. (13), the average spectral radiance at the top of the atmosphere, $\langle L_{\lambda}(\mu) \rangle$, averaged over a wavelength interval $\Delta\lambda$ is given by:

$$\begin{aligned} \langle L_{\lambda}(\mu) \rangle &= \frac{1}{\Delta\lambda} \int_{\lambda_1}^{\lambda_2} L_{\lambda}(\mu) d\lambda = \frac{1}{\Delta\lambda} \int_{\lambda_1}^{\lambda_2} \left\{ L_{\lambda}(0, \mu) \tilde{T}_{(j+1)-n}(\lambda, \mu) \right. \\ &\quad \left. + \sum_{i=j+1}^n L_{\lambda}^b(T_i, \mu) \left[\tilde{T}_{i-n}(\lambda, \mu) - \frac{\tilde{T}_{(i+1)-n}(\lambda, \mu)}{t_{s_{i-n}}(\lambda, \mu)} \right] \right\} d\lambda \quad (20) \end{aligned}$$

Since $L_{\lambda}^b(T_i, \mu)$ and $t_{s_{i-n}}(\lambda, \mu)$ are slow varying functions of wavelength, $\langle L_{\lambda}(\mu) \rangle$ can be expressed as:

$$\begin{aligned} \langle L_{\lambda}(\mu) \rangle &= \frac{1}{\Delta\lambda} \int_{\lambda_1}^{\lambda_2} L_{\lambda}(0, \mu) \tilde{T}_{(j+1)-n}(\lambda, \mu) d\lambda \\ &\quad + \sum_{i=j+1}^n \langle L_{\lambda}^b(T_i, \mu) \rangle \left[\langle \tilde{T}_{i-n}(\lambda, \mu) \rangle - \frac{\langle \tilde{T}_{(i+1)-n}(\lambda, \mu) \rangle}{\langle t_{s_{i-n}}(\lambda, \mu) \rangle} \right] \quad (21) \end{aligned}$$

where $\langle L_{\lambda}^b(T_i, \mu) \rangle$, $\langle \tilde{T}_{i-n}(\lambda, \mu) \rangle$, and $\langle \tilde{T}_{(i+1)-n}(\lambda, \mu) \rangle$ are average values, averaged over the wavelength interval $\Delta\lambda$. Since it is desirable to eliminate the integral term of Eq. (21), an "effective cloud transmission", $\tilde{T}_c(\lambda, \mu)$, is defined as:

$$\tilde{T}_c(\lambda, \mu) = \frac{L_{\lambda}^s(0, \mu)}{L_{\lambda}(\tau_0, \mu)} \quad (22)$$

Because of the nature of scattering and absorption processes in clouds, $\tilde{T}_c(\lambda, \mu)$ will be a slow varying function of wavelength. In particular, for wavelength intervals of approximately $0.10 \mu\text{m}$, $\tilde{T}_c(\lambda, \mu)$ will remain constant throughout the interval. It is referred to as an "effective cloud transmission" because it is not solely a fundamental parameter of the cloud, but also depends upon the angular distribution of the source function $L_{\lambda}(\tau_0, \mu)$ which, in general, is different for each value of surface temperature and distribution of atmospheric parameters. Its use, however, allows the average spectral radiance at the top of the atmosphere, $\langle L_{\lambda}(\mu) \rangle$, to be expressed in terms of average values of spectral radiance and spectral transmission, averaged over the wavelength interval $\Delta\lambda$. Combining Eq. (12), (17), (21), and (22), we have:

$$\begin{aligned} \langle L_{\lambda}(\mu) \rangle = & \langle L_{\lambda}^g(T_s, \mu) \rangle \langle \tilde{T}_{0-n}(\lambda, \mu) \rangle \langle \tilde{T}_c(\lambda, \mu) \rangle \\ & + \sum_{i=1}^j \langle L_{\lambda}^b(T_i, \mu) \rangle \left[\langle \tilde{T}_{i-n}(\lambda, \mu) \rangle - \frac{\langle \tilde{T}_{(i+1)-n}(\lambda, \mu) \rangle}{\langle t_{s_{i-n}}(\lambda, \mu) \rangle} \right] \langle \tilde{T}_c(\lambda, \mu) \rangle \\ & + \langle L_{\lambda}^{(o)}(\lambda, \mu) \rangle \langle \tilde{T}_{(j+1)-n}(\lambda, \mu) \rangle \\ & + \sum_{i=j+1}^n \langle L_{\lambda}^b(T_i, \mu) \rangle \left[\langle \tilde{T}_{i-n}(\lambda, \mu) \rangle - \frac{\langle T_{(i+1)-n}(\lambda, \mu) \rangle}{\langle t_{s_{i-n}}(\lambda, \mu) \rangle} \right] \end{aligned} \quad (23)$$

The first term in Eq. (23) is the radiance contribution from the sea surface. The second term is the radiance contribution from the atmosphere below the cloud. The third term is the contribution from the cloud resulting from thermal radiation generated within the cloud. The last term is the contribution from the atmosphere above the cloud. Evaluating Eq. (23) for a given sea temperature and atmospheric condition involves three basically independent spectral calculations for each spectral interval $\Delta\lambda$.

- (1) Determine the transmittance from the top of the atmosphere to each atmospheric layer: the transmittance being determined by molecular absorption, haze absorption, and haze scattering.
- (2) Determine the magnitude of the "effective cloud transmission" and the cloud radiance resulting from thermal emission within the cloud.
- (3) Determine the magnitude of Planck's function for each atmospheric layer.

3.1. METHODS FOR ESTIMATING MOLECULAR ABSORPTION AND HAZE EXTINCTION

There are two general classes of atmospheric constituents which give rise to absorption, scattering, and emission in a noncloudy atmosphere, the infrared-active molecules H_2O , CO_2 , O_3 , CH_4 , and N_2O , and atmospheric haze. Molecular absorption by atmospheric gases is well understood, as is the methods for estimating their effect on the transmission of infrared energy. Haze absorption and scattering processes are well known only for particles which are spherical. Since, however, atmospheric haze is primarily composed of liquid water droplets which are nearly spherical, the methods developed for estimating the effects of haze on the transmission of infrared energy yield satisfactory results. The atmospheric transmission between the top of the atmosphere and the i -th layer (\tilde{T}) is given to a good approximation by the product of the transmittance of each of the absorbing gases and the haze absorption (\tilde{T}_α) and scattering transmittances (\tilde{T}_s). Hence,

$$\tilde{T} = \tilde{T}_{\text{H}_2\text{O}} \tilde{T}_{\text{CO}_2} \tilde{T}_{\text{O}_3} \tilde{T}_{\text{N}_2\text{O}} \tilde{T}_{\text{CH}_4} \tilde{T}_{\text{CO}} \tilde{T}_\alpha \tilde{T}_s \quad (24)$$

3.1.1. METHODS FOR ESTIMATING MOLECULAR ABSORPTION

The transmittance for each of the molecular gases is evaluated through the use of band models, which involve assumptions and approximations which are subject to question; however, if band models are applied judiciously, transmittances which compare well with actual field measurements are obtainable. [1] Thus, the method should also be valid for use in the calculation of emitted radiance.

In general, the molecular transmittance for a spectral interval $\Delta\lambda$ is expressed as an infinite sum of all molecular absorption lines in the interval $\Delta\lambda$. Band models are simply closed-form mathematical expressions which approximate the infinite sum. The band-model equations are functions of average absorption coefficients for the interval $\Delta\lambda$ and equivalent homogeneous (constant temperature, pressure, and density) path parameters which are related to the amount of absorbing gas in the path and the distribution of pressure and temperature along the path. The absorption coefficients are determined by empirically fitting the band-model functions to spectral absorption data.

The band-model equations and the spectral absorption coefficients used in the present analysis are given in Appendix II. Although they are representative of the state-of-the-art, they yield questionable results for certain spectral regions and for certain atmospheric conditions. However, for the spectral regions in which remote-sensing measurements will most likely be performed, the results obtained by the use of these band-model functions are quite satisfactory.

3.1.2. METHODS FOR ESTIMATING HAZE EXTINCTION

The total extinction between the i -th layer of the atmosphere and the top of the atmosphere is composed of haze absorption and scattering as well as molecular gas absorption. The magnitudes of haze absorption and scattering for a path length, ℓ , are given respectively by:

$$\begin{aligned}\tilde{T}_\alpha &= e^{-\beta_\alpha(\lambda)\ell N} \\ \tilde{T}_s &= e^{-\beta_s(\lambda)\ell N}\end{aligned}\tag{25}$$

where $\beta_\alpha(\lambda)$ and $\beta_s(\lambda)$ are the spectral absorption and scattering coefficients, respectively. N is the particle density. For the present analysis, these coefficients are obtained by the application of classical Mie theory to liquid H_2O spheres. From Mie theory, the absorption and scattering coefficients are given by the following expressions:

$$\begin{aligned}\beta_\alpha(\lambda) &= \int_0^\infty Q_a(\lambda, a)\pi a^2 N(a) da \\ \beta_s(\lambda) &= \int_0^\infty Q_s(\lambda, a)\pi a^2 N(a) da\end{aligned}\tag{26}$$

where a = particle radius

$N(a)$ = number of scatterers as a function of particle size

$Q_a(\lambda, a)$, $Q_s(\lambda, a)$ = efficiency factors

The efficiency factors are given by

$$\begin{aligned}Q_a(\lambda, a) &= \frac{2}{\xi^2} \sum_{n=1}^{\infty} (2n+1) \text{Real}\{A_n[\xi, M(\lambda)] + B_n[\xi, M(\lambda)]\} \\ Q_s(\lambda, a) &= \frac{2}{\xi^2} \sum_{n=1}^{\infty} (2n+1) \left\{ |A_n[\xi, M(\lambda)]|^2 + |B_n[\xi, M(\lambda)]|^2 \right\}\end{aligned}\tag{27}$$

where

$\xi = 2\pi a/\lambda$, the scattering cross section

$M(\lambda)$ = complex index of refraction of water

$A_n[\xi, M(\lambda)]$, $B_n[\xi, M(\lambda)]$ = scattering parameters

The scattering parameters, A_n and B_n , were calculated from expressions containing series of Ricatti-Bessel functions and are discussed in detail in Born and Wolfe [2] and Van De Hulst [3].

In order to calculate the spectral absorption and scattering coefficients, it is necessary to first specify the complex index of refraction of water, $M(\lambda)$, and the size distribution of the

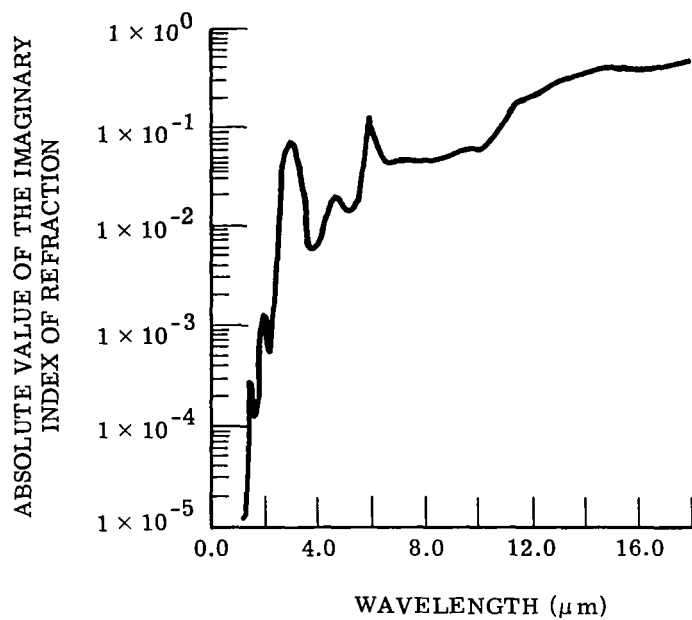
water droplets, $N(a)$. The optical properties used for liquid water in the present study were taken from Centeno [4] and are presented in Fig. 2. The size distribution of water droplets used was that of a standard maritime haze and is shown in Fig. 3. The absorption and scattering coefficients calculated by the use of the above procedure and the described input parameters are presented in Fig. 4 for a particle density of $100 \text{ particles/cm}^3$. For performing haze extinction calculations for atmospheric paths, the size distribution of the water particles was assumed constant, the only variable being the distribution of particle density, N , with altitude. The distribution used for the present study was taken from Elterman [5] and is shown in Fig. 5. In general, the effect of haze on the spectral radiance observed at space altitude is small at thermal-infrared wavelengths (i.e., greater than $4.0 \mu\text{m}$) compared to the effects of molecular absorption, even in the spectral regions of low molecular absorption. Therefore, even if the values of haze extinction calculated were somewhat unrealistic, because of incorrectly assumed values of size and density distribution of scatterers, the final results of the present study would not be significantly affected.

3.2. METHOD FOR ESTIMATING CLOUD RADIANCE AND CLOUD EXTINCTION

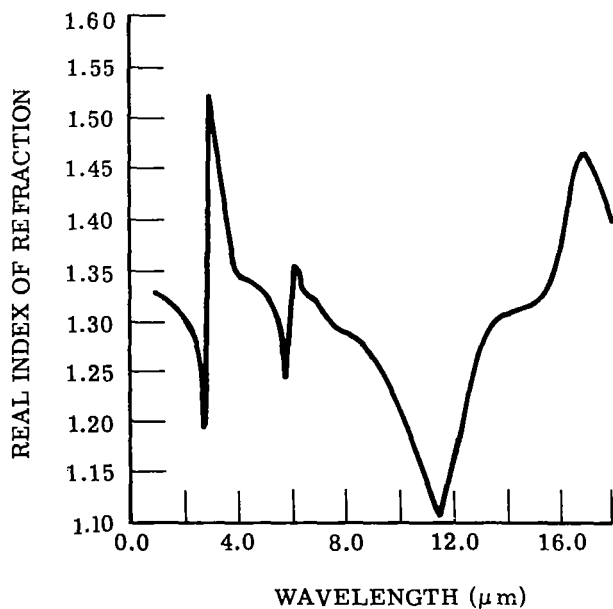
There are two cloud related quantities which need to be calculated in order to account for the effects of clouds on the spectral radiance defined by Eq. (23). The effective cloud transmission, $\tilde{T}_c(\lambda, \mu)$, and the cloud radiance resulting from thermal emission within the cloud, $L_\lambda^{(o)}(\lambda, \mu)$. Given the optical properties of the cloud particles, their size distribution and their number density, classical Mie theory can be applied to obtain for each wavelength interval $\Delta\lambda$: the scattering phase function, $\rho(\mu, \mu')$; the scattering and absorption coefficients, α and β ; and the single-scattering albedo, ω_o . Then, given the cloud thickness and cloud temperature, Eqs. (18) and (19) can be evaluated to obtain values of $L_\lambda^{(o)}(0, \mu)$ and $L_S^S(0, \mu)$, and the cloud transmission can be calculated from Eq. (22).

Unfortunately, the computational labor required to perform these calculations is voluminous, even with the aid of a digital computer; therefore, calculations could not be performed during the present study without sacrificing other important aspects of the investigation. For this reason, the required cloud data was obtained from the results of other researchers.

An extensive literature search was performed with the optimistic view that directional spectral radiance and directional spectral transmittance data, covering the spectral region from approximately 4.0 to $14 \mu\text{m}$, would be obtainable for a representative sample of cloud conditions and thicknesses. Unfortunately, the published data are very limited. Directional spectral radiance data covering the desired spectral region were given only for opaque clouds. For semitransparent clouds, directional radiance data were given for only a few wavelength regions. The only spectral data available for semitransparent clouds were the spectral hemispherical emittance and transmittance, which could not be used directly, since directional



(a) Imaginary



(b) Real

FIGURE 2. SPECTRAL INDEX OF REFRACTION OF WATER

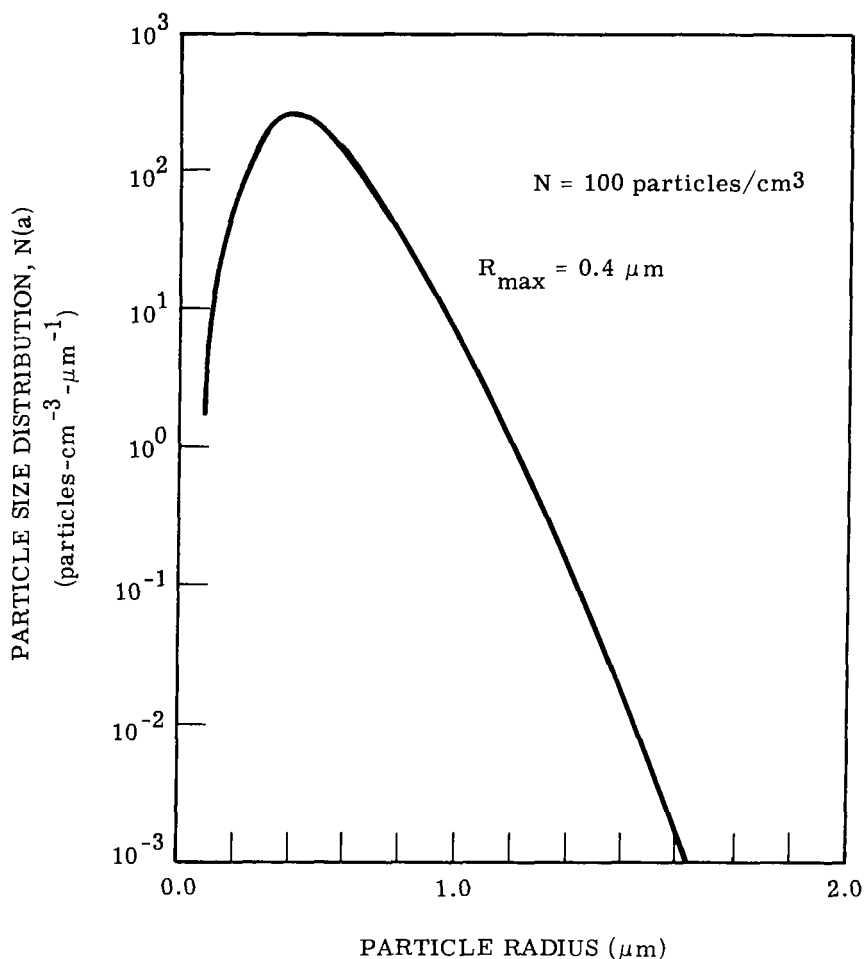


FIGURE 3. MARITIME HAZE DROPLET DISTRIBUTION

values are required. Because of the lack of available comprehensive data and the fact that it was not possible to implement the general Mie theory calculational procedure within the time frame of the present contract, the required values of cloud radiance and transmittance were estimated by the use of empirically derived relationships, which were based upon the published data.

Recall that the two quantities required are the directional spectral radiance at the cloud top resulting from thermal radiation generated within the cloud, $L_{\lambda}^{(o)}(0, \mu)$, and that caused by the external function, $L_{\lambda}^s(\tau_o, \mu)$. $L_{\lambda}^{(o)}(0, \mu)$ can be expressed as:

$$L_{\lambda}^{(o)}(0, \mu) = \epsilon_{\lambda}(\mu) L_{\lambda}^b(T_c) \quad (28)$$

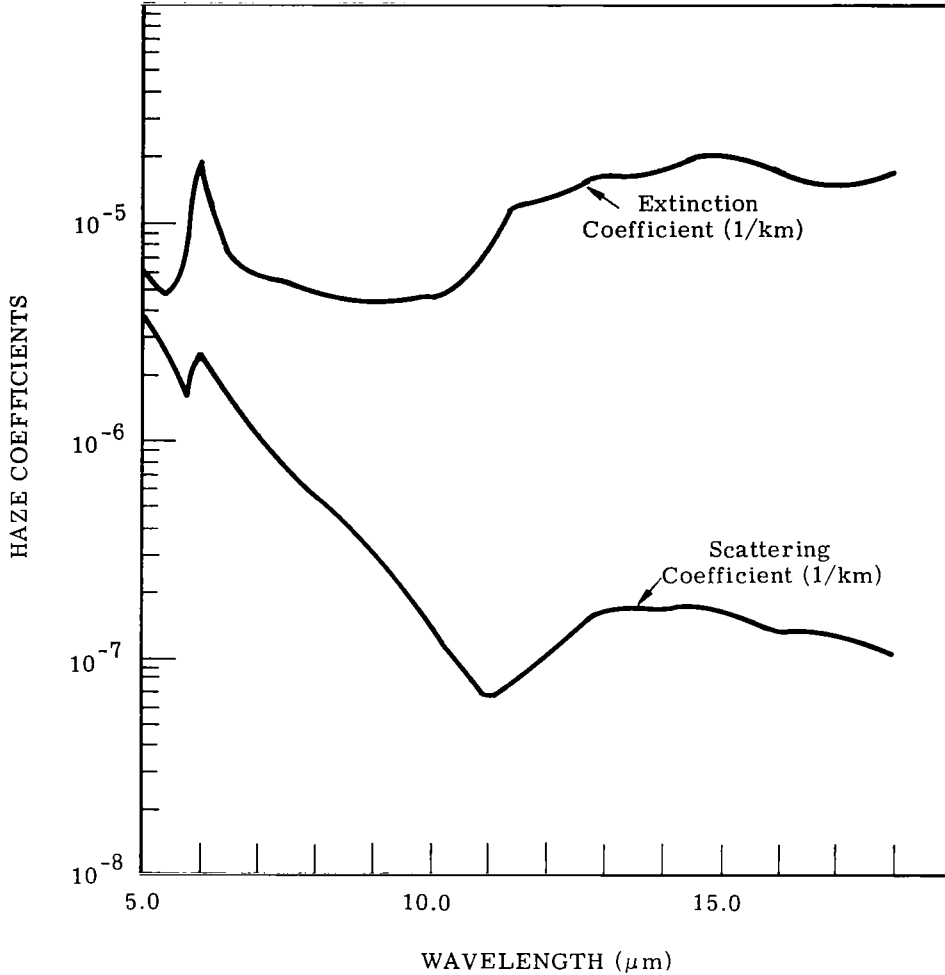


FIGURE 4. SCATTERING AND EXTINCTION COEFFICIENTS FOR H_2O ,
100 PARTICLES/ cm^3

where $\epsilon_\lambda(\mu)$ is the effective directional spectral emittance of the cloud. For opaque clouds, the directional emittance and the hemispherical emittance are approximately equal since $\epsilon_\lambda(\mu)$ is constant for $\theta < 70^\circ$; therefore, the published results could be used directly to calculate $L_\lambda^{(o)}(0, \mu)$ for opaque clouds. The values of spectral emittance used were taken from Havard [6] and are presented in Fig. 6. Havard obtained these data through the application of the general Mie theory to liquid water spheres. The optical properties of water used were those of Centeno [4], and the size distribution of water droplets used is given in Fig. 7.

In order to calculate $L_\lambda^{(o)}(0, \mu)$ for semitransparent clouds, it was first necessary to derive expressions for the directional emittance, $\epsilon_\lambda(z_o, \mu)$, and the directional transmittance, $\tilde{T}_\lambda(z_o, \mu)$. The hemispherical transmittance of a semitransparent cloud of thickness z_o , $\tilde{T}_\lambda^h(z_o)$, can

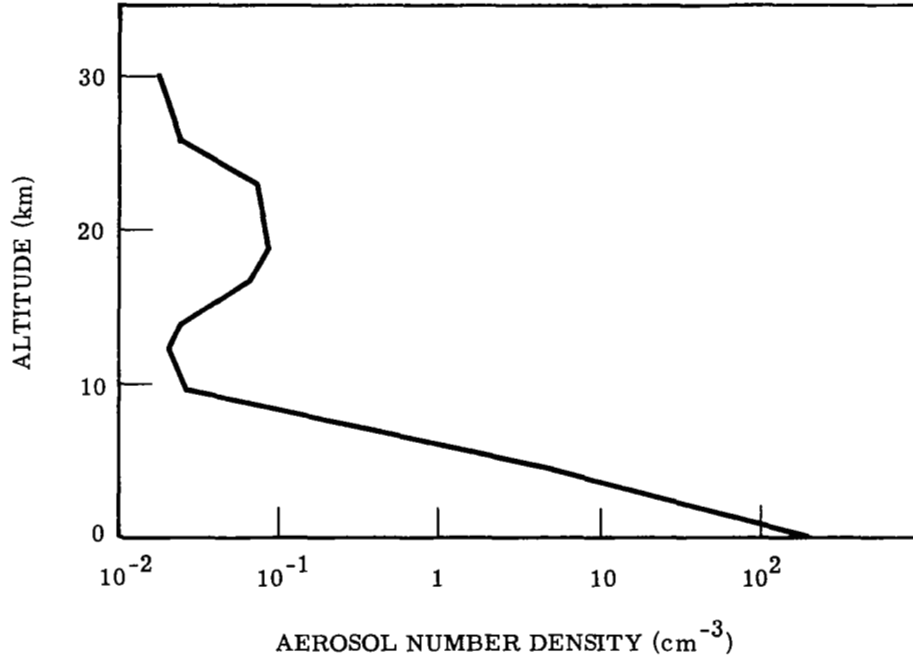


FIGURE 5. AEROSOL NUMBER DENSITY VERSUS ALTITUDE

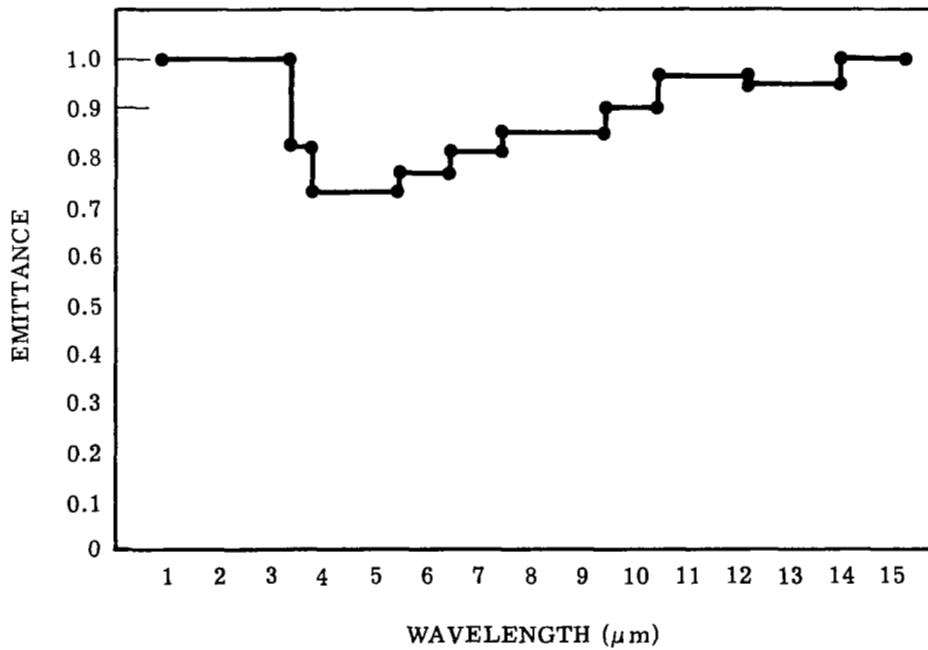


FIGURE 6. SPECTRAL EMITTANCE OF AN OPAQUE WATER-DROP CLOUD

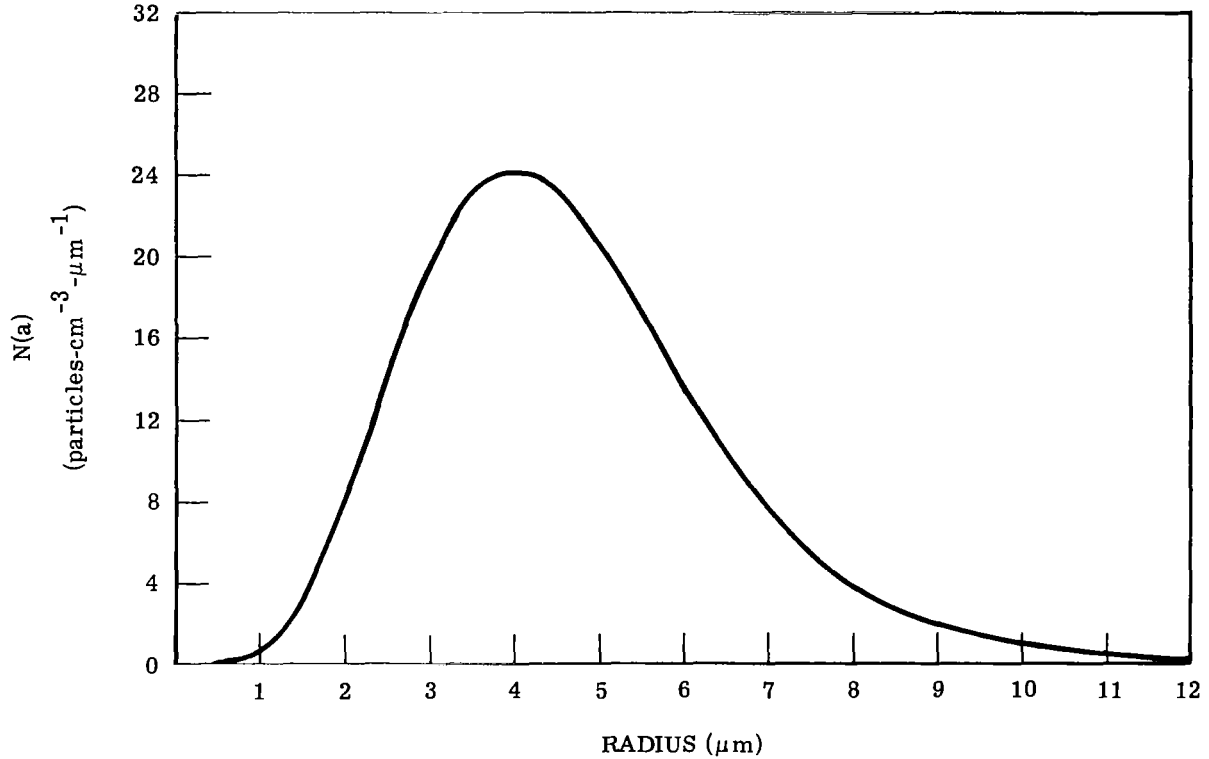


FIGURE 7. PARTICLE SIZE DISTRIBUTION OF WATER-DROP CLOUD

be expressed as:

$$\tilde{T}_{\lambda}^h(z_0) = \frac{1}{\pi} \int_{\text{hemisphere}} \tilde{T}_{\lambda}(z_0, \mu) d\Omega \quad (29)$$

where $d\Omega$ is the incremental solid angle. The procedure used to define $\tilde{T}_{\lambda}(z_0, \mu)$ was to empirically derive an analytical function which, when integrated over the hemisphere, gave a least squares best fit to Havard's hemispherical emittance data for clouds of various thicknesses ranging from 20 m to infinity. The derived directional transmittance relationship is:

$$\tilde{T}_{\lambda}(z_0, \mu) = e^{-\alpha z_0/\mu} e^{-(a+bz_0/\mu)\beta z_0/\mu} \quad (30)$$

where $a = 0.305$ and $b = 1.79$ are empirically derived constants.

An analogous procedure was used to obtain the directional emittance relationship from the hemispherical emittance, which can be expressed as:

$$\epsilon_{\lambda}^h(z_0) = \frac{1}{\pi} \int_{\text{hemisphere}} \epsilon_{\lambda}(z_0, \mu) d\Omega \quad (31)$$

The relationship derived from Havard's data is:

$$\epsilon_{\lambda}(z_0, \mu) = (1 - \omega)[1 - \tilde{T}_{\lambda}(z_0, \mu)] \quad (32)$$

where ω is the albedo at the top of a semi-infinite cloud. Note that (31) and (32) yield the correct values of emittance and transmittance for the limiting values of cloud thickness. For example, as the cloud thickness becomes large (i.e., z_0 approaches infinity), the transmittance approaches zero and the emittance approaches $1 - \omega$, the hemispherical emittance of an opaque cloud. Also, as the cloud thickness becomes small (i.e., z_0 approaches zero), the transmittance approaches unity and the emittance approaches zero. In Fig. 8, the spectral emittance and spectral transmittance, as calculated by (31) and (32), are given for clouds of three thicknesses at normal incidence.

4

CALCULATIONS OF SPECTRAL RADIANCE

In order to define a multichannel system capable of providing estimates of the sea-surface temperature on a global basis, it would be necessary to define the upwelling spectral radiance at space altitudes for a sufficient range of sea temperatures and atmospheric conditions to encompass all values of spectral radiance which would be encountered in a global application. As a preliminary step to performing such calculations and subsequent analysis, the present study restricted the range of sea temperature and atmospheric conditions to those common to the LaJolla-San Clemente geographical locale. This was done to minimize the computational labor required to synthesize the spectral-radiance data, allowing the major effort to be devoted to demonstrating the feasibility of using multichannel remote-sensing techniques for estimating accurately the sea-surface temperature. Such a restriction in sea temperature and atmospheric conditions does not affect the demonstration of feasibility; it may, however, affect the predictability of the error in the estimate of sea temperature for a geographical locale which has a significantly different meteorology.

4.1. DEFINITION OF ATMOSPHERIC STATES

The data required to calculate the radiance for a given atmospheric state, as given by Eq. (23), are as follows:

- (1) pressure, temperature, and the partial density of each of the molecular absorbing gases (H_2O , CO_2 , O_3 , N_2O , and CH_4) as a function of altitude
- (2) spectral absorption and scattering coefficients for atmospheric haze
- (3) directional spectral emittance and transmittance of either an opaque or semitransparent cloud, its altitude and temperature
- (4) the directional emittance and temperature of the sea surface

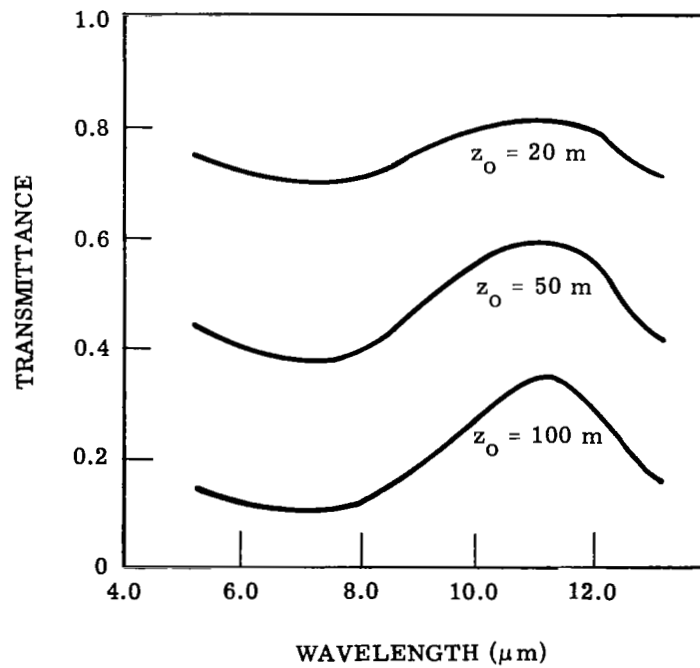
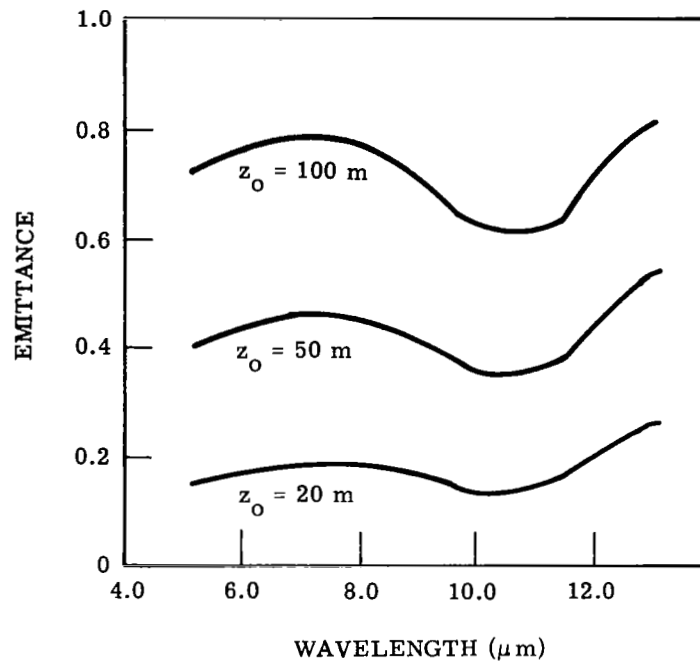


FIGURE 8. SPECTRAL TRANSMITTANCE AND EMITTANCE OF SEMITRANSSPARENT CLOUDS

For the present analysis of these atmospheric parameters, the only ones considered variable were the distribution of atmospheric water vapor and temperature, the emittance and transmittance of semitransparent clouds (the thickness was varied), the altitude and temperature of opaque and semitransparent clouds, and the sea temperature. Pressure and the concentration of the stable molecular constituents in the atmosphere (i.e., CO₂, N₂O, and CH₄) were assumed fixed. Since there is little likelihood of obtaining information about sea temperature in the spectral region of ozone absorption and emission (i.e., near 9.6 μm), variations in the concentration of ozone were also ignored.

To establish the range of parameters (i.e., sea temperature, water vapor, and atmospheric temperature) to be used in the present study, radiosonde and surface data for San Clemente, San Nicholas, and San Diego over a one-year period were acquired from the National Weather Records Center. A detailed computerized survey of these meteorological data was performed, and three temperature profiles and five water profiles were selected, the composite of these comprising five atmospheric states which give rise to maximum and minimum effects of the atmosphere on the spectral radiance.

In Fig. 9, the three temperature profiles are presented. The winter profile represents the coldest temperature profile, the summer profile the warmest, and the curve labeled "mean" is the average value of the temperature data, averaged over the one-year period. Figure 10 presents the five water profiles selected. These data represent the extremes for both summer and winter conditions and the mean value for the one-year period. Radiosonde data for water vapor did not exist for altitudes greater than approximately 12 km, so the values shown were taken from Gutnick [7]: they represent the mean water concentration for a midlatitude atmosphere. The use of Gutnick's data for these altitudes is permissible because the effect of high-altitude water vapor on the spectral radiance is negligible in those spectral regions which are likely to be useful for remote sensing of sea temperature.

The five model atmospheres selected from the temperature and water-vapor data are listed below. The temperature and water-vapor profiles used to define each atmosphere are also listed.

MODEL ATMOSPHERE NAME	TEMPERATURE PROFILE	WATER VAPOR PROFILE
Summer Wet (SWET)	Summer	Summer Wet
Summer Dry (SDRY)	Summer	Summer Dry
Winter Wet (WWET)	Winter	Winter Wet
Winter Dry (WDRY)	Winter	Winter Dry
Mean 30° North	Mean	Mean

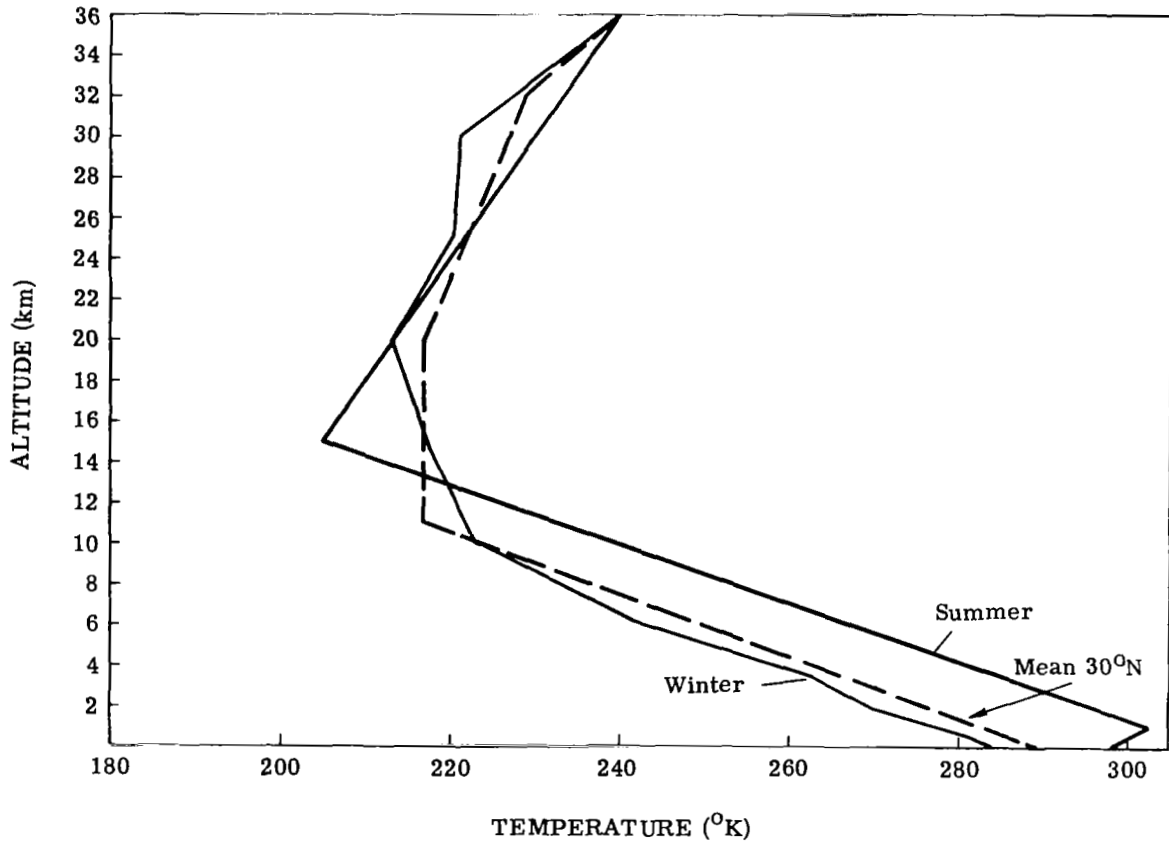


FIGURE 9. TEMPERATURE PROFILES FOR LA JOLLA AREA

4.2. SYNTHESIS OF SPECTRA

With (1) the five model atmospheres, (2) the spectral emittance and transmittance values for opaque and semitransparent clouds given in Section 3.2, (3) the absorption and scattering coefficients for a maritime haze given in Section 3.1.2, and (4) the spectral emittance of the sea surface as a function of direction taken from Buettner [8] (see Fig. 11), the spectral radiance from 4.0 to 30 μm observed at an altitude of 100-km was calculated for the following conditions:

- (1) For noncloudy atmospheres, radiance spectra were calculated for each of the five model atmospheres, each of three zenith angles* (0° , 60° , and 75°), and for each of five sea temperatures (280, 285, 290, 295, and 300°K).
- (2) For each of the five model atmospheres, radiance spectra were calculated with opaque clouds at four altitudes (0, 2, 5, and 12 km) for each of three zenith angles (0° , 60° , and 75°).

*The zenith angle is defined as the angle between the nadir and the optical line of sight at the sea surface.

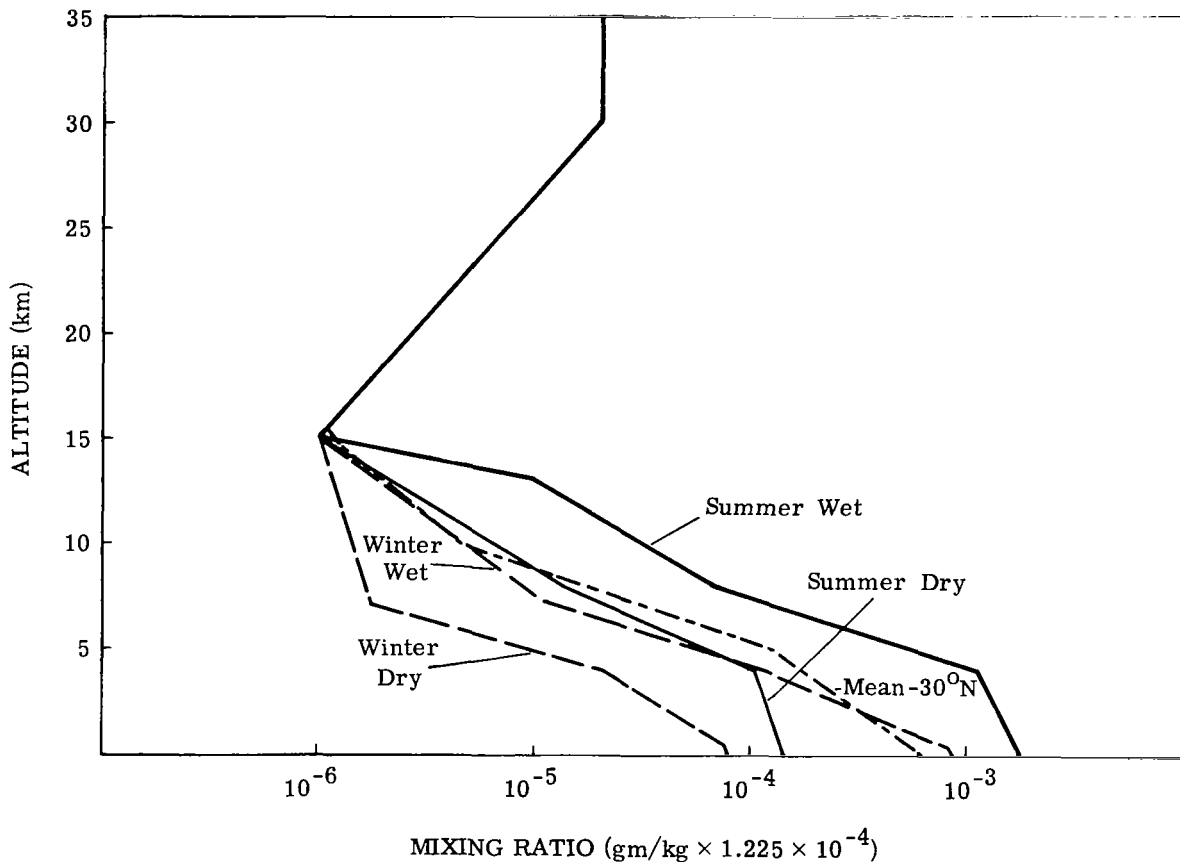


FIGURE 10. WATER VAPOR PROFILES FOR LA JOLLA AREA

- (3) For each of the five model atmospheres, three zenith angles, four cloud altitudes, and five sea temperatures, spectra were calculated for three amounts of fractional cloud cover (10%, 50%, and 90%).
- (4) For the mean 30°N atmosphere and a zenith angle of 0°, spectra were calculated for three semitransparent clouds (20, 50, and 100 m in thickness) at each of four altitudes (0, 2, 5, and 12 km), for each of the five sea temperatures.
- (5) To determine the distinguishing features between the spectral radiance emanating from fields of view completely obscured by semitransparent clouds and that which contains partial obscuration by opaque clouds for each spectrum of item (4), a spectrum was calculated for identical conditions (i.e., the same sea-surface temperature, model atmosphere, zenith angle, and cloud altitude) except that the semitransparent cloud was replaced with a certain fraction of opaque cloud, and the fractional coverage was chosen so the spectral radiance at 11 μm for the two spectra were identical.

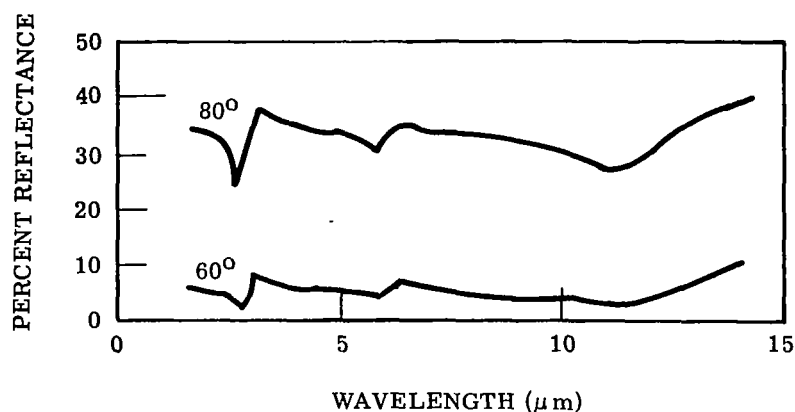


FIGURE 11. LIQUID WATER REFLECTANCE 60° AND 80° ANGLE OF INCIDENCE

The radiance spectra calculated provides a comprehensive description of the upwelling spectral-radiance field at a point in space for meteorological conditions characteristic of the LaJolla-San Clemente area. These data were used as a basis for developing multispectral-sensing techniques for estimating the sea temperature, detecting the presence of clouds, and estimating the fractional cover of opaque clouds.

4.3. DISCUSSION OF REPRESENTATIVE SPECTRA

Because of the large number of spectra calculated, it would be impractical to include all of the results. Therefore, only a representative sample of the results obtained is presented.*

In Fig. 12, the upwelling spectral radiance at 100 km for a noncloudy mean 30°N atmosphere is presented for six sea temperatures at a zenith viewing angle of 0°. The calculations included the effects of haze. The 0°K surface temperature was included to demonstrate the magnitude of the spectral radiance which emanates from only the atmosphere. The data presented are self-explanatory in that each radiance spectrum is the radiance emitted by a sea surface having a given temperature and emittance as modified by atmospheric molecular absorption and emission and the effects of atmospheric haze. Near the center of the intense absorbing regions (i.e., 6.3-μm H₂O band and the 15-μm CO₂ band), the spectra are the same for all sea temperatures. This occurs because the atmosphere is opaque in these spectral regions. In general, the larger the variation in radiance with sea temperature, the higher the transparency of the atmosphere. For the atmospheric conditions included in the present study, this occurs near 11 μm and, in general, is true for any atmospheric condition. However, for very dry, cold atmospheres as found in polar regions, the spectral region near 9 μm may be more transparent.

*All of the spectra calculated for noncloudy atmospheres (i.e., five model atmospheres, three zenith angles, and six sea temperatures) are given in Appendix III.

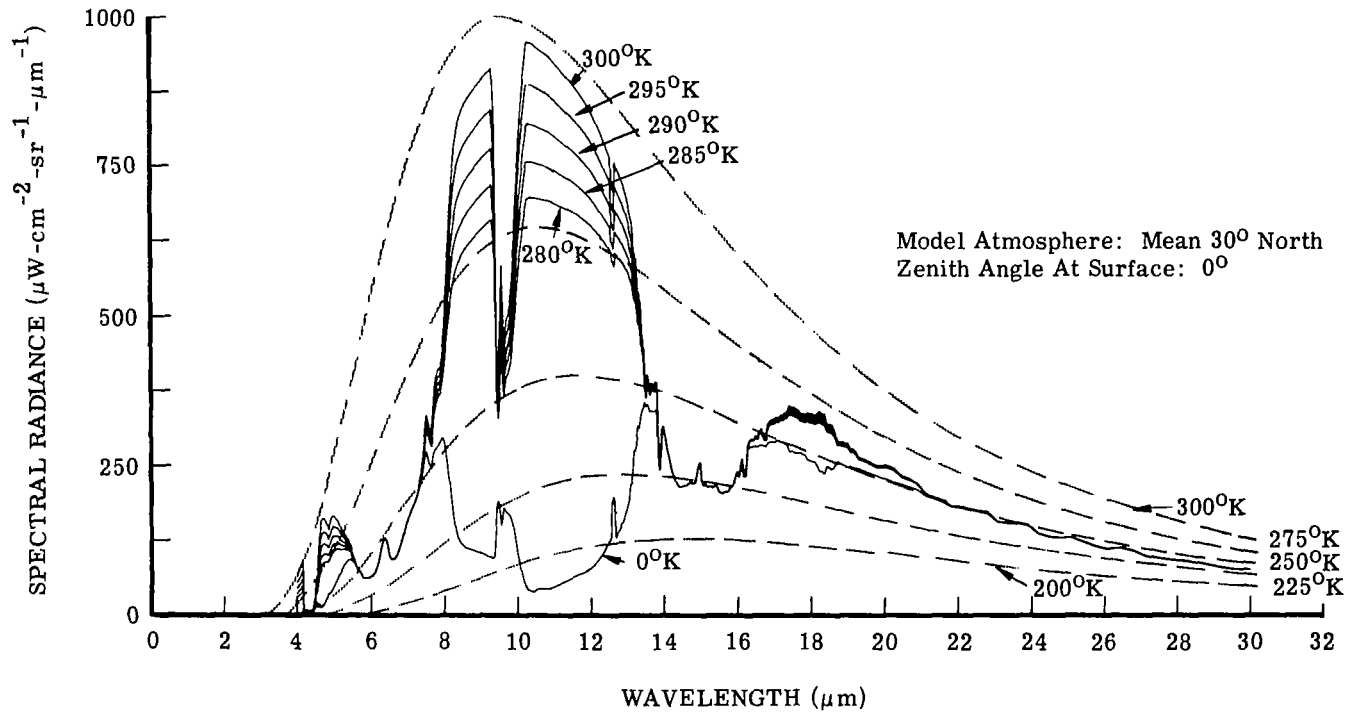


FIGURE 12. UPWELLING SPECTRAL RADIANCE AT 100 km FOR A NONCLOUDY ATMOSPHERE WITH SEA TEMPERATURE AS A PARAMETER

Figure 13 demonstrates the effects of the zenith viewing angle on the observed radiance. In most spectral regions, the radiance decreases at the larger zenith angles because of a decrease in the atmospheric transparency and an increase in the atmospheric radiance at the cooler high-altitude temperatures. In the center of the 15- μm CO_2 band, the radiance increases at the larger zenith angles. This is caused by an increase in atmospheric emission from the warm mesosphere. Figure 14 demonstrates the effect of changing the atmospheric state on the spectral radiance. The model atmosphere yielding the largest values of spectral radiance is WDRY, the lowest SWET. The effect may not appear to be large, but the magnitude of the change in radiance near 11 μm corresponds to changes in the effective radiometric temperature of approximately 2.0 $^\circ\text{K}$. If a similar set of radiance spectra were calculated for near horizon viewing, the spread in the radiometric temperature near 11.0 μm would be approximately 4.0 $^\circ\text{K}$.

Figure 15 represents the upwelling spectral radiance for an atmosphere which contains opaque clouds at four altitudes. The model atmosphere used was mean 30 $^\circ\text{N}$, and the zenith viewing angle is 0 $^\circ$. The upper curve is for a clear atmosphere with the sea temperature 290 $^\circ\text{K}$. Since the clouds are opaque, the spectral radiance results from the emission from the cloud, as affected by the molecular absorption and emission of the atmosphere above the clouds. As the cloud altitude is increased, the effect of the atmosphere decreases, and the spectral shape of the radiance spectra tends toward that of a blackbody as shown by the lower curve of Fig. 15. The radiance spectra presented in Fig. 16 were generated for the same conditions as those used to generate the spectra in Fig. 15, except the opaque cloud was replaced by a semitransparent cloud having a thickness of 50 m. Since the cloud is semitransparent, the spectral shape of the radiance spectra is similar to those for a clear atmosphere. The primary difference between the spectral shape of these data and those for a clear atmosphere is the large spread in the radiance values in the edges of the absorption bands of water vapor and CO_2 (i.e., near 8.0 and 13 μm) for the semitransparent cloud data, compared to almost no spread in the radiance values at these wavelengths for a clear atmosphere.

Figures 17 and 18 are examples of the calculated spectra stated in item (5). The model atmosphere, zenith angle, cloud altitude, and sea temperature are noted on the figures. Figure 17 is for semitransparent clouds of various thicknesses (0, 20, 50, and 100 m and opaque); Fig. 18 is for various values of fractional cover of opaque clouds. If the two sets of spectra are superposed, it is observed that the radiance values are approximately the same near 11 μm , and that the radiance values for the semitransparent cloud spectra are significantly smaller than those for the fractional opaque cloud spectra near 9 and 13 μm . Because of this difference in spectral shape, it is possible to distinguish the two cases using multispectral-sensing techniques.

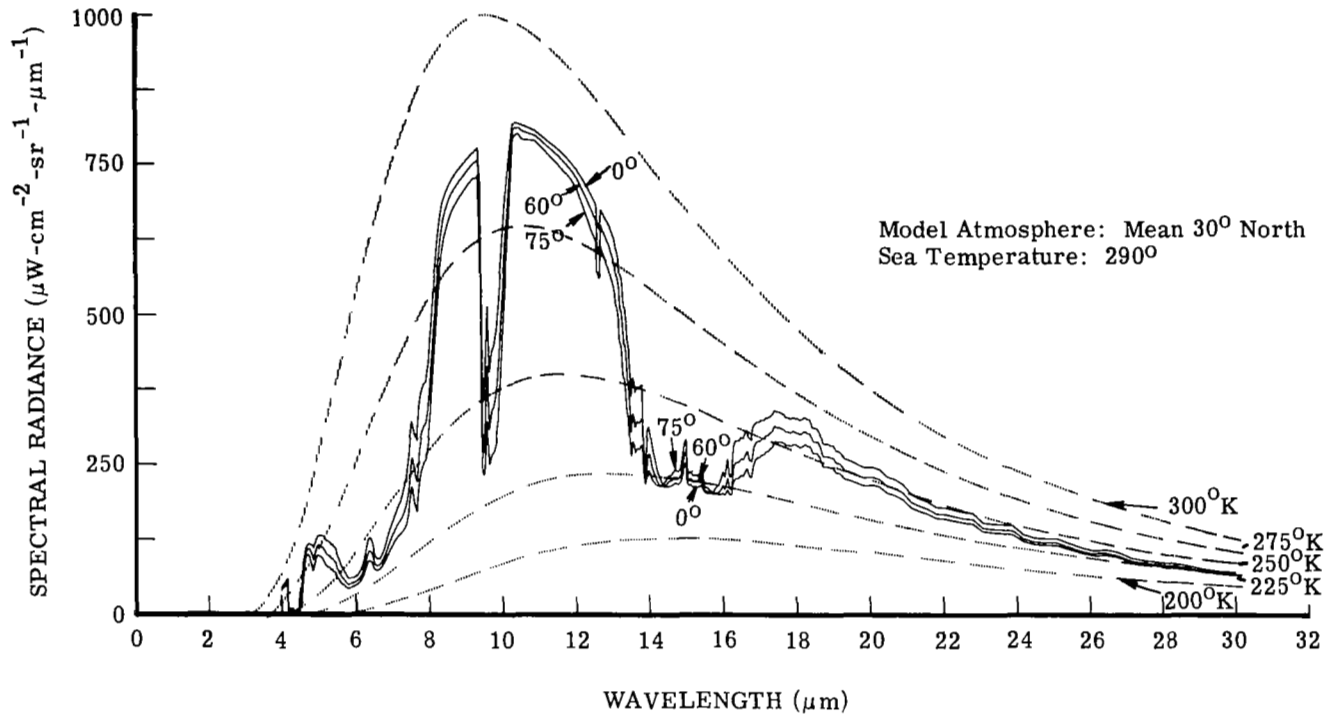


FIGURE 13. UPWELLING SPECTRAL RADIANCE AT 100 km FOR A NONCLOUDY ATMOSPHERE WITH ZENITH ANGLE AS A PARAMETER

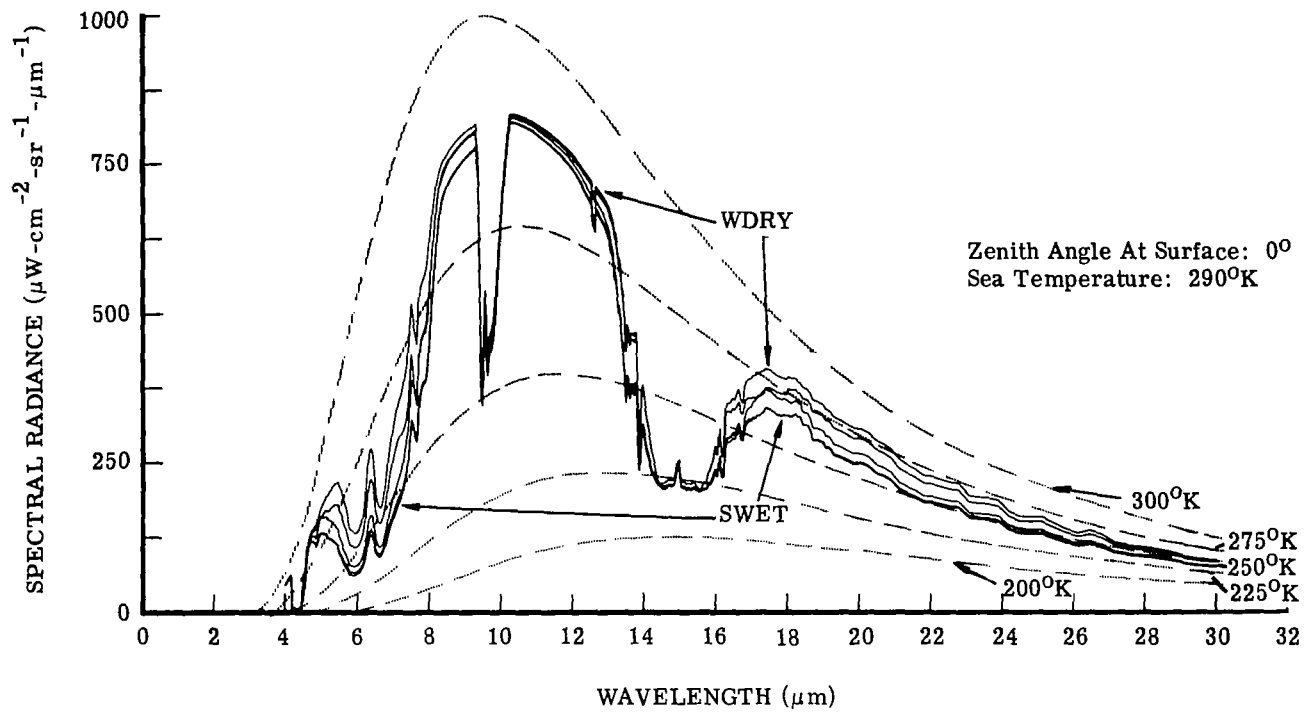


FIGURE 14. UPWELLING SPECTRAL RADIANCE AT 100 km FOR NONCLOUDY ATMOSPHERES WITH MODEL ATMOSPHERE AS A PARAMETER

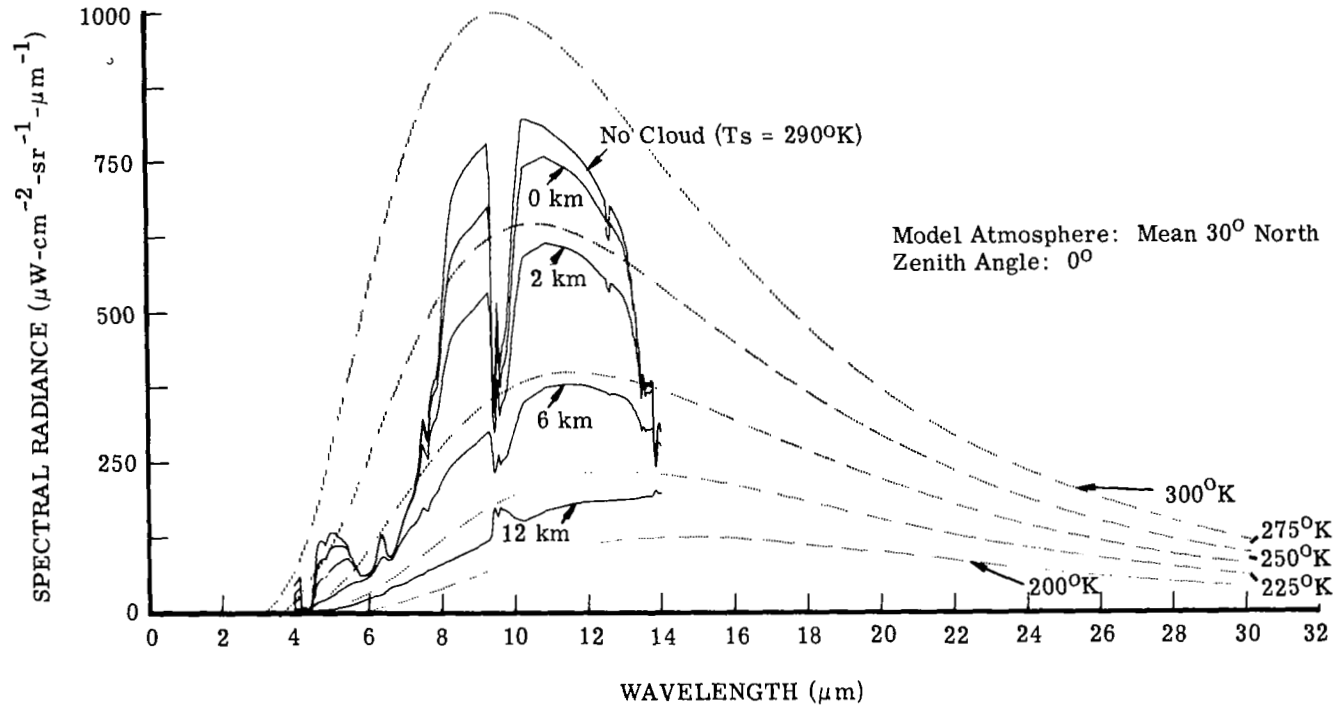


FIGURE 15. UPWELLING SPECTRAL RADIANCE AT 100 km WITH OPAQUE CLOUDS AT FOUR ALTITUDES

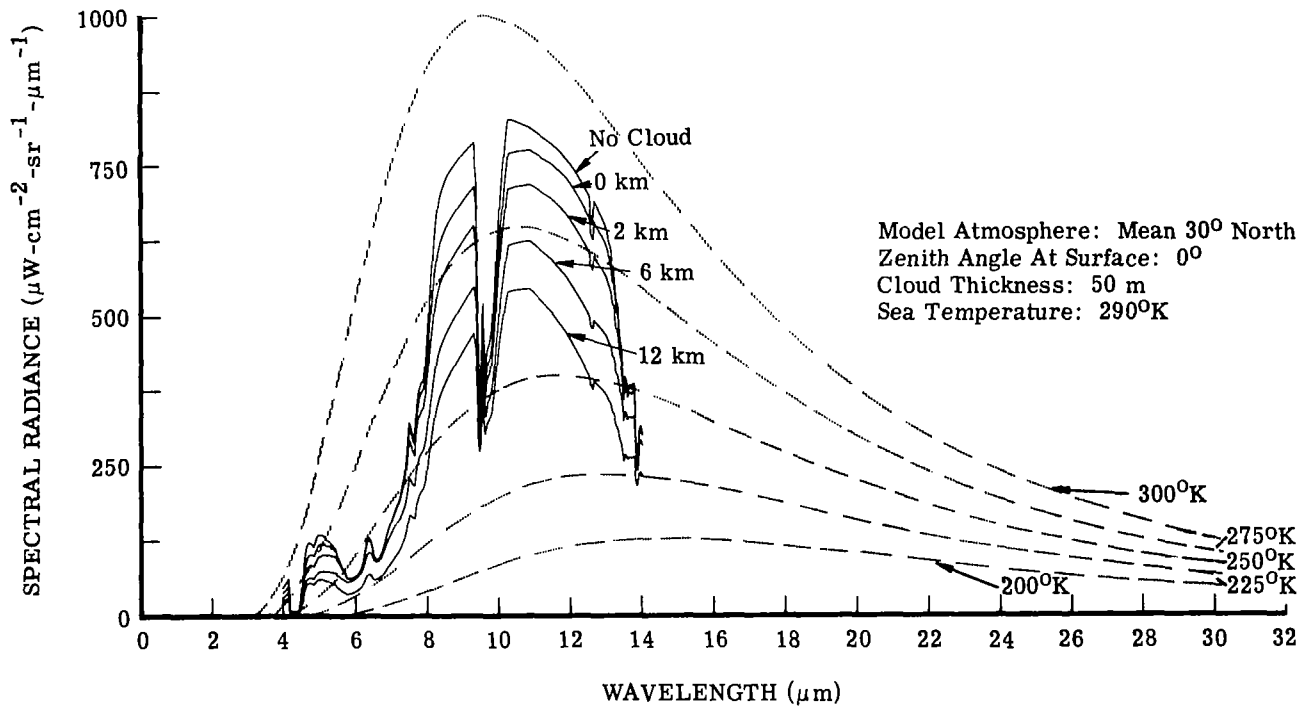


FIGURE 16. UPWELLING SPECTRAL RADIANCE AT 100 km WITH A SEMITRANSSPARENT CLOUD AT FOUR ALTITUDES

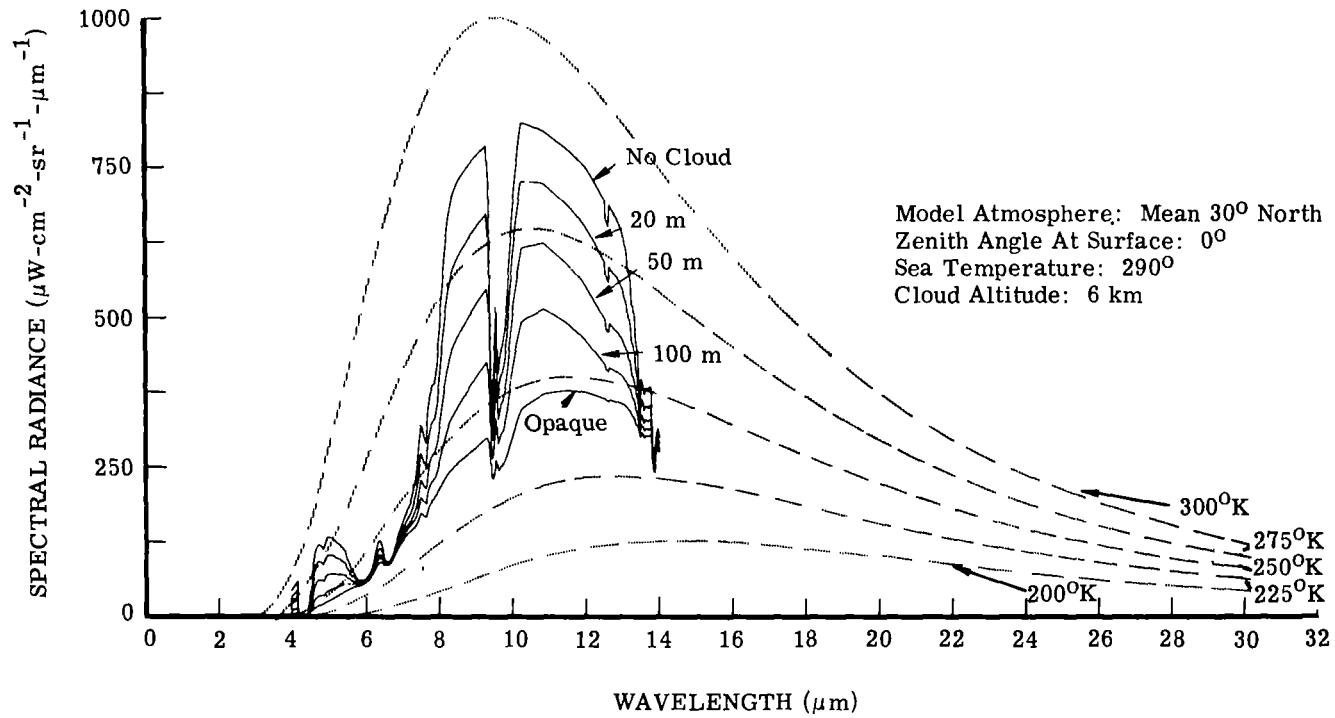


FIGURE 17. UPWELLING SPECTRAL RADIANCE AT 100 km FOR SEMITRANSSPARENT CLOUDS WITH CLOUD THICKNESS AS A PARAMETER

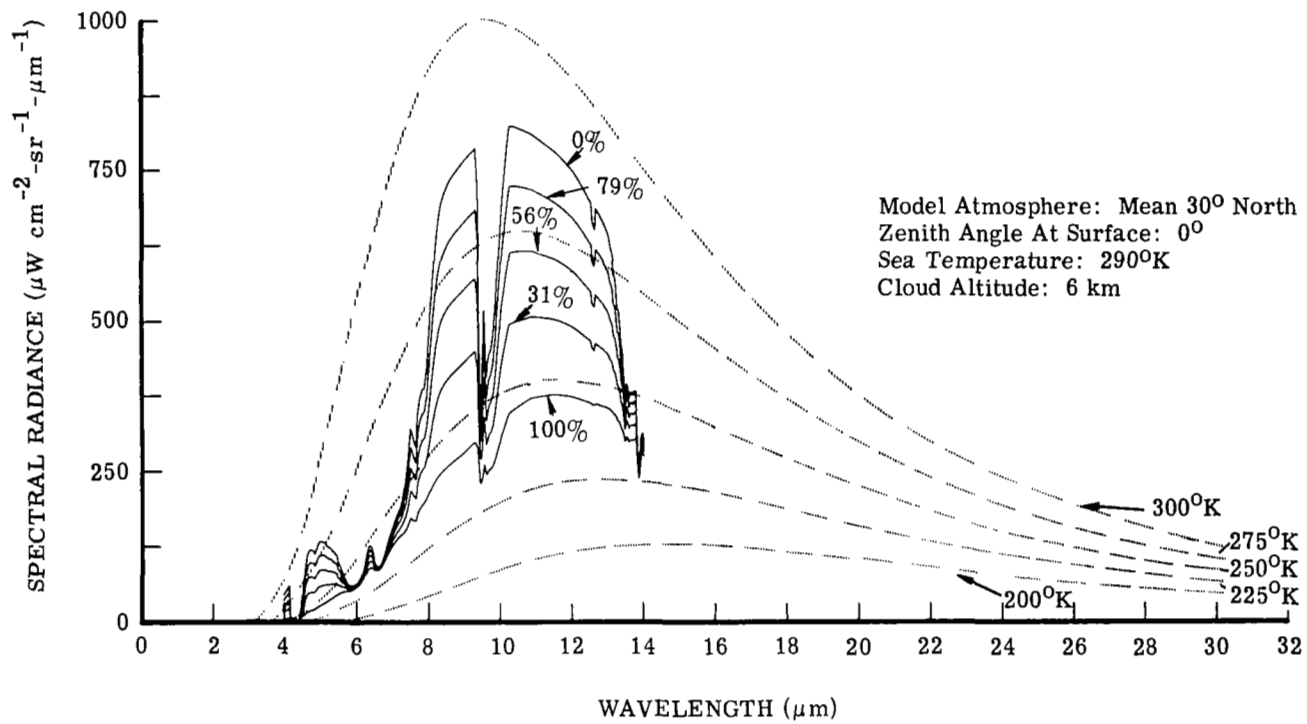


FIGURE 18. UPWELLING SPECTRAL RADIANCE AT 100 km FOR OPAQUE CLOUDS WITH PERCENT CLOUD COVER AS A PARAMETER

4.4. COMPARISON OF CALCULATED SPECTRA TO MEASURED SPECTRA

The composite of the calculated spectra may be considered as the results of a simulated spaceborne experiment, in which the atmospheric and sea temperature conditions were precisely known. Clearly, if such an experiment could be implemented, multispectral pattern-recognition techniques could be applied directly to the experimental results, and the amount of spectral information required (i.e., the number of spectral bands, their location, and spectral-filter definition) to identify a given atmospheric condition or sea temperature could be established. The utilization of spectral-radiance data obtained through the use of analytical models (i.e., the results of a simulated experiment) should provide results that are equally valid, assuming the spectra are representative of the real world. Since measurements of spectral radiance for known atmospheric conditions exist only for fields of view which are free of clouds, the representative nature of the calculated spectra could only be established for cloud-free conditions. This was achieved by comparing the results of calculations with data obtained with the Nimbus III Infrared Interferometer Spectrometer (IRIS) for known clear atmospheric conditions. Seven such comparisons were made for various geographical locations within the continental United States. At the time of each IRIS measurement, radiosonde data for pressure, atmospheric temperature, water vapor, and surface temperature were obtained, and these data were used to calculate the radiance spectrum for each case. Two such comparisons are shown in Figs. 19 and 20. Although minor differences are observable, the agreement is satisfactory in those spectral regions which will be potentially useful for the remote measurement of sea temperature. These comparisons demonstrate that the state-of-the-art of analytical procedures for calculating the upwelling spectral radiance for known clear atmosphere conditions is very good.

5

DEVELOPMENT OF MULTISPECTRAL SYSTEMS

The objective of the present study is to define potentially useful multispectral systems for estimating sea temperature. A multispectral system is one which measures the radiance in some number of spectral bands and processes this information to obtain an estimate of the atmospheric conditions or sea temperature. This section discusses procedures for defining such systems in regard to the spectral bands and data processing. The data base which was used to devise and test various systems is the spectral-radiance data discussed in Section 4. For these data, the input conditions for each simulated experimental output were precisely known. Therefore, the accuracy to which a given multispectral system could estimate the input conditions could be established.

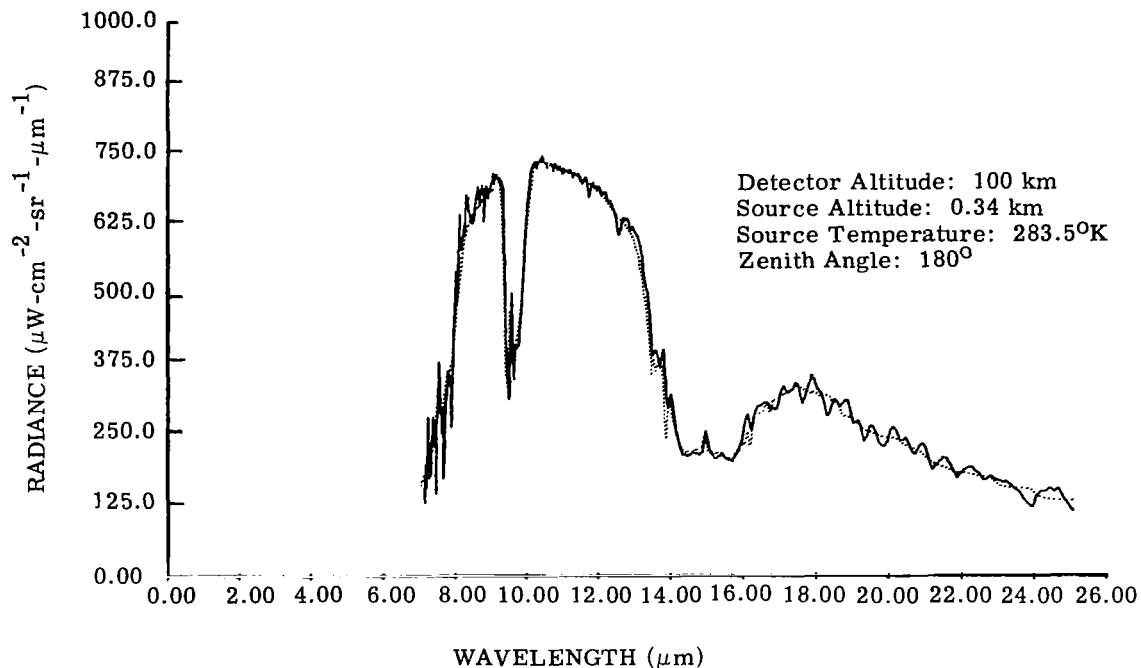


FIGURE 19. COMPARISON OF CALCULATED SPECTRAL RADIANCE WITH MEASUREMENTS FOR A CLEAR ATMOSPHERE. Spectral radiance (-----) calculated with The University of Michigan computer code, and spectral radiance (——) measured by Nimbus III.

In defining potentially useful multispectral systems, it is convenient to represent each output of the previously described simulated experiment (i.e., the spectral radiance observed at space altitudes) by an n -dimensional vector, L , where n is the number of defined wavelength points in a given spectrum. Let h be the value of an input condition which is to be estimated by the system (for example, sea temperature or fractional cloud cover). The vector L is a function of the input condition h as well as other input conditions. Since these other conditions are variable, there will be a collection of vectors for each value of h , which will be denoted by $L(h)$. The problem, therefore, is to determine the most likely value of the input condition, h , given an experimental output vector, L . This can be achieved by choosing that value of h which maximizes the probability density function of h given L . The probability density of h given L , $p(h|L)$, is:

$$p(h|L) = \frac{p(L|h)p(h)}{p(L)} \quad (33)$$

where $p(L|h)$ is the probability density of L given h , and $p(h)$ and $p(L)$ are the a priori probability densities of h and L , respectively. Maximizing $p(h|L)$ requires:

$$\frac{\partial p(h|L)}{\partial h} = \frac{1}{p(L)} \left[p(h) \frac{\partial p(L|h)}{\partial h} + p(L|h) \frac{\partial p(h)}{\partial h} \right] = 0 \quad (34)$$

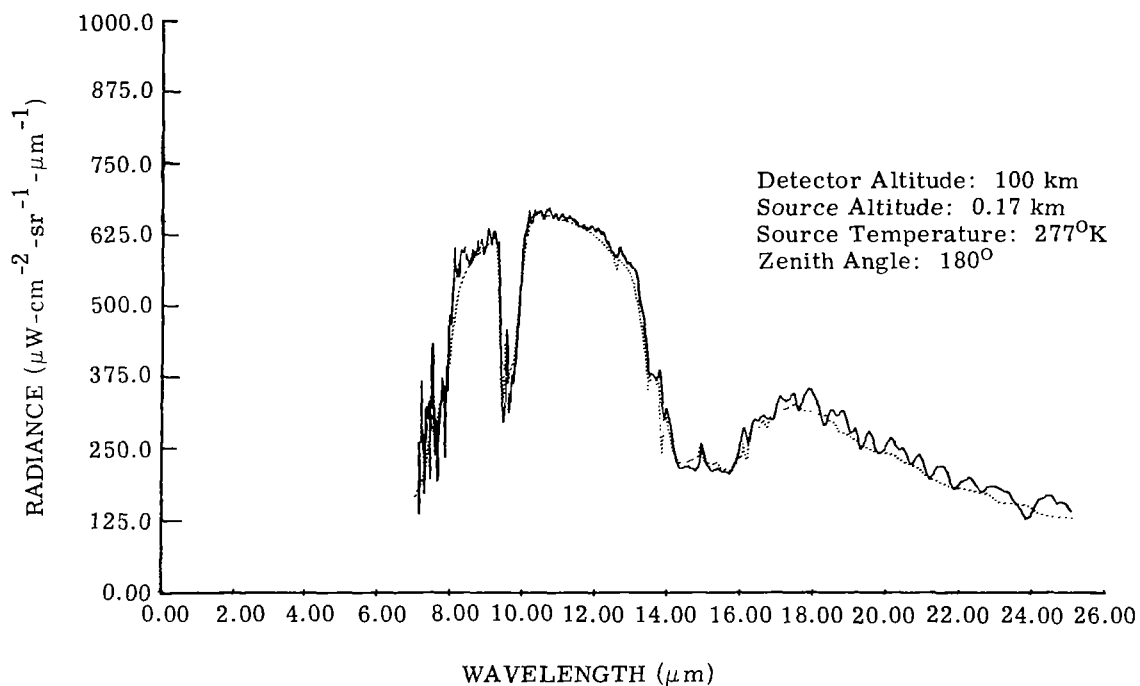


FIGURE 20. COMPARISON OF CALCULATED SPECTRAL RADIANCE WITH MEASUREMENTS FOR A CLEAR ATMOSPHERE. Spectral radiance (-----) calculated with The University of Michigan computer code, and spectral radiance (——) measured by Nimbus III.

If $p(h)$ is assumed the same for all h , then the quantity which must be maximized is the likelihood function $p(L|h)$. It can be easily shown that finding the maximum of a density function is equivalent to finding the maximum of its logarithm. The problem then is to choose h such that:

$$\frac{\partial \log_e p(L|h)}{\partial h} = 0 \quad (35)$$

In order to obtain a solution to Eq. (35), it is necessary to assume a statistical form for the likelihood function $p(L|h)$. For the present application, a reasonable functional form of $p(L|h)$ is a multivariate normal with mean value $A(h)$ and covariance matrix $B(h)$. $A(h)$ is given by:

$$A(h) = \frac{1}{n} \sum_{k=1}^n L^k(h) \quad (36)$$

where $L^k(h)$ is a specific vector of the collection $L(h)$ and the sum is taken over all vectors resulting from the input condition h . The covariance matrix of $L(h)$ is $B(h)$, and its element $B_{(a,b)}(h)$ is the covariance between the spectral radiances at wavelength points a and b , $\text{Cov}_{a,b}[L(h)]$, and is given by:

$$\text{Cov}_{a,b}[L(h)] = \frac{1}{n-1} \sum_{k=1}^n [L_a^k(h) - A_a(h)][L_b^k(h) - A_b(h)] \quad (37)$$

where $L_a^k(h)$ and $L_b^k(h)$ are the spectral radiances at wavelength points a and b respectively, and the sum is again taken over all vectors resulting from the input condition h. For the multivariate normal distribution, $p(L|h)$ is given by:

$$p(L|h) = \frac{1}{(2\pi)^{n/2} |B(h)|^{1/2}} e^{-\frac{1}{2} [L(h)-A(h)] B^{-1}(h) [L(h)-A(h)]^t} \quad (38)$$

where $|B(h)|$ is the determinant of the covariance matrix, $B(h)$; B^{-1} is the inverse of the covariance matrix, $B(h)$; and $[L(h) - A(h)]^t$ is the transpose of the matrix $[L(h) - A(h)]$, which is assumed by convention to be a matrix of 1 row and n columns. From Eqs. (34) and (38) we have:

$$\frac{\partial \log_e p(L|h)}{\partial h} = -\frac{1}{2} \frac{\partial}{\partial h} \log_e |B(h)| - \frac{1}{2} \frac{\partial}{\partial h} \{ [L(h) - A(h)] B^{-1}(h) [L(h) - A(h)]^t \} \quad (39)$$

$L(h)$, $A(h)$, and $B(h)$ can be assumed to be linear functions of h over some sufficiently small range of values. Let h_0 and h_1 be two bounding values of the input condition L which span such a linear range, and let the mean value and covariance of $L(h_0)$ and $L(h_1)$ be known. Thus:

$$A(h) = \frac{(h - h_0)A(h_1) + (h_1 - h)A(h_0)}{h_1 - h_0} \quad (40)$$

$$B(h) = \frac{(h - h_0)B(h_1) + (h_1 - h)B(h_0)}{h_1 - h_0} \quad (41)$$

In general, the only conditions for which a unique solution to Eq. (39) exists is when $B(h_0)$ and $B(h_1)$ are identical [9]. For the applications of the present study, the covariance matrices for collections of vectors for various values of the input condition h will not be identical, but, in general, will be identical except for a slight rotation. For this case, a rigorous mathematical solution to Eq. (39) is not obtainable; however, a reasonable estimate of the value of h which yields a particular output vector $L^k(h)$ is obtainable. The procedure for obtaining this estimate is developed heuristically using a rationale motivated by the solution of the maximum likelihood function for the identical matrix case which is given below.

5.1. MAXIMUM LIKELIHOOD ESTIMATE OF h FOR COVARIANCE MATRICES IDENTICAL

From Eq. (39), a value of h must be chosen to minimize

$$[L^k(h) - A(h)] B^{-1}(h) [L^k(h) - A(h)]^t + \log_e |B(h)|$$

where $A(h)$ and $B(h)$ are given by Eqs. (40) and (41), respectively. Since $B(h_0)$ and $B(h_1)$ are, by assumption, identical, $|B(h)|$ is a constant, and the partial derivative of the logarithm term is, therefore, zero. Also, it is convenient to transform the vectors, $L(h)$, such that $B(h_0)$ and $B(h_1)$ become identity matrices. Such a transformation eliminates the covariance term from Eq. (39)

and simplifies the procedure for selecting that value of h which minimizes the likelihood function.

The first step in performing such a transformation is to find an orthogonal transformation which transforms a covariance matrix, B , into a new matrix, B' , which is a diagonal matrix, denoted by D , where the diagonal elements of D are the eigenvalues, δ_i , of B . The transformation which accomplishes this is:

$$B' = D = HBH^t \quad (42)$$

where H is a matrix which has the eigenvectors of B as its rows. This transformation is equivalent to transforming each vector L into a new vector L' by:*

$$L' = LH^t \quad (43)$$

consequently:

$$A' = AH^t \quad (44)$$

The first transformation, in effect, performs a coordinate rotation which is shown schematically in Figs. 21a and 21b for a two-dimensional case. The next step is to transform B into the identity matrix by:

$$B'' = \sqrt{(B')^{-1}} B' (\sqrt{(B')^{-1}})^t = \sqrt{D^{-1}} D (\sqrt{D^{-1}})^t = I \quad (45)$$

Therefore,

$$L'' = L' (\sqrt{D^{-1}})^t \quad (46)$$

and

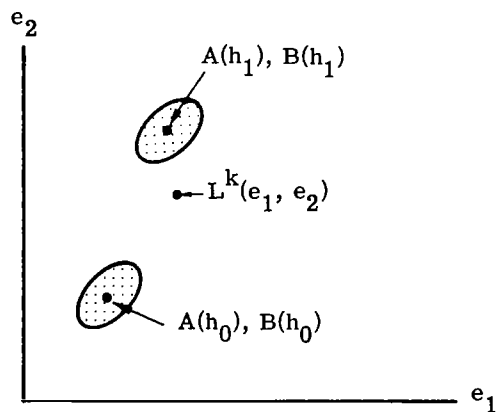
$$A'' = A' (\sqrt{D^{-1}})^t \quad (47)$$

The result of this transformation is shown in Fig. 21c.

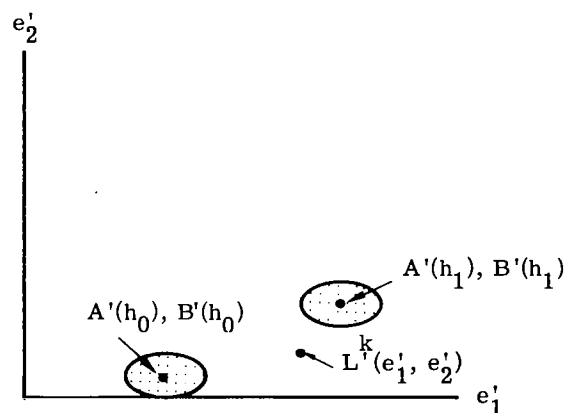
In the transformed coordinate system, the estimate of h , denoted by \hat{h} , will be that h which minimizes $[L^{k''}(h) - A''(h)][L^{k''}(h) - A''(h)]^t$. This is achieved by finding the point on the line

*By definition $B' = E\{[L' - E(L')][L' - E(L')]^t\}$. The order of the operations of expectation, difference, and transpose can be interchanged, so that, $B' = E[L'^t L'] - E[L'^t]E[L']$; from Eq. (43), $L'^t L' = (LH^t)^t LH^t = H(L^t L)H^t$. Therefore:

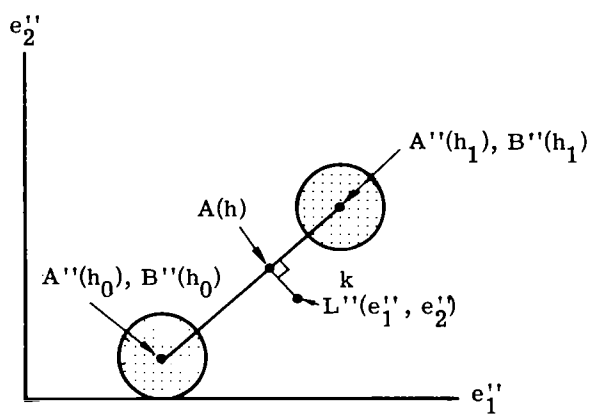
$$\begin{aligned} B' &= E[H(L^t L)H^t] - E(HL^t)E(LH^t) \\ &= HE(L^t L)H^t - HE(L^t)E(L)H^t \\ &= H[E(L^t L) - E(L^t)E(L)]H^t \\ &= HBH^t \end{aligned}$$



(a) Untransformed



(b) Coordinates Rotated



(c) Covariance Matrices Normalized

FIGURE 21. SKETCH SHOWING THE EFFECT OF A COORDINATE TRANSFORMATION ON EACH OF TWO COLLECTIONS OF OUTPUT VECTORS

passing through $A''(h_0)$ and $A''(h_1)$ which is closest to $L''(h)$. Mathematically:

$$\hat{h} = h_0 + (h_1 - h_0) \frac{[L^k(h) - A''(h_0)][A''(h_1) - A''(h_0)]^t}{[A''(h_1) - A''(h_0)][A''(h_1) - A''(h_0)]^t} \quad (48)$$

Since $[L^k(h) - A''(h_0)]$ and $[A''(h_1) - A''(h_0)]$ are row vectors, and $[A''(h_1) - A''(h_0)]^t$ is a column vector, the vector products in Eq. (48) are vector dot-products and are consequently scalar quantities. The scalar fraction is a number between zero and one and can be thought of as a fraction of the geometrical distance between $A''(h_0)$ and $A''(h_1)$.

Using Eqs. (43), (44), (46), (47), and (48), Eq. (48) can be expressed as an operation on the radiance vector $L(h)$, or:

$$\hat{h} = h_0 + (h_1 - h_0) \frac{[L^k(h) - A(h_0)]H^t(\sqrt{D^{-1}})^t \sqrt{D^{-1}}H[A(h_1) - A(h_0)]^t}{[A(h_1) - A(h_0)]H^t(\sqrt{D^{-1}})^t \sqrt{D^{-1}}H[A(h_1) - A(h_0)]^t} \quad (49)$$

From Eq. (42), it can be shown that:

$$H^t(\sqrt{D^{-1}})^t \sqrt{D^{-1}}H = B^{-1} \quad (50)$$

Substituting Eq. (50) into Eq. (49), the estimation formula becomes:

$$\hat{h} = \left[h_0 - (h_1 - h_0)A(h_0)w^t \right] + (h_1 - h_0)L^k(h)w^t \quad (51)$$

where

$$w^t = \frac{B^{-1}[A(h_1) - A(h_0)]^t}{[A(h_1) - A(h_0)]B^{-1}[A(h_1) - A(h_0)]^t} \quad (52)$$

The geometrical interpretation of this estimation procedure is shown in Fig. 22. In effect, the value of h is estimated by interpolating the observed point $L^k(h)$ between two parallel planes which contain the mean values $A(h_0)$ and $A(h_1)$ and whose normal vector is w .

Since the denominator in Eq. (52) is a scalar, w^t is a vector in the direction $B^{-1}[A(h_1) - A(h_0)]^t$. If the data points of the set $L(h)$ are very closely confined to a hyperplane, w is very well approximated by a vector in the direction v_ℓ where v_ℓ is the eigenvector of B which corresponds to the least eigenvalue, δ_ℓ , of B .

For this approximation:

$$\hat{h} = h_0 + (h_1 - h_0) \frac{[L^k(h) - A(h_0)]v_\ell^t}{[A(h_1) - A(h_0)]v_\ell^t} \quad (53)$$

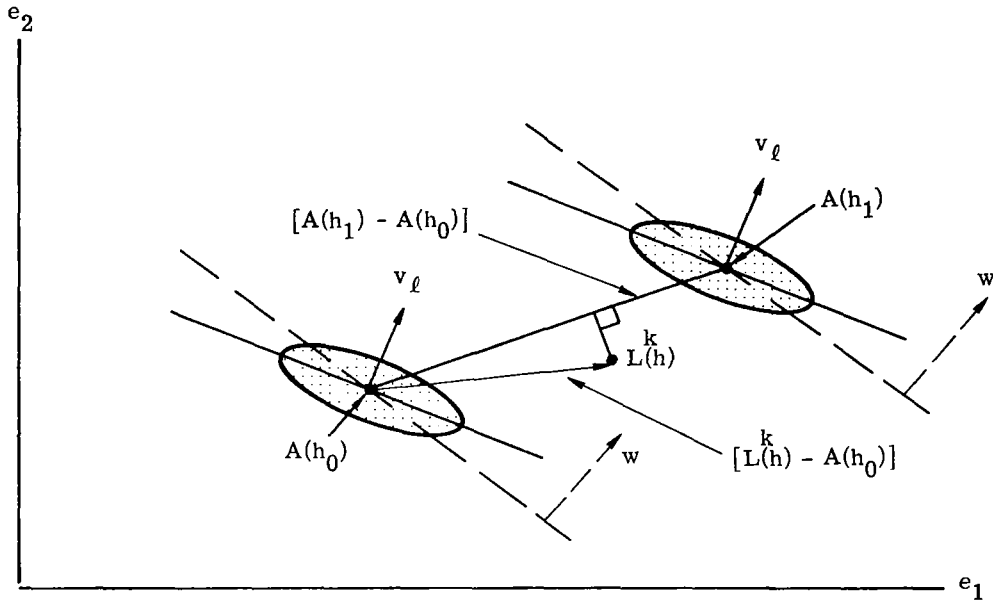


FIGURE 22. TWO-DIMENSIONAL GEOMETRICAL INTERPRETATION OF INTERPOLATION PROCEDURES GIVEN BY EQS. (51) AND (53)

The geometrical interpretation is also shown in Fig. 22. The observed point $L^k(h)$ is interpolated between two parallel planes which contain the means $A(h_0)$ and $A(h_1)$, and whose common normal is v_ℓ . In the limit, as the scatter in the data points about the hyperplane becomes very small, w and v_ℓ become equal and Eqs. (51) and (53) are equivalent.

The estimation formula given by Eq. (53) motivated a choice of a more generalized estimation formula when covariance matrices $B(h_0)$ and $B(h_1)$ are slightly different, which is, in general, true for the applications of the present study.

5.2. MAXIMUM LIKELIHOOD ESTIMATE OF h FOR COVARIANCE MATRICES SLIGHTLY DIFFERENT

In Fig. 23, two sets of data points are shown, each represented by a hyperplane whose unit normals are the eigenvectors $v_\ell(h_0)$ and $v_\ell(h_1)$, of the respective covariance matrices in $B(h_0)$ and $B(h_1)$, which corresponds to the respective eigenvalues $\delta_\ell(h_0)$ and $\delta_\ell(h_1)$ which are small compared to all others. Even in this simplified case (i.e., δ_ℓ very small), a different interpolation concept is required than in the case where covariance matrices were identical. A good one appears to be:

$$\hat{h} = h_0 + (h_1 - h_0) \frac{d_0}{d_0 - d_1} \quad (54)$$

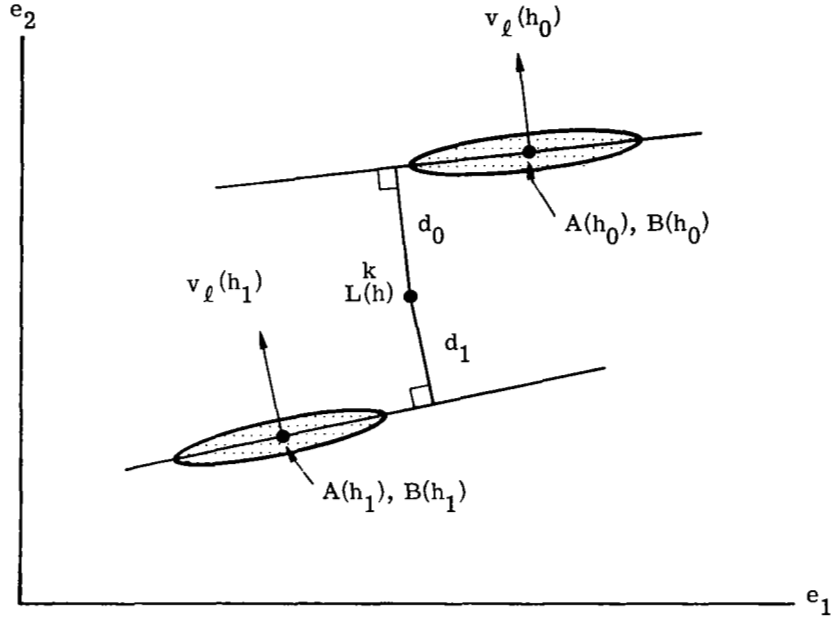


FIGURE 23. TWO-DIMENSIONAL GEOMETRICAL INTERPRETATION OF INTERPOLATION PROCEDURES GIVEN BY EQS. (54) AND (55)

where d_0 and d_1 are given by:

$$d_0 = [L^k(h) - A(h_0)] \cdot v_l(h_0) = [L^k(h) - A(h_0)][v_l(h_0)]^t \quad (55)$$

$$d_1 = [L^k(h) - A(h_1)] \cdot v_l(h_1) = [L^k(h) - A(h_1)][v_l(h_1)]^t$$

The above estimation procedure is the one which was used to estimate fractional cloud cover and is discussed in Section 6.1.

In case the above simplification cannot be made, a useful estimation formula is obtained by redefining d_0 and d_1 as follows:

$$d_0 = [L^k(h) - A(h_0)]w(h_0)^t \quad (56)$$

$$d_1 = [L^k(h) - A(h_1)]w(h_1)^t$$

where the w 's are defined in a manner similar to Eq. (52) but are normalized to unit vectors; i.e.:

$$w(h_0)^t = \frac{B(h_0)^{-1}[A(h_1) - A(h_0)]^t}{\|B(h_0)^{-1}[A(h_1) - A(h_0)]^t\|} \quad w(h_1)^t = \frac{B(h_1)^{-1}[A(h_1) - A(h_0)]^t}{\|B(h_1)^{-1}[A(h_1) - A(h_0)]^t\|} \quad (57)$$

where the parallel bars denote the magnitude of the vector quantity. The estimation formula for this case is then:

$$h = h_0 + (h_1 - h_0) \frac{[L^k(h) - A(h_0)]B(h_0)^{-1}[A(h_1) - A(h_0)]^t}{[L^k(h) - A(h_0)]B(h_0)^{-1}[A(h_1) - A(h_0)]^t - [L^k(h) - A(h_1)]B(h_1)^{-1}[A(h_1) - A(h_0)]^t} \mathbf{R} \quad (58)$$

where

$$\mathbf{R} = \frac{||B(h_0)^{-1}[A(h_1) - A(h_0)]^t||}{||B(h_1)^{-1}[A(h_1) - A(h_0)]^t||}$$

Note that as $B(h_1)$ approaches $B(h_0)$, Eq. (58) converges to Eq. (51), the estimation formula for identical covariance matrices.

In review of the interpolation rules developed, Eq. (51) represents the rigorous solution to the problem of maximizing the likelihood function of h given a vector $L^k(h)$, when the covariance matrices of the distributions of $L(h_0)$ and $L(h_1)$ are identical. Equation (53) is an approximation which is useful if the points of the distribution are confined closely to a hyperplane. The form of the solution for the identical matrix case suggests the estimation formula given by Eq. (58) when the covariance matrices are slightly different. Although Eq. (58) is not an exact solution to the maximization of the likelihood function, we feel that it will provide very good and useful approximations for the interpolations required in this study.

6

APPLICATIONS OF REMOTE-SENSING PROCEDURE

The remote-sensing procedures outlined in Section 5 can be applied to any collection of radiance spectra to estimate any given property (or properties) of the atmospheric or sea-temperature conditions giving rise to a particular spectral-radiance signature. The precision to which a given property can be estimated depends upon the uniqueness of the collection of vectors, $L(h)$, representing a given property of the input conditions. Clearly, some properties can be determined more easily than others (and with greater precision), simply because the uniqueness requirement is a function of the property to be estimated. In the present study, the objective was to demonstrate the successful application of the outlined procedure to estimate the sea temperature for atmospheres which are noncloudy and to estimate the fraction of opaque clouds within the field of view of a hypothetical, spaceborne system.

6.1. ESTIMATE OF SEA TEMPERATURE FOR CLEAR ATMOSPHERES

As outlined previously, the first step in defining a remote-sensing system for estimating the sea temperature for clear atmosphere is to determine the number of spectral bands required. For this particular application, this was achieved, in part, by examining the nature of physical processes affecting the upwelling spectral irradiance.

Figures 12, 13, and 14 are representative samples of clear-atmosphere spectra. The atmosphere has a minimum effect on the spectral radiance in the spectral regions between the intense absorption bands in the so-called atmospheric windows. However, even in these spectral regions, the effects of atmospheric absorption and emission are significant. For example, at zenith angles corresponding to near-horizon viewing and for very moist atmospheres, the spectral radiance near $11.0 \mu\text{m}$, the clearest atmospheric window, would correspond to temperatures approximately 4.0°C cooler than the surface temperature that would be inferred from radiance measurements performed at the sea surface. Even at near-nadir viewing through relatively dry, clear atmospheres, the equivalent radiometric temperature near $11.0 \mu\text{m}$ would be approximately 1.0°C cooler than the surface temperature. The effect in the atmospheric window near $9.0 \mu\text{m}$ is, in general, slightly larger than the effect near $11.0 \mu\text{m}$. Therefore, accurate estimates of the sea temperature can only be achieved by correcting for the effects of atmospheric absorption and emission.

In the two window regions, $7.0 \mu\text{m}$ to $9.5 \mu\text{m}$ and $10.0 \mu\text{m}$ to $12.0 \mu\text{m}$, the only atmospheric constituent which significantly absorbs and emits radiation is water vapor, the absorption resulting primarily from the far wings of the intense spectral absorption lines in the $6.3\text{-}\mu\text{m}$ absorption band and those in the rotational water band (which begins to absorb strongly beyond $15.0 \mu\text{m}$). Since the effects of only one atmospheric constituent need be observed and compensated for in order to obtain satisfactory estimates of sea temperature, it appears that only two spectral bands are required. Furthermore, since the physical process which causes the absorption and emission in both window regions is the same, with the effect near $9.0 \mu\text{m}$ simply a slight magnification of the effect near $11.0 \mu\text{m}$, a simultaneous measurement of the radiance in each window region should provide the necessary data to estimate the magnitude of water-vapor absorption and emission. The problem is to specify the two bands which will yield the optimum results.

For this application, each radiance spectrum may be represented by a two-dimensional vector, $L^k(e_1, e_2)$, where e_1 and e_2 are the average values of radiance in band 1 and band 2, respectively. The procedure is to represent all possible output vectors by a collection of vector subsets $L(T_1), L(T_2), \dots, L(T_m)$, where $L(T_m)$ is the set of all output vectors for a sea temperature equal to T_m . Since the space is two-dimensional, these subsets can be represented by hyperlines. A representation for m such subsets is shown schematically in Fig. 24. $A(T_1)$

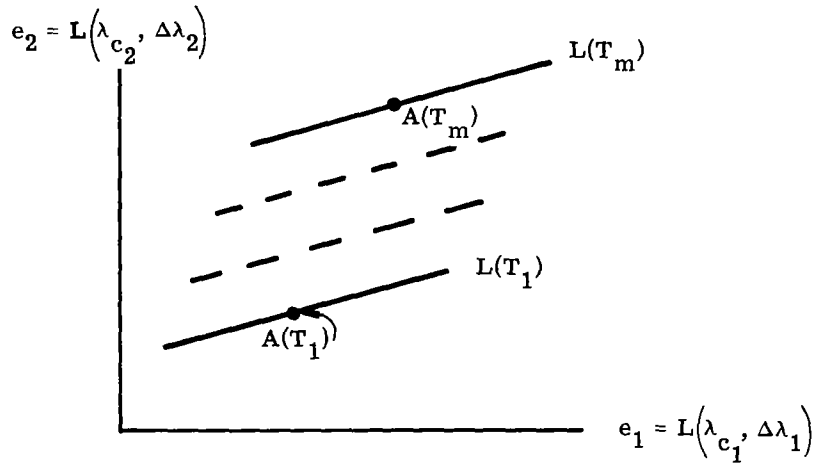


FIGURE 24. SCHEMATIC OF HYPERLINES FOR A TWO-DIMENSIONAL VECTOR REPRESENTATION OF OUTPUT SPECTRA

and $A(T_m)$ are the mean-value vectors for the subsets representing sea temperatures T_1 and T_m . The objective was to select the two spectral bands such that the subsets were accurately represented by nearly parallel, straight lines and the rms distance of the data points for a given temperature from its corresponding hyperline was a minimum value.

Recall that 75 spectra were calculated for clear atmosphere conditions (i.e., five model atmospheres, three zenith angles, and five sea temperatures). Within each of the two window regions, the average spectral radiance was calculated every $0.1 \mu\text{m}$ for spectral intervals 0.5, 1.0, and $1.5 \mu\text{m}$ wide. Using these data, five hyperlines were determined (one for each of the five sea temperatures) for each possible combination of two spectral bands. For many band pairs, nonlinearities were observed, and, in many cases, the scatter in the data points was extremely large. The band pair which gave the best results in regard to linearity and minimum scatter was: $\lambda_c = 9.1 \mu\text{m}$, $\Delta\lambda = 0.5 \mu\text{m}$; and $\lambda_c = 11.0 \mu\text{m}$, $\Delta\lambda = 1.0 \mu\text{m}$, where λ_c is the center wavelength of the band, and $\Delta\lambda$ is the spectral width of the spectral interval. A plot of the result is shown in Fig. 25. Since the lines are of approximately the same slope and are reasonably evenly spaced, further linearization by including hyperlines for more temperatures was unwarranted. The interpolation-extrapolation procedure to estimate the input sea temperature, given the values of average spectral radiance in each of the two spectral bands [i.e., the value of the vector $L(T)$], was based on these five hyperlines. From Section 5, the sea temperature giving rise to an output vector value of $L(T)$, which lies between the hyperline corresponding to sea temperatures T_1 and T_2 , is given by:

$$T_i = T_1 + (T_2 - T_1) \frac{d_1}{d_1 - d_2} \quad (59)$$

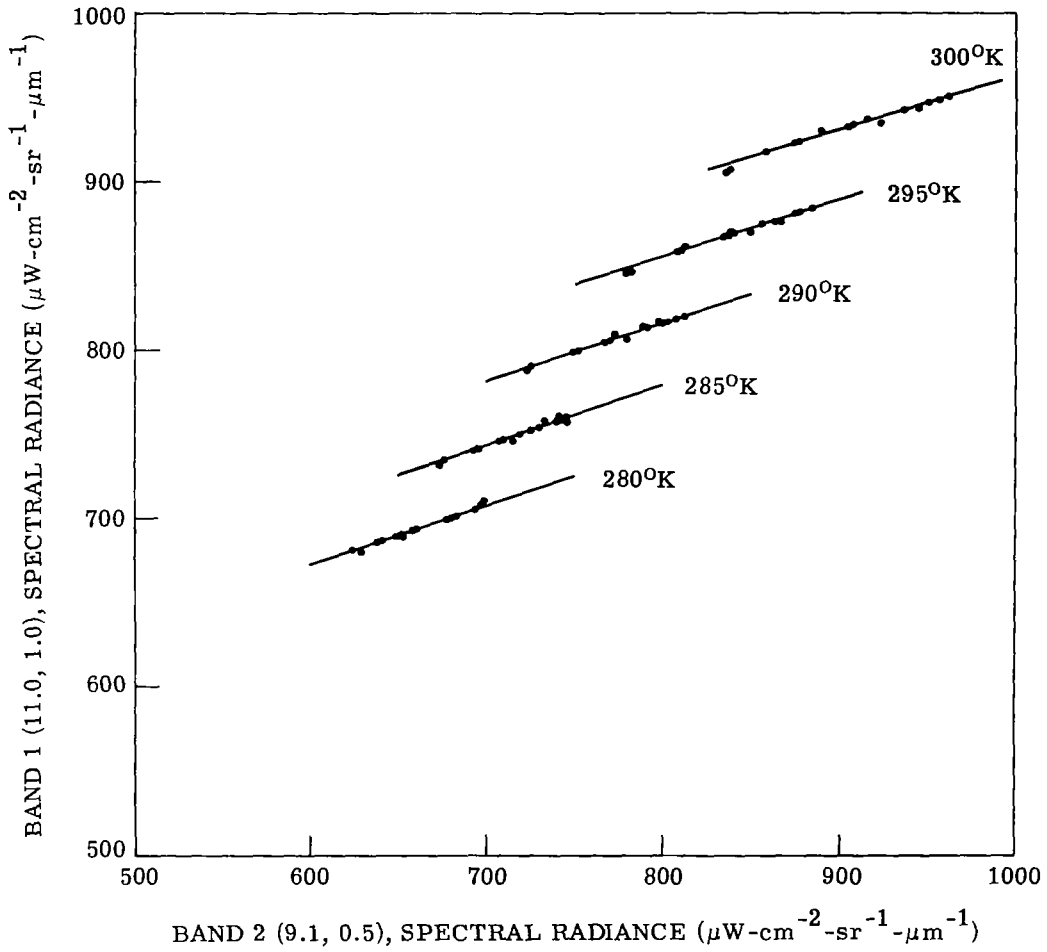


FIGURE 25. SPECTRAL RADIANCE IN BAND 1 VERSUS THAT IN BAND 2 AS A FUNCTION OF ATMOSPHERIC STATE. Parameters = zenith angle at target and sea-surface temperature.

where d_1 and d_2 are the respective distances from lines $L(T_1)$ and $L(T_2)$ and are given by:

$$d_1 = [L^k(T) - A(T_1)][v_\ell(T_1)]^t$$

and

(60)

$$d_2 = [L^k(T) - A(T_2)][v_\ell(T_2)]^t$$

where $v_\ell(T_1)$ and $v_\ell(T_2)$ are the vectors normal to the representative hyperlines.

To estimate the error in the estimate of sea temperature that would be realized using this procedure, for every value of input sea temperature, T_s , used to obtain the 75 clear-atmosphere

spectra, an estimated temperature, T_i , was calculated from Eq. (59). The rms error was then calculated by:

$$E = \sqrt{\frac{1}{75} \sum_{i=1}^{75} (T_i - T_s)^2}$$

For the selected band pair, this error was 0.15°K , and the maximum error for any T_i was only 0.23°K . This occurred when viewing the sea surface near the horizon through a moist atmosphere.

The physical interpretation of the result obtained is straightforward. Given the radiance in one spectral band and the sea temperature, the spectral radiance in the other band is accurately predictable. In essence, the amount of atmospheric absorption and emission can be predicted. Conversely, given the radiance in each of the two spectral bands for any arbitrary distribution of atmospheric water vapor and temperature, the sea temperature can be accurately estimated. The existence of a band pair showing linearly related radiance values is not surprising. Since the physical processes which cause the absorption and atmospheric emission is the same in both spectral regions with the effect in the $9.1\text{-}\mu\text{m}$ band simply a slight magnification of that near $11.0\ \mu\text{m}$, a high correlation between the radiance values was expected. The linearity results from the fact that the atmospheric absorption and emission in both spectral regions is small and well represented by linear functions.

6.2. ESTIMATION OF FRACTIONAL CLOUD COVER

The selection of the number of spectral bands and the spectral regions of greatest potential for estimating fractional cloud cover was based on the spectral differences between the emissivity of opaque water-drop clouds and the emissivity of the water surface. In Fig. 26, the spectral emittance at the nadir of a typical sea surface [8] is compared to the spectral emittance of a water-drop cloud [6]. The maximum difference between cloud and water-surface emittance occurs near $5.0\ \mu\text{m}$. According to these data, if the spectral radiance emitted from a cloud was simultaneously measured near $5.0\ \mu\text{m}$ and near $11.0\ \mu\text{m}$, and each measured value of radiance was converted into an equivalent blackbody temperature, the temperature derived from the $5.0\text{-}\mu\text{m}$ data would be significantly lower than that derived from the $11.0\text{-}\mu\text{m}$ data. If a similar experiment were performed for a water surface, the two derived temperatures would be approximately the same, since the emittance of water in these two spectral regions is approximately equal.

This result suggests that, in the absence of an intervening atmosphere, simultaneous radiometric measurements in only two spectral bands (i.e., near $5.0\ \mu\text{m}$ and $11.0\ \mu\text{m}$) would provide the necessary information to estimate accurately the fractional cloud cover. If the equivalent blackbody temperatures for the two spectral bands were equal, then the field of view would be

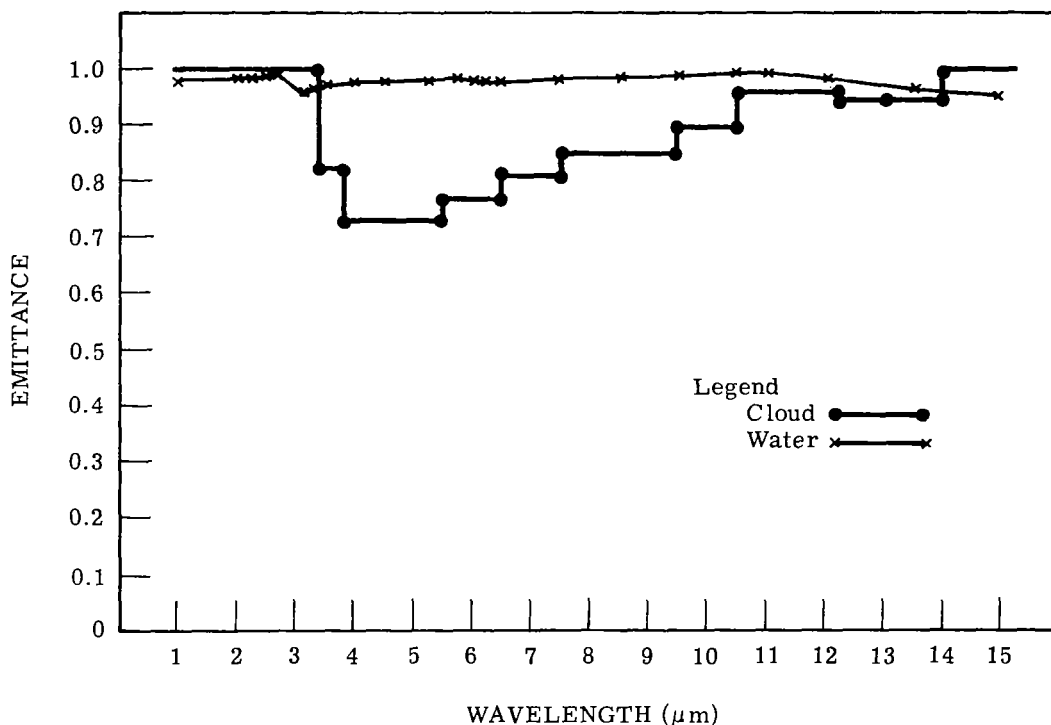


FIGURE 26. SPECTRAL EMITTANCE OF LIQUID WATER AND OPAQUE WATER-DROP CLOUD

assumed clear. If the equivalent blackbody temperatures were different, then clouds would be present, and the magnitude of the temperature difference would be a direct measure of the fractional cloud cover.

Unfortunately, because of the effects of the intervening atmosphere on the spectral radiance observed at space altitudes, a two-band system would be inadequate. Variations in the atmospheric meteorology would cause variations in the equivalent blackbody temperatures that would have no relevance to cloud cover. Therefore, a larger number of spectral bands are required.

In Section 6.1, it was demonstrated that by performing simultaneous radiometric measurements in two spectral bands, one in each of the two atmospheric windows, the effects of atmospheric water-vapor absorption and emission could be compensated for, and estimates of the true radiometric temperature of the sea surface could be obtained. It appears, therefore, that by performing radiometric measurements in a third spectral band, located in a spectral region where water vapor has the primary effect on the observed spectral radiance, that the effect of the atmosphere on the observed radiance near $5.0 \mu\text{m}$ and $11.0 \mu\text{m}$ could be compensated for and the relative effects of cloud and sea emittance on the observed radiance, as previously described, would be observable. The problem, therefore, is to determine the three spectral bands which would provide the best atmospheric compensation and, consequently, yield the best esti-

mate of fractional cloud cover. The approach used to select the three spectral bands was analogous to that used in selecting the two spectral bands for estimating the sea temperature for noncloudy atmospheres.

For this application, each output vector was denoted by $L^k(e_1, e_2, e_3)$, where e_1 , e_2 , and e_3 were the average values of spectral radiance in band 1, band 2, and band 3, respectively. As before, the procedure was to represent all possible output vectors by a collection of subsets $[L(C_1), L(C_2), \dots, L(C_m)]$, where $L(C_m)$ was the subset of all output vectors for a fractional cloud cover equal to C_m . The objective was to select three spectral bands such that the subsets were accurately represented by nearly parallel planes, and the rms distance of the data points from their corresponding hyperplane was a minimum.

The 1125 calculated radiance spectra (i.e., five model atmospheres, five sea temperatures, four cloud altitudes, and five values of fractional cloud cover) were subdivided into five sets of spectra, each set representing a given fraction of cloud cover (i.e., 0%, 10%, 50%, 90%, and 100%). For each set of spectra, the average spectral radiance was calculated every $0.1 \mu\text{m}$ for spectral intervals 0.5 , 1.0 , and $1.5 \mu\text{m}$ wide throughout the respective spectral regions: 4.4 to $6.0 \mu\text{m}$, 7.0 to $9.5 \mu\text{m}$, and 10.0 to $12.0 \mu\text{m}$. For each possible combination of three spectral bands, the covariance matrix was evaluated for each value of fractional cloud cover, and for each covariance matrix the associated eigenvectors and eigenvalues were determined. The three spectral bands which gave the best results according to the previously stated selection criteria (i.e., nearly parallel hyperplanes and a minimum value of the average rms distance of the data points from their corresponding hyperplane) was: $\lambda_c = 4.9 \mu\text{m}$, $\Delta\lambda = 0.5 \mu\text{m}$; $\lambda_c = 9.1 \mu\text{m}$, $\Delta\lambda = 0.5 \mu\text{m}$; and $\lambda_c = 11.0 \mu\text{m}$, $\Delta\lambda = 1.0 \mu\text{m}$.

A schematic representation of the planes for 0% and 100% cloud cover is given in Fig. 27. For each percent cloud cover, the mean values, eigenvalues, and rms distance of the 4 points (expressed in units of percent cloud cover) from their corresponding hyperplane are given in Table 1a. The eigenvalues are a direct measure of the nature of the distribution of data points for a given fractional cloud cover. For example, for each set of data points corresponding to a given fractional cloud cover, one eigenvalue is orders of magnitude less than the other two eigenvalues. This demonstrates the planer nature of the distribution. Note that the least eigenvalue is approximately the same for each data set and is approximately 6% of the least eigenvalue for the distribution of data points for all fractions of cloud cover. This is comparable to the rms distance of the data points from their corresponding hyperplane, as expected, and may be thought of as a measure of the geometrical thickness of a given plane relative to the thickness of the distribution for all data points. From Table 1b, note that the eigenvectors corresponding to the least eigenvalues (the vectors normal to the planes) are approximately the same for each of the five planes and are, therefore, approximately parallel. Also, since the distance between

TABLE 1(a). DESCRIPTION OF THE DATA POINT DISTRIBUTION FOR EACH HYPERPLANE

Fraction Cloud Cover (%)	$L(\lambda_c, \Delta\lambda)$ ($\mu W \cdot cm^{-2} \cdot sr^{-1} \cdot \mu m^{-1}$)			Eigenvalues			rms Distance from Plane (% Cloud Cover)
	$\lambda_c = 4.9;$	9.1;	11.0	δ_1	δ_2	δ_3	
0	135.8	779.9	806.1	3.1	246.9	16414	6.1
10	130.6	758.1	789.9	2.9	198.9	14214	5.9
50	109.6	671.0	725.4	2.5	109.1	18885	5.7
90	89.3	584.0	660.8	3.0	83.7	45227	6.9
100	84.1	562.2	644.7	3.9	85.7	55198	7.6
0, 10, 50, 90, 100	109.9	671.0	725.4	50.8	274.1	42301	

TABLE 1(b). EIGENVECTORS CORRESPONDING TO LEAST EIGENVALUE (VECTOR NORMAL TO HYPERPLANE)

Fractional Cloud Cover (%)	Eigenvector Normal to Plane		
	e_1	e_2	e_3
0	0.601	-0.625	0.499
10	0.593	-0.628	0.503
50	0.570	-0.642	0.513
90	0.550	-0.651	0.524
100	0.558	-0.648	0.519

planes is a nearly linear function of fractional cloud cover, these hyperplanes are sufficient to define a linear interpolation procedure.

From Section 5, the fractional cloud cover giving rise to an output vector, $L(C_i)$, which lies between the hyperplanes corresponding to a fractional cloud cover of C_1 and C_2 respectively, is given by:

$$C_i = C_1 + (C_2 - C_1) \frac{d_1}{d_1 - d_2} \quad (61)$$

where d_1 and d_2 are the respective distances from plane $L(C_1)$ and $L(C_2)$ and are given by:

$$d_1 = [L^k(C_i) - A(C_1)][v_\ell(C_1)]^t$$

and

$$d_2 = [L^k(C_i) - A(C_2)][v_\ell(C_2)]^t \quad (62)$$

where $v_\ell(C_1)$ and $v_\ell(C_2)$ are the vectors normal to the respective hyperplanes.

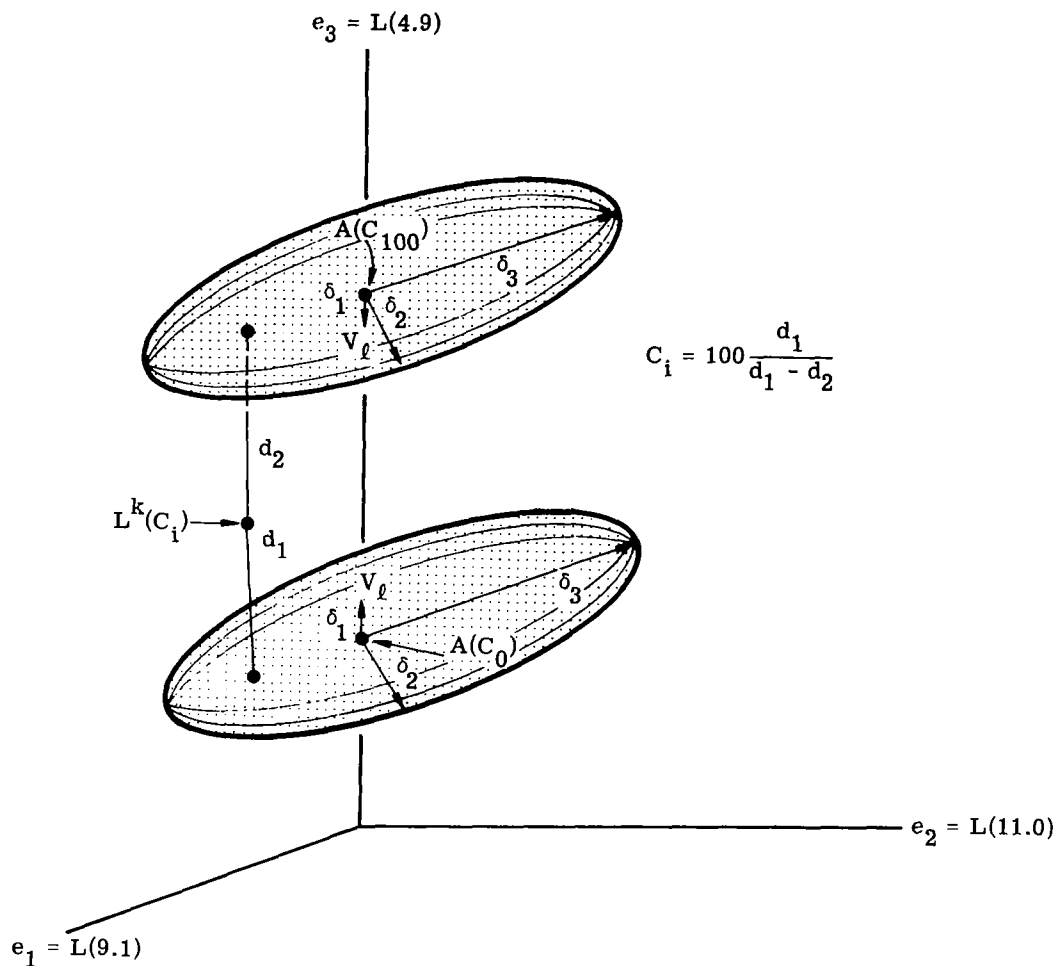


FIGURE 27. SCHEMATIC REPRESENTATION OF HYPERPLANES FOR FRACTIONAL CLOUD COVER DETERMINATION

It may appear surprising that the distribution of all output data points can be represented by a series of nearly parallel planes, each plane corresponding to a given fraction of cloud cover; however, the result is not unexpected after consideration of the relative effects on the three band-radiance values of atmospheric temperature, atmospheric water vapor, sea temperature, cloud temperature, and cloud and sea-surface emittance. Consider a given output vector, L , which corresponds to a given set of input conditions, with the output vector being represented, as before, by the average radiance in each of the respective three spectral bands. Now consider the directional change in the output vector with respect to a change in each of the respective input conditions. In other words, consider the direction of the following gradients:

$$\frac{\partial L}{\partial T^A}, \frac{\partial L}{\partial H_2O}, \frac{\partial L}{\partial T_s}, \frac{\partial L}{\partial C_f}, \frac{\partial L}{\partial C_A}, \frac{\partial L}{\partial T_c}$$

where T^A = atmospheric temperature distribution

H_2O = atmospheric water vapor distribution

T_s = sea temperature

C_f = fractional cloud cover

C_A = cloud altitude

T_c = cloud temperature

From the results of the present study, the following conditions were observed:

$$\frac{\partial L}{\partial T^A} \cong \frac{\partial L}{\partial H_2O} \cong \frac{\partial L}{\partial C_A} \quad (63)$$

and

$$\frac{\partial L}{\partial T_s} \cong \frac{\partial L}{\partial T_c} \quad (64)$$

Equation (63) represents the directional change in the vector L with respect to a change in the atmospheric temperature distribution and is approximately equal to the directional change in the vector L with respect to a change in either the atmospheric water-vapor distribution or the altitude of the cloud. The magnitude of the change may be different in each case; however, the direction of the three gradients are approximately equal. Therefore, these points lie nearly on a line in three-dimensional space. From Eq. (64), the directional change in the vector L with respect to a change in sea temperature is approximately equal to a change in the vector L with respect to a change in the cloud temperature. The direction of these two gradients is, however, different than the gradients given in Eq. (63). Therefore, since all linear combinations of any two vectors define a plane, all output vectors, for a fixed value of fractional cloud cover and cloud spectral emittance, will lie very nearly on a plane in three-dimensional space.

The result that the total collection of output vectors can be represented by a series of nearly parallel, equally spaced planes comes about because (1) the directionally of all gradients remains nearly constant for all operating points (i.e., any given set of input conditions), (2) the directional change in the vector L , with respect to a change in fractional cloud cover, $\frac{\partial L}{\partial C_f}$, does not lie within the previously defined plane, and (3) the magnitude of the gradient, $\frac{\partial L}{\partial C_f}$, is approximately constant for all values of fractional cloud cover.

To obtain some measure of the error that would be realized using the above procedure to estimate fractional cloud cover, the average spectral radiance was calculated for each of the

1125 radiance spectra in each of the defined spectral bands, and an estimate of the fractional cloud cover was calculated from Eq. (61). For each known value of input cloud cover (i.e., 0, 0.10, 0.50, 0.90, and 1.0), the average value of the estimated cloud cover and the standard deviation in the difference between input and estimated cloud cover was calculated. The results are shown in Fig. 28. The dotted line represents zero error in estimated cloud cover. Note that the average value of the estimated cloud cover is nearly equal to the input value with a maximum deviation of 4.5% which occurs at 50% cloud cover. The standard deviation in the estimated fractional cloud cover, for all values of fractional cloud cover, is nearly constant and equal to approximately 6%. Note that the use of the interpolation procedure yields values of estimated fractional cloud cover that are greater than 100% and less than zero. This is a valid and meaningful result. Recall that all output vectors for zero and 100% cloud cover are represented by respective planes which were obtained by making a best fit to the respective collections of output vectors. Therefore, some of the vectors for each case will lie above and below its corresponding plane. Consequently, an output vector corresponding to an input value of fractional cloud cover of either zero or 100% could yield fractional cloud cover estimates greater than one or less than zero. Designing the interpolation procedure in this manner allows the frac-

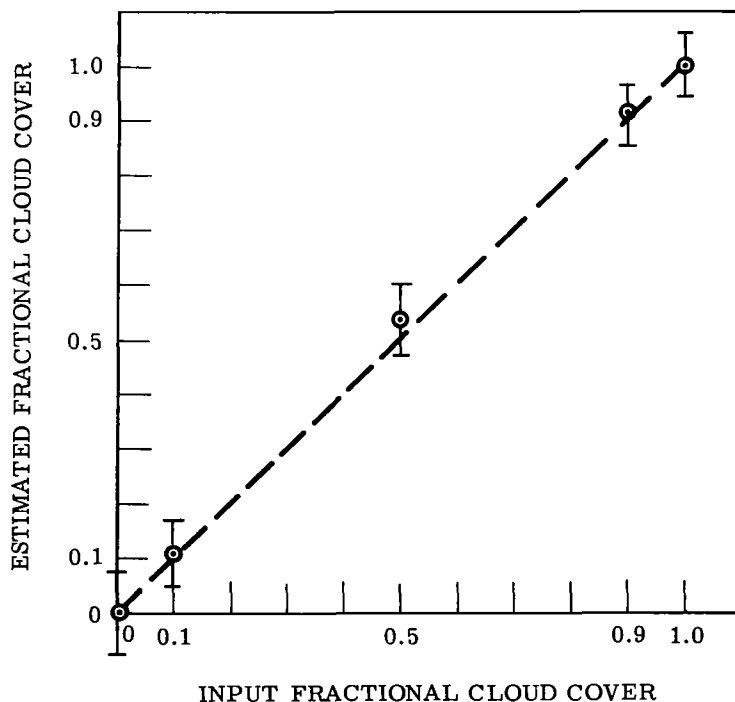


FIGURE 28. ERROR IN ESTIMATE OF FRACTIONAL CLOUD COVER

tional cloud-cover threshold, for deciding whether a field of view is cloud free, to be set at a lower value.

Let us now consider the effect of a defined fractional cloud-cover threshold on the ability of the three-band system to estimate accurately the sea temperature. Suppose the threshold is set at 10% cloud cover. According to the results shown in Fig. 28, approximately 15% cloud cover could exist and the estimated value of fractional cloud cover could be less than 10%. If these clouds were at high altitude, the estimate of the sea temperature, obtained from the 9.1- and 11.0- μm spectral bands, could be 4°K or 5°K different than the actual sea temperature. If the threshold is set at a lower value to reduce this error, then some fields of view which are actually noncloudy, would be deemed cloudy.

The results are not, however, as inadequate as they may appear if analyzed in conjunction with field-of-view size and cloud distribution. For example, if the field of view defined a ground resolution of a few feet, then the fractional cloud cover would be, in general, either zero or 100%, and the three-band system would perform very well. However, if the ground resolution was in the range of 100 miles, the fractional cover could be any value from zero to 100%, and the system would perform exactly as indicated in Fig. 28.

Proposed satellite systems will have a ground resolution of approximately 1-2 km. For fields of view of this size, only small cellular clouds would give rise to partial cloud cover. Cellular clouds have average effective diameters of approximately 0.2 to 0.4 km, and the average distance between such clouds is approximately equal to the average diameter. Therefore, if cellular clouds existed within the field of view, the average value of fractional cloud cover would be approximately 30% at the nadir, and approximately 50% at 60° from the nadir. This suggests that if a threshold value of 10% were not exceeded, then it could be assumed, fairly conclusively, that the field of view is clear and the temperature estimate obtained from the 9.1- and 11.0- μm spectral bands would be that of the sea surface.

There is one further aspect of the study that requires comment. Since the spectral emittance of clouds was assumed fixed, the effect of a variable spectral emittance on the ability of the defined three-band system to estimate fractional cloud cover is not known. It is well known that various cloud types have different water-droplet size distributions, which will give rise to differences in their spectral emittance. Yet to be determined is the directional change in the vector L with respect to a change in the spectral emittance of the cloud. It is felt that the direction of this gradient will be approximately equal to the direction of $\frac{\partial L}{\partial C_f}$. If this is true, then a certain cloud type of, say 50% fractional cover, may yield the same result as a different cloud type of, say 40 or 45% fractional cover. Indeed, such answers are necessary and are presently being pursued.

6.3. DETECTION OF SEMITRANSSPARENT CLOUDS

Thus far, the ability of the three-band system to detect only the presence of opaque water-drop clouds within the field of view has been discussed. To demonstrate its ability to indicate the presence of semitransparent clouds within the field of view, the following analysis was performed.

Recall from Section 4 that values of spectral radiance were calculated for a 30°N atmosphere and a zenith angle of 0° for semitransparent clouds of three thicknesses (20, 50, and 100 meters) at each of four altitudes (0, 2.0, 5.0, and 12.0 km) for each of five sea temperatures (see Fig. 17). These data were integrated over each of the three spectral bands (i.e., 4.9, 9.1, and $11.0\ \mu\text{m}$) and values of average spectral radiance in each band were obtained. Since an estimate of fractional cloud cover, as applied to a semitransparent cloud, has little meaning, these data were processed in a slightly different manner than those for opaque clouds.

With the procedures described in Section 6.1, a temperature estimating algorithm was developed for the 4.9-, 9.1- μm band pair. This algorithm was identical, in principle, to that for the 9.1-, 11- μm band pair. The difference lies in the mathematical description of the hyperlines for each of the five sea temperatures. The result for the 4.9-, 9.1- μm band pair is shown in Fig. 29. Note that the spread in the data points from their corresponding hyperlines is much larger for the 4.9-, 9.1- μm band pair than for the 9.1-, 11- μm band pair (see Fig. 25). This occurs because the magnitude of the atmospheric absorption and emission near $4.9\ \mu\text{m}$ is not highly correlated with the magnitude of the absorption and emission near $9.1\ \mu\text{m}$, particularly when viewing the sea surface through moist, warm atmospheres at large zenith angles. If the 4.9-, 9.1- μm band pair were used to estimate the sea temperature, the rms error in the estimate would be 1.36°K as compared to 0.15°K for the 9.1-, 11.0- μm band pair.

With each of the two band pairs, two values of effective radiometric temperature were determined for each of the semitransparent cloud radiance spectra. The results are given in Table 2 where T_1 denotes the temperature estimated by the 4.9-, 9.1- μm band pair, T_2 denotes the temperature estimated by the 9.1-, 11.0- μm band pair, and ΔT denotes the difference between T_1 and T_2 . Since the results shown are for only a 0° zenith angle, the average value of ΔT for clear atmospheres at 0° zenith angle was calculated for comparative purposes. This value was 0.21°K . Note that as the cloud thickness increases, the temperature difference increases from approximately 2°K for a 20-m cloud, to greater than 9°K for a 100-m cloud. It appears, therefore, that the three-band system will conclusively indicate the presence of semitransparent clouds, even if they are very thin and occur at very low altitudes, simply by noting the difference in temperature recorded by the two band pairs. If the temperature difference is on the order of 0.21°K , the field of view could be assumed cloud free, and the temperature estimated by the 9.1-, 11.0- μm band pair could be assumed the true radiometric temperature of

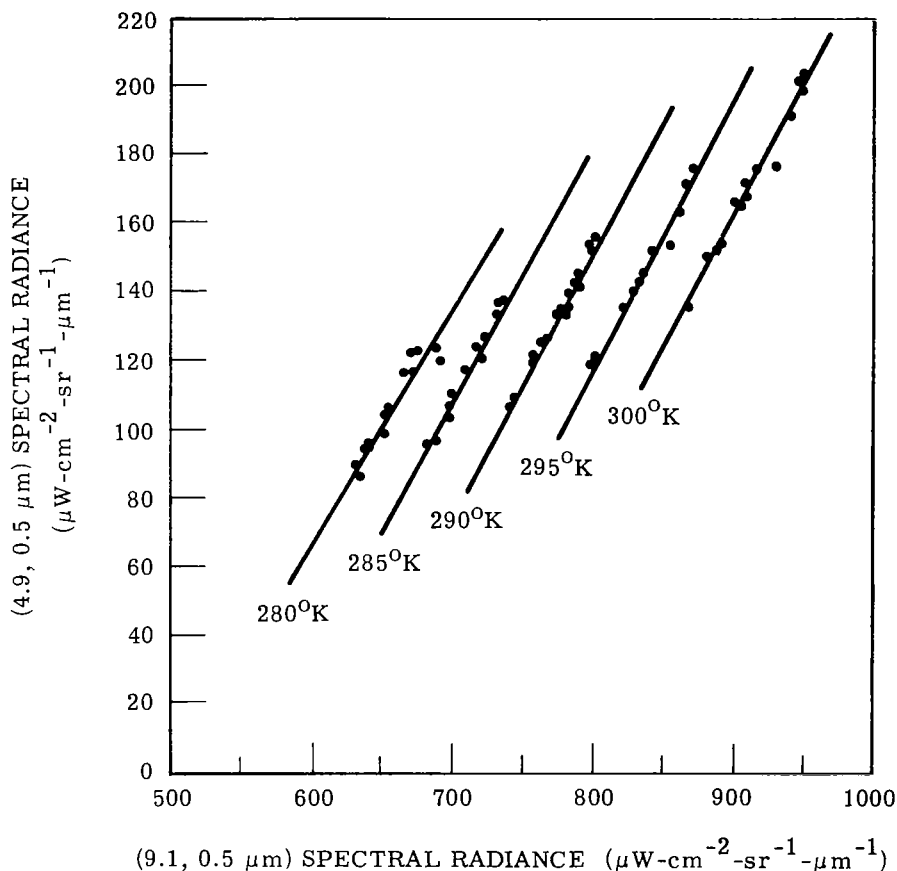


FIGURE 29. SPECTRAL RADIANCE IN BAND 1 VERSUS THAT IN BAND 2 AS A FUNCTION OF ATMOSPHERIC STATE. Parameters = zenith angle and sea temperature.

the sea. If the temperature difference were significantly larger than 0.21°K , say greater than 0.50°K , the field of view could be assumed contaminated by clouds and the data points so assigned.

It is interesting to note the magnitude of the error caused by semitransparent clouds in the estimate of the sea temperature that could be realized if only a two-band system were used, namely, the 9.1-, 11.0- μm band pair. For example, a 20-m cloud at 2 km would reduce the observed radiometric temperature of the sea from its actual value of 300°K to 295.39°K , a degradation of over 4.5°K .

6.4. CRITIQUE OF THREE-BAND SYSTEM

The present investigation has shown that the effects of the atmosphere on the spectral radiance emanating from the sea surface can be significant and must be compensated for if accurate estimates of sea temperature are to be obtained. It has been demonstrated that if the at-

TABLE 2. COMPARISON BETWEEN THE TEMPERATURE ESTIMATED BY THE 4.9-, 9.1- μm BAND PAIR AND THE TEMPERATURE ESTIMATED BY THE 9.1-, 11.0- μm BAND PAIR AS A FUNCTION OF CLOUD THICKNESS, CLOUD ALTITUDE, AND SEA TEMPERATURE

Cloud Thickness (km)	Cloud Altitude (km)	Sea-Surface Temperature ($^{\circ}\text{K}$)	T_1	T_2	ΔT
0.02	0.0	280	278.94	281.11	2.17
		285	282.89	285.13	2.24
		290	286.92	289.16	2.24
		295	291.00	293.21	2.21
		300	295.16	297.32	2.16
	2.0	280	276.82	278.97	2.15
		285	280.78	282.99	2.21
		290	284.79	287.09	2.30
		295	288.88	291.22	2.36
		300	293.04	295.39	2.35
	6.0	280	273.12	275.30	2.18
		285	277.08	279.32	2.24
		290	281.11	283.50	2.39
		295	285.24	287.73	2.49
		300	289.42	291.99	2.57
	12.0	280	269.65	271.96	2.31
		285	273.67	275.99	2.32
		290	277.77	280.17	2.40
		295	281.93	284.51	2.58
		300	286.19	288.86	2.67
0.05	0.0	280	278.76	282.64	3.88
		285	281.52	285.59	4.07
		290	284.35	288.57	4.22
		295	287.20	291.60	4.40
		300	290.12	294.69	4.57
	2.0	280	273.83	277.87	4.04
		285	276.59	280.84	4.25
		290	279.38	283.93	4.55
		295	282.25	287.06	4.81
		300	285.16	290.25	5.09
	6.0	280	265.12	269.69	4.58
		285	267.91	272.68	4.77
		290	270.74	275.77	5.03
		295	273.62	278.97	5.35
		300	276.54	282.30	5.76
	12.0	280	256.47	262.25	5.78
		285	259.39	265.23	5.84
		290	262.34	268.34	6.00
		295	265.32	271.55	6.23
		300	268.33	274.89	6.56
0.10	0.0	280	281.02	284.19	3.17
		285	282.39	285.92	3.53
		290	283.81	287.70	3.89
		295	285.27	289.55	4.28
		300	286.76	291.40	4.64
	2.0	280	272.46	276.35	3.89
		285	273.85	278.13	4.28
		290	275.28	279.97	4.69
		295	276.76	281.89	5.13
		300	278.27	283.87	5.60
	6.0	280	257.34	263.04	5.70
		285	258.81	264.82	6.01
		290	260.32	266.68	6.36
		295	261.89	268.61	6.72
		300	263.47	270.60	7.13
	12.0	280	241.56	250.94	9.38
		285	243.20	252.73	9.53
		290	244.87	254.62	9.75
		295	246.59	256.56	9.97
		300	248.32	258.57	10.25

mosphere is cloud free, these atmospheric effects can be compensated for almost completely for any atmospheric state and any zenith observation angle by performing simultaneous radiometric measurements in two spectral bands [(9.1, 0.5 μm), (11.0, 1.0 μm)]. The validity of this conclusion was established by demonstrating consistent agreement between calculated values of spectral radiance for clear atmospheres (upon which the study was based) and values of spectral radiance measured by Nimbus III for known atmospheric conditions.

For atmospheres which contain clouds, it has been shown that by including a third spectral band, (4.9, 0.5 μm), the presence of opaque or semitransparent water-drop clouds within the field of view can be determined. The precision with which this determination can be made depends upon the field-of-view size relative to cellular cloud distribution which has not been thoroughly investigated. Further, the cloud-emittance data used in the analysis were based on application of Mie scattering theory to liquid-water spheres. These data have not been thoroughly verified; however, it appears that they correctly represent the relative distribution of emittance as a function of wavelength, but may be in error in their absolute value. Since the selection of the three-band system is primarily dependent on relative values of spectral-cloud emittance, it is felt that a realistic possibility of detecting the presence of clouds in the field of view using a three-band system has been demonstrated. The spectral bands chosen should not, however, be considered optimum until further analysis of the radiative characteristics of clouds are performed. Cloud research, which should provide a useful input to such an investigation, is currently being performed in this laboratory.

Appendix I
SOLUTION OF THE EQUATION OF TRANSFER FOR HOMOGENEOUS CLOUDS

Definition of symbols:

- L = spectral radiance in $\mu\text{W}\cdot\text{cm}^{-2}\cdot\text{sr}^{-1}\cdot\mu\text{m}^{-1}$
 τ = optical depth
 μ = cosine of the angle with the normal to the cloud surface
 φ = cosine of the azimuthal angle
 ω_0 = single-scattering albedo
 p = single-scattering phase function
 $B(\tau)$ = Planck's function at optical depth τ
 E = spectral irradiance in $\mu\text{W}\cdot\text{cm}^{-2}\cdot\mu\text{m}^{-1}$

If expressions can be found which are a first approximation to the radiances caused by the internal source and the external source, then they can be substituted into the integral equations given in the text and expressions which are a higher order approximation to the radiances can be obtained.

Consider the radiative transfer equation

$$\mu \frac{dL}{d\tau} = L(\tau, \mu, \varphi) - \frac{\omega_0}{4\pi} \int_0^1 \int_{-1}^1 p(\mu, \varphi, \mu', \varphi') L(\tau, \mu', \varphi') d\mu' d\varphi' - (1 - \omega_0) B(\tau) \quad (65)$$

where $B(\tau) = 0$ if $L(\tau, \mu, \varphi)$ is considered to be only the external source radiance. Equation (65) will be solved in general and then two separate cases will be considered where $L(\tau, \mu, \varphi)$ is equal to the externally and internally generated radiance respectively. Multiplying Eq. (65) by $d\mu d\varphi$ and integrating from 0 to 1, 0 to 2π ; then from -1 to 0, 0 to 2π ; we obtain, respectively

$$\begin{aligned} \frac{d}{d\tau} \int_0^1 \int_0^{2\pi} \mu L(\tau, \mu, \varphi) d\mu d\varphi &= \int_0^1 \int_0^{2\pi} L(\tau, \mu, \varphi) d\mu d\varphi + \\ &- \frac{\omega_0}{4\pi} \int_0^1 \int_0^{2\pi} \int_0^1 \int_{-1}^1 p(\mu, \varphi, \mu', \varphi') L(\tau, \mu', \varphi') d\mu' d\varphi' d\mu d\varphi \\ &- (1 - \omega_0) B_0 \int_0^1 \int_0^{2\pi} d\mu d\varphi \end{aligned} \quad (66)$$

and

$$\frac{d}{d\tau} \int_0^1 \int_{-1}^0 \mu L(\tau, \mu, \varphi) d\mu d\varphi = \int_0^1 \int_{-1}^0 L(\tau, \mu, \varphi) d\mu d\varphi +$$

$$\begin{aligned}
& - \frac{\omega_o}{4\pi} \int_0^{2\pi} \int_{-1}^0 \int_0^{2\pi} \int_{-1}^1 p(\mu, \varphi, \mu', \varphi') L(\tau, \mu', \varphi') d\mu' d\varphi' d\mu d\varphi \\
& - (1 - \omega_o) B_o \int_0^{2\pi} \int_{-1}^0 d\mu d\varphi
\end{aligned} \tag{67}$$

where it is assumed that the Planck function $B(\tau)$ is a constant function of optical depth and equal to B_o .

We define

$$L_+(\tau) = \int_0^{2\pi} \int_0^1 L(\tau, \mu, \varphi) d\mu d\varphi \tag{68}$$

$$L_-(\tau) = \int_0^{2\pi} \int_{-1}^0 L(\tau, \mu, \varphi) d\mu d\varphi \tag{69}$$

where (+) denotes upwelling radiation and (-) denotes downwelling radiation. The upward and downward irradiances are, respectively,

$$E_+(\tau) = \int_0^{2\pi} \int_0^1 \mu L(\tau, \mu, \varphi) d\mu d\varphi \tag{70}$$

$$E_-(\tau) = - \int_0^{2\pi} \int_{-1}^0 \mu L(\tau, \mu, \varphi) d\mu d\varphi \tag{71}$$

in which all quantities are always positive.

Defining the parameter η as the fraction of the radiation which is scattered into the upward hemisphere, we have

$$\eta = \frac{1}{4\pi} \int_0^{2\pi} \int_0^1 p(\mu, \varphi, \mu', \varphi') d\mu d\varphi \tag{72}$$

$$1 - \eta = \frac{1}{4\pi} \int_0^{2\pi} \int_0^1 p(\mu, \varphi, -\mu', \varphi') d\mu d\varphi \tag{73}$$

Therefore, Eqs. (66) and (67) become

$$\begin{aligned}
\frac{dE_+(\tau)}{d\tau} &= L_+(\tau) - \eta \omega_o \int_0^{2\pi} \int_0^1 L(\tau, \mu', \varphi') d\mu' d\varphi' \\
& - (1 - \eta) \omega_o \int_0^{2\pi} \int_0^1 L(\tau, -\mu', \varphi') d\mu' d\varphi' - 2\pi(1 - \omega_o) B_o
\end{aligned} \tag{74}$$

$$\begin{aligned} \frac{dE_{-}(\tau)}{d\tau} &= L_{-}(\tau) - (1 - \eta)\omega_0 \int_0^{2\pi} \int_0^1 L(\tau, \mu', \varphi') d\mu' d\varphi' \\ &\quad - \eta\omega_0 \int_0^{2\pi} \int_0^1 L(\tau, -\mu', \varphi') d\mu' d\varphi' - 2\pi(1 - \omega_0)B_0 \end{aligned} \quad (75)$$

or

$$\frac{dE_{+}(\tau)}{d\tau} = (1 - \eta\omega_0)L_{+}(\tau) - (1 - \eta)\omega_0 L_{-}(\tau) - 2\pi(1 - \omega_0)B_0 \quad (76)$$

$$\frac{dE_{-}(\tau)}{d\tau} = (1 - \eta\omega_0)L_{-}(\tau) - (1 - \eta)\omega_0 L_{+}(\tau) - 2\pi(1 - \omega_0)B_0 \quad (77)$$

Since there are no collimated sources of radiation, the radiation field is almost isotropic. Thus,

$$L_{+}(\tau) = \int_0^{2\pi} \int_0^1 L(\tau, \mu, \varphi) d\mu d\varphi \cong 2\pi L^u(\tau) \quad (78)$$

$$L_{-}(\tau) = \int_0^{2\pi} \int_{-1}^0 L(\tau, \mu, \varphi) d\mu d\varphi \cong 2\pi L^d(\tau) \quad (79)$$

where $L^u(\tau)$ and $L^d(\tau)$ are the upwelling and downwelling radiances, respectively, and are constant for all μ and φ , and

$$E_{+}(\tau) = \int_0^{2\pi} \int_0^1 \mu L(\tau, \mu, \varphi) d\mu d\varphi \cong \pi L^u(\tau) \quad (80)$$

$$E_{-}(\tau) = - \int_0^{2\pi} \int_{-1}^0 \mu L(\tau, \mu, \varphi) d\mu d\varphi \cong \pi L^d(\tau) \quad (81)$$

and therefore

$$L_{\pm}(\tau) \cong 2E_{\pm}(\tau) \quad (82)$$

Expression (82) is called the Schuster-Schwarzschild approximation.

Hence, the differential equations become

$$\frac{d[E_{+}(\tau) - E_{-}(\tau)]}{d\tau} = 2(1 - \omega_0)[E_{+}(\tau) + E_{-}(\tau)] - 4\pi(1 - \omega_0)B_0 \quad (83)$$

$$\frac{d[E_{+}(\tau) + E_{-}(\tau)]}{d\tau} = 2[1 + \omega_0(1 - 2\eta)][E_{+}(\tau) - E_{-}(\tau)] \quad (84)$$

or

$$\frac{dF_-(\tau)}{d\tau} = 2(1 - \omega_0)F_+(\tau) - 4\pi(1 - \omega_0)B_0 \quad (85)$$

$$\frac{dF_+(\tau)}{d\tau} = 2[1 + \omega_0(1 - 2\eta)]F_-(\tau) \quad (86)$$

where

$$F_+(\tau) = E_+(\tau) + E_-(\tau); \quad F_-(\tau) = E_+(\tau) - E_-(\tau) \quad (87)$$

Differentiating Eq. (87) and substituting Eq. (86) into the result gives

$$\frac{d^2F_+(\tau)}{d\tau^2} = 2[1 + \omega_0(1 - 2\eta)][2(1 - \omega_0)F_+(\tau) - 4\pi(1 - \omega_0)B_0] = k^2F_+(\tau) - 2\pi k^2B_0 \quad (88)$$

where

$$k = 2\sqrt{(1 - \omega_0)[1 + \omega_0(1 - 2\eta)]} \quad (89)$$

The solution of Eq. (88) is then simply

$$F_+(\tau) = c_1 e^{k\tau} + c_2 e^{-k\tau} + 2\pi B_0 \quad (90)$$

Substituting Eq. (90) into Eq. (86) gives

$$F_-(\tau) = \frac{2(1 - \omega_0)}{k^2} \frac{dF_+(\tau)}{d\tau} = \frac{2(1 - \omega_0)}{k} (c_1 e^{k\tau} - c_2 e^{-k\tau}) \quad (91)$$

From Eq. (87)

$$E_+(\tau) = \left[1 + \frac{2(1 - \omega_0)}{k}\right] \frac{c_1}{2} e^{k\tau} + \left[1 - \frac{2(1 - \omega_0)}{k}\right] \frac{c_2}{2} e^{-k\tau} + \pi B_0 \quad (92)$$

and

$$E_-(\tau) = \left[1 - \frac{2(1 - \omega_0)}{k}\right] \frac{c_1}{2} e^{k\tau} + \left[1 + \frac{2(1 - \omega_0)}{k}\right] \frac{c_2}{2} e^{-k\tau} + \pi B_0 \quad (93)$$

where c_1 and c_2 are constants determined by the boundary conditions:

$$E_-(0) = 0 \quad (94)$$

and

$$E_+(\tau_0) = \int_0^{2\pi} \int_0^1 \mu F(\mu, \varphi) d\mu d\varphi = \pi F_0 \quad (95)$$

where $F(\mu, \varphi)$ is the external source radiance and F_0 is a constant defined by the form of $F(\mu, \varphi)$. Defining

$$\Lambda_{\pm} = 1 \pm \frac{2(1 - \omega_0)}{k} \quad (96)$$

and with the boundary conditions (94) and (95), we obtain

$$\Lambda_+ c_1 e^{k\tau_0} + \Lambda_- c_2 e^{-k\tau_0} = 2\pi(F_0 - B_0) \quad (97)$$

and

$$\Lambda_- c_1 + \Lambda_+ c_2 = -2\pi B_0 \quad (98)$$

Thus, one can easily see that the constants c_1 and c_2 are

$$c_1 = \frac{2\pi \left[\Lambda_+(F_0 - B_0) + \Lambda_- B_0 e^{-k\tau_0} \right]}{\Delta} \quad (99)$$

$$c_2 = \frac{-2\pi \left[\Lambda_-(F_0 - B_0) + \Lambda_+ B_0 e^{k\tau_0} \right]}{\Delta} \quad (100)$$

where

$$\Delta = \Lambda_+^2 e^{k\tau_0} - \Lambda_-^2 e^{-k\tau_0} \quad (101)$$

Therefore, the general solution for the irradiances in the upward and downward directions is

$$E_+(\tau) = \frac{\pi}{\Delta} \left\{ \Lambda_+ \left[\Lambda_+(F_0 - B_0) + \Lambda_- B_0 e^{-k\tau_0} \right] e^{k\tau} - \Lambda_- \left[\Lambda_-(F_0 - B_0) + \Lambda_+ B_0 e^{k\tau_0} \right] e^{-k\tau} \right\} + \pi B_0 \quad (102)$$

$$E_-(\tau) = \frac{\pi}{\Delta} \left\{ \Lambda_- \left[\Lambda_+(F_0 - B_0) + \Lambda_- B_0 e^{-k\tau_0} \right] e^{k\tau} - \Lambda_+ \left[\Lambda_-(F_0 - B_0) + \Lambda_+ B_0 e^{k\tau_0} \right] e^{-k\tau} \right\} + \pi B_0 \quad (103)$$

and for $\tau = 0$ and $\tau = \tau_0$ respectively, we have

$$E_+(0) = \frac{\pi}{\Delta} \left\{ \left(\Lambda_+^2 - \Lambda_-^2 \right) (F_0 - B_0) + \Lambda_+ \Lambda_- B_0 \left(e^{-k\tau_0} - e^{k\tau_0} \right) \right\} + \pi B_0 \quad (104)$$

$$E_-(\tau_0) = \frac{\pi}{\Delta} \left\{ \left(\Lambda_-^2 - \Lambda_+^2 \right) B_0 + \Lambda_+ \Lambda_- (F_0 - B_0) \left(e^{k\tau_0} - e^{-k\tau_0} \right) \right\} + \pi B_0 \quad (105)$$

providing that $\omega_0 \neq 1$.

It is interesting to consider the special case of a semi-infinitely thick cloud (i.e., let $\tau_0 \rightarrow \infty$). For this case,

$$\Delta \rightarrow \Lambda_+^2 e^{k\tau_0} \quad (106)$$

and, therefore,

$$E_+(\tau) = \pi B_0 \left(1 - \frac{\Lambda_-}{\Lambda_+} e^{-k\tau} \right) \quad (107)$$

$$E_-(\tau) = \pi B_0 (1 - e^{-k\tau}) \quad (108)$$

and

$$E_+(0) = \pi B_0 \left(1 - \frac{\Lambda_-}{\Lambda_+} \right) = \frac{4\pi B_0 (1 - \omega_0)}{k + 2(1 - \omega_0)} \quad (109)$$

$$E_-(\tau_0) = \pi B_0 \quad (110)$$

Now consider the special cases: pure scattering ($\omega_0 = 1$) and pure absorption ($\omega_0 = 0$).

Pure Scattering:

Equations (85) and (86) become

$$\frac{dF_-(\tau)}{d\tau} = 0 \quad (111)$$

$$\frac{dF_+(\tau)}{d\tau} = 4(1 - \eta)F_-(\tau) \quad (112)$$

or

$$F_+(\tau) = c_3$$

$$F_-(\tau) = 4(1 - \eta)c_3\tau + c_4$$

and

$$E_+(\tau) = [4(1 - \eta)\tau + 1] \frac{c_3}{2} + \frac{c_4}{2} \quad (113)$$

$$E_-(\tau) = [4(1 - \eta)\tau - 1] \frac{c_3}{2} + \frac{c_4}{2} \quad (114)$$

Applying the boundary conditions from Eqs. (94) and (95), we obtain

$$\begin{aligned} [4(1 - \eta)\tau_0 + 1]c_3 + c_4 &= 2\pi F_0 \\ -c_3 + c_4 &= 0 \end{aligned}$$

or

$$c_3 = c_4 = \frac{\pi F_0}{1 + 2(1 - \eta)\tau_0} \quad (115)$$

and we obtain for the upward and downward irradiances

$$E_+(\tau) = \pi F_0 \left[\frac{1 + 2(1 - \eta)\tau}{1 + 2(1 - \eta)\tau_0} \right] \quad (116)$$

$$E_-(\tau) = \frac{2\pi F_0(1 - \eta)\tau}{1 + 2(1 - \eta)\tau_0} \quad (117)$$

and

$$E_+(0) = \frac{\pi F_0}{1 + 2(1 - \eta)\tau_0} \quad (118)$$

$$E_-(\tau_0) = \frac{2\pi F_0(1 - \eta)\tau_0}{1 + 2(1 - \eta)\tau_0} \quad (119)$$

Pure Absorption:

In this case, $k = 2$, $\Lambda_+ = 2$, $\Lambda_- = 0$, and $\Delta = 4e^{2\tau_0}$. It is easily shown that Eqs. (102) and (103) become

$$E_+(\tau) = \pi F_0 e^{-2(\tau_0 - \tau)} + \pi B_0 \left[1 - e^{-2(\tau_0 - \tau)} \right] \quad (120)$$

$$E_-(\tau) = \pi B_0 (1 - e^{-2\tau}) \quad (121)$$

and

$$E_+(0) = \pi F_0 e^{-2\tau_0} + \pi B_0 \left(1 - e^{-2\tau_0} \right) \quad (122)$$

$$E_-(\tau_0) = \pi B_0 \left(1 - e^{-2\tau_0} \right) \quad (123)$$

Thus far we have considered only the solution of the radiative transfer equation for the irradiances. Let us now consider the solution for the radiances. From Eq. (82), a first order approximation to the radiance is given by

$$L(\tau, \mu, \varphi) = \frac{L^u(\tau) + L^d(\tau)}{2}$$

From Eqs. (78) and (79)

$$L(\tau, \mu, \varphi) = \frac{L_+(\tau) + L_-(\tau)}{4\pi} = \frac{[E_+(\tau) + E_-(\tau)]}{2\pi} \quad (124)$$

or, from Eqs. (102) and (103)

$$L(\tau, \mu, \varphi) = D_+ e^{k\tau} + D_- e^{-k\tau} + B_0 \quad (125)$$

where

$$D_{\pm} = \frac{\pm 1}{\Delta} \left[\Lambda_{\pm} (F_0 - B_0) + \Lambda_{\mp} B_0 e^{\mp k\tau_0} \right] \quad (126)$$

Inserting Eq. (125) into the following integral expressions

$$L(\tau, \mu, \varphi) = L(\tau_0, \mu, \varphi) e^{-(\tau_0 - \tau)/\mu} + \frac{\omega_0}{4\pi\mu} \int_0^{2\pi} \int_{-1}^1 p(\mu, \varphi, \mu', \varphi') \times \\ \int_{\tau}^{\tau_0} e^{-(\tau' - \tau)/\mu} L(\tau', \mu', \varphi') d\tau' d\mu' d\varphi' + (1 - \omega_0) B_0 \left[1 - e^{-(\tau_0 - \tau)/\mu} \right] \quad (127)$$

and

$$L(\tau, -\mu, \varphi) = L(0, -\mu, \varphi) e^{-\tau/\mu} + \frac{\omega_0}{4\pi\mu} \int_0^{2\pi} \int_{-1}^1 p(-\mu, \varphi, \mu', \varphi') \times \\ \int_{\tau}^{\tau_0} e^{-(\tau - \tau')/\mu} L(\tau', \mu', \varphi') d\tau' d\mu' d\varphi' + (1 - \omega_0) B_0 (1 - e^{-\tau/\mu}) \quad (128)$$

we obtain

$$\int_{\tau}^{\tau_0} e^{-(\tau' - \tau)/\mu} (D_+ e^{k\tau'} + D_- e^{-k\tau'} + B_0) d\tau' \\ = \frac{-D_+}{\left(k - \frac{1}{\mu}\right)} \left[e^{k\tau} - e^{k\tau_0} e^{-(\tau_0 - \tau)/\mu} \right] + \frac{D_-}{\left(k + \frac{1}{\mu}\right)} \left[e^{-k\tau} - e^{-k\tau_0} e^{-(\tau_0 - \tau)/\mu} \right] \\ + B_0 \mu \left[1 - e^{-(\tau_0 - \tau)/\mu} \right] \quad (129)$$

and

$$\int_0^{\tau} e^{-(\tau - \tau')/\mu} (D_+ e^{k\tau'} + D_- e^{-k\tau'} + B_0) d\tau'$$

$$= \frac{D_+}{\left(k + \frac{1}{\mu}\right)} (e^{k\tau} - e^{-\tau/\mu}) - \frac{D_-}{\left(k - \frac{1}{\mu}\right)} (e^{-k\tau} - e^{-\tau/\mu}) + B_0 \mu (1 - e^{-\tau/\mu}) \quad (130)$$

With the boundary conditions given by Eqs. (94) and (95), we obtain

$$\begin{aligned} L(\tau, \mu, \varphi) = & F(\mu, \varphi) e^{-(\tau_0 - \tau)/\mu} - \omega_0 \left(\frac{D_+ e^{k\tau}}{k\mu - 1} - \frac{D_- e^{-k\tau}}{k\mu + 1} \right) \\ & + \left[\omega_0 \left(\frac{D_+ e^{k\tau_0}}{k\mu - 1} - \frac{D_- e^{-k\tau_0}}{k\mu + 1} \right) - B_0 \right] e^{-(\tau_0 - \tau)/\mu} + B_0 \end{aligned} \quad (131)$$

and

$$\begin{aligned} L(\tau, -\mu, \varphi) = & \omega_0 \left(\frac{D_+ e^{k\tau}}{k\mu + 1} - \frac{D_- e^{-k\tau}}{k\mu - 1} \right) \\ & - \left[\omega_0 \left(\frac{D_+}{k\mu + 1} - \frac{D_-}{k\mu - 1} \right) + B_0 \right] e^{-\tau/\mu} + B_0 \end{aligned} \quad (132)$$

In particular, the upward radiance at the top of the cloud is

$$\begin{aligned} L(0, \mu, \varphi) = & F(\mu, \varphi) e^{-\tau_0/\mu} - \omega_0 \left(\frac{D_+}{k\mu - 1} - \frac{D_-}{k\mu + 1} \right) \\ & + \left[\omega_0 \left(\frac{D_+ e^{k\tau_0}}{k\mu - 1} - \frac{D_- e^{-k\tau_0}}{k\mu + 1} \right) - B_0 \right] e^{-\tau_0/\mu} + B_0 \end{aligned} \quad (133)$$

and the downward radiance at the bottom of the cloud is

$$\begin{aligned} L(\tau_0, -\mu, \varphi) = & \omega_0 \left(\frac{D_+ e^{k\tau_0}}{k\mu + 1} - \frac{D_- e^{-k\tau_0}}{k\mu - 1} \right) \\ & - \left[\omega_0 \left(\frac{D_+}{k\mu + 1} - \frac{D_-}{k\mu - 1} \right) + B_0 \right] e^{-\tau_0/\mu} + B_0 \end{aligned} \quad (134)$$

We now separate the radiation field into its two components, the internally generated radiance, $L_i(\tau, \mu, \varphi)$, and the externally generated radiance, $L_s(\tau, \mu, \varphi)$. The upward and downward

components of $L_i(\tau, \mu, \varphi)$ are given by

$$L_i(\tau, \mu, \varphi) = -\omega_o \left(\frac{D'_+ e^{k\tau}}{k\mu - 1} - \frac{D'_- e^{-k\tau}}{k\mu + 1} \right) + \left[\omega_o \left(\frac{D'_+ e^{k\tau_o}}{k\mu - 1} - \frac{D'_- e^{-k\tau_o}}{k\mu + 1} \right) - B_o \right] e^{-(\tau_o - \tau)/\mu} + B_o \quad (135)$$

and

$$L_i(\tau, -\mu, \varphi) = \omega_o \left(\frac{D'_+ e^{k\tau}}{k\mu + 1} - \frac{D'_- e^{-k\tau}}{k\mu - 1} \right) - \left[\omega_o \left(\frac{D'_+}{k\mu + 1} - \frac{D'_-}{k\mu - 1} \right) + B_o \right] e^{-\tau/\mu} + B_o \quad (136)$$

where D'_\pm is obtained by letting $F_o = 0$ in Eq. (126). In particular,

$$L_i(0, \mu, \varphi) = -\omega_o \left(\frac{D'_+}{k\mu - 1} - \frac{D'_-}{k\mu + 1} \right) + \left[\omega_o \left(\frac{D'_+ e^{k\tau_o}}{k\mu - 1} - \frac{D'_- e^{-k\tau_o}}{k\mu + 1} \right) - B_o \right] e^{-\tau_o/\mu} + B_o \quad (137)$$

and

$$L_i(\tau_o, -\mu, \varphi) = \omega_o \left(\frac{D'_+ e^{k\tau_o}}{k\mu + 1} - \frac{D'_- e^{-k\tau_o}}{k\mu - 1} \right) - \left[\omega_o \left(\frac{D'_+}{k\mu + 1} - \frac{D'_-}{k\mu - 1} \right) + B_o \right] e^{-\tau_o/\mu} + B_o \quad (138)$$

The upward and downward components of $L_s(\tau, \mu, \varphi)$ are given by

$$L_s(\tau, \mu, \varphi) = F(\mu, \varphi) e^{-(\tau_o - \tau)/\mu} - \omega_o \left(\frac{D''_+ e^{k\tau}}{k\mu - 1} - \frac{D''_- e^{-k\tau}}{k\mu + 1} \right) + \omega_o \left(\frac{D''_+ e^{k\tau_o}}{k\mu - 1} - \frac{D''_- e^{-k\tau_o}}{k\mu + 1} \right) e^{-(\tau_o - \tau)/\mu} \quad (139)$$

and

$$L_S(\tau, -\mu, \varphi) = \omega_0 \left(\frac{D_+'' e^{k\tau}}{k\mu + 1} - \frac{D_-'' e^{-k\tau}}{k\mu - 1} \right) - \omega_0 \left(\frac{D_+''}{k\mu + 1} - \frac{D_-''}{k\mu - 1} \right) e^{-\tau/\mu} \quad (140)$$

where D_{\pm}'' is obtained by letting $B_0 = 0$ in Eq. (126). In particular,

$$L_S(0, \mu, \varphi) = F(\mu, \varphi) e^{-\tau_0/\mu} - \omega_0 \left(\frac{D_+}{k\mu - 1} - \frac{D_-}{k\mu + 1} \right) + \omega_0 \left(\frac{D_+ e^{k\tau_0}}{k\mu - 1} - \frac{D_- e^{-k\tau_0}}{k\mu + 1} \right) e^{-\tau_0/\mu} \quad (141)$$

and

$$L_S(\tau_0, -\mu, \varphi) = \omega_0 \left(\frac{D_+ e^{k\tau_0}}{k\mu + 1} - \frac{D_- e^{-k\tau_0}}{k\mu - 1} \right) - \omega_0 \left(\frac{D_+}{k\mu + 1} - \frac{D_-}{k\mu - 1} \right) e^{-\tau_0/\mu} \quad (142)$$

For the special case of a semi-infinite cloud, we have

$$\Delta \rightarrow \Lambda_+^2 e^{k\tau_0}$$

and

$$D_+ \rightarrow 0; \quad D_- \rightarrow -\frac{B_0}{\Lambda_+}$$

and

$$L(\tau, \mu, \varphi) = \frac{\omega_0 D_-}{k\mu + 1} e^{-k\tau} + B_0 \quad (143)$$

$$L(\tau, -\mu, \varphi) = -\frac{\omega_0 D_- e^{-k\tau}}{k\mu - 1} + \left[\omega_0 \left(\frac{D_-}{k\mu - 1} \right) - B_0 \right] e^{-\tau/\mu} + B_0 \quad (144)$$

In particular,

$$L(0, \mu, \varphi) = \frac{\omega_0 D_-}{k\mu + 1} + B_0 \quad (145)$$

$$L(\tau_0, -\mu, \varphi) = B_0 \quad (146)$$

Appendix II
BAND MODELS FOR CALCULATING ATMOSPHERIC TRANSMITTANCE

II.1. WATER VAPOR

Two different band-model functions are used to calculate the transmittance of water vapor for the spectral region from 4.274 to 30.0 μm .

II.1.1. BAND MODEL FOR THE INTERVAL FROM 4.274 TO 15.0 μm

The band model used for this spectral region was developed by Altshuler [10]. It utilizes the strong-line approximation to the statistical model empirically fitted to the laboratory data taken by Howard, Burch, and Williams [11]. The transmission for a resolution element $\Delta\lambda$ is given by

$$\tilde{T}(\Delta\lambda) = \exp - [W' \cdot K(\Delta\lambda)]^{1/2} \quad (147)$$

where $K(\Delta\lambda)$ is the spectral absorption coefficient for a resolution element $\Delta\lambda$ and varies from approximately 0.4 μm near 4.0 μm to approximately 1.0 μm near 15.0 μm . The coefficients are listed in Table 3. W' is the equivalent optical depth* (in centimeters) of liquid water at standard temperature and pressure (STP). For an atmospheric path of range R , the optical depth is given by

$$W' = \rho \int_0^R M \left(\frac{P}{P_0} \right)^2 \left(\frac{T_0}{T} \right)^{1.5} dr \quad (148)$$

- where P = atmospheric pressure (mm Hg)
- T = atmospheric temperature ($^{\circ}\text{K}$)
- r = range (cm)
- ρ = atmospheric density (g/cm^3)
- M = water mixing ratio ($\text{g H}_2\text{O}/\text{g air}$)
- P_0 = standard pressure
- T_0 = standard temperature

II.1.2. BAND MODEL FOR INTERVAL FROM 15.0 TO 30.0 μm

The band model used for this spectral region is the Goody model for an exponential distribution of line intensity. The transmission is given by

*The equivalent optical depth is that amount of water vapor at standard temperature and pressure that would give rise to the same amount of absorption as the water vapor along a given optical line of sight, taking into account the effect of a variable temperature and pressure on the absorption-line Lorentz half-width.

$$\tilde{T}(\Delta\lambda) = \exp - \left(\frac{\frac{S}{d} W}{\sqrt{1 + \frac{2}{\bar{P}} \frac{S}{2\pi\alpha'_0} W}} \right) \quad (149)$$

where S/d and $S/2\pi\alpha'_0$ * are spectral absorption coefficients. W is the optical depth (in cm) of liquid water at STP, and \bar{P} is the Curtis-Godson equivalent broadening pressure (in mm Hg) for an atmospheric path of total range R . These quantities are given, respectively, by

$$W = \rho \int_0^R M \left(\frac{P}{P_0} \right) \left(\frac{T_0}{T} \right) \quad (150)$$

and

$$\bar{P} = \frac{\rho P_0 \int_0^R M \left(\frac{P}{P_0} \right)^2 \left(\frac{T_0}{T} \right) dr}{W} \quad (151)$$

A tabulation of the values of S/d and $S/2\pi\alpha'_0$ are also given in Table 3.

II.2. CARBON DIOXIDE

II.2.1. BAND MODEL FOR THE INTERVAL FROM 4.465 TO 11.8 μm

As for water vapor, two band models are used to calculate the transmissivities for CO_2 . The first is an empirical model developed by Altshuler [10] and is applicable to the spectral region from 4.464 to 11.8 μm . Altshuler, using the data of Howard et al. [11], empirically determined the functional relationship between transmission and the product, $W' \cdot K(\Delta\lambda)$, as well as the spectral absorption coefficient, $K(\Delta\lambda)$. The transmission is given by

$$\tilde{T}(\Delta\lambda) = \tau[W' \cdot K(\Delta\lambda)] \quad (152)$$

where W' is the equivalent optical depth of CO_2 in centimeters of pure CO_2 gas at STP. For a path of range R , the optical depth is given by

$$W' = \int_0^R M \left(\frac{P}{P_0} \right)^2 \left(\frac{T_0}{T} \right)^{1.5} dr \quad (153)$$

where M is the mixing ratio of CO_2 in percent by volume. Values for the function $W' \cdot K(\Delta\lambda)$ are given in Table 4. The values for $K(\Delta\lambda)$ are listed in Table 5.

*In the notation α'_0 , the prime (') denotes half-width per unit pressure and the subscript (o) denotes the half-width at $T = 300^\circ\text{K}$.

TABLE 3. SPECTRAL ABSORPTION COEFFICIENTS FOR H₂O

Wavelength	K($\Delta\lambda$)	Wavelength	K($\Delta\lambda$)	Wavelength	K($\Delta\lambda$)	Wavelength	K($\Delta\lambda$)	Wavelength	K($\Delta\lambda$)
(μm)	(cm^{-1})	(μm)	(cm^{-1})	(μm)	(cm^{-1})	(μm)	(cm^{-1})	(μm)	(cm^{-1})
4.274	1.70E-3	6.126	1.37E 02	7.737	2.00E 00	10.070	2.65E-03	13.400	4.95E-02
4.405	4.25E-4	6.163	1.22E 02	7.797	1.74E 00	10.190	1.98E-03	13.440	5.14E-02
4.600	5.00E-3	6.202	1.02E 02	7.859	1.56E 00	10.290	1.86E-03	13.480	5.33E-02
4.800	7.20E-2	6.240	7.47E 01	7.921	1.77E 00	10.440	1.90E-03	13.510	5.47E-02
5.000	3.89E-01	6.279	4.99E 01	7.984	1.54E 00	10.550	2.00E-03	13.550	5.66E-02
5.025	4.70E-01	6.319	3.60E 01	8.048	8.30E-01	10.900	2.50E-03	13.590	5.85E-02
5.075	6.51E-01	6.359	2.96E 01	8.114	4.36E-01	11.500	4.52E-03	13.620	6.10E-02
5.105	7.53E-01	6.400	3.02E 01	8.180	2.41E-01	11.670	5.33E-03	13.660	6.52E-02
5.130	8.82E-01	6.441	3.64E 01	8.247	1.42E-01	11.790	6.23E-03	13.700	6.95E-02
5.145	9.56E-01	6.483	5.54E 01	8.316	8.30E-02	11.900	7.15E-03	13.740	7.38E-02
5.160	1.06E 00	6.525	1.11E 02	8.386	5.46E-02	12.050	8.17E-03	13.770	7.72E-02
5.180	1.17E 00	6.568	1.58E 02	8.457	4.67E-02	12.200	1.01E-02	13.810	8.19E-02
5.220	1.49E 00	6.612	1.94E 02	8.529	4.19E-02	12.350	1.28E-02	13.850	8.66E-02
5.260	1.86E 00	6.656	2.18E 02	8.602	3.89E-02	12.500	1.71E-02	13.890	8.82E-02
5.290	2.25E 00	6.700	2.12E 02	8.677	3.67E-02	12.530	1.81E-02	13.950	9.07E-02
5.320	2.61E 00	6.745	1.77E 02	8.753	3.49E-02	12.560	1.92E-02	13.990	9.24E-02
5.355	3.36E 00	6.791	1.40E 02	8.830	3.32E-02	12.590	2.00E-02	14.030	9.58E-02
5.380	3.56E 00	6.838	1.04E 02	8.909	3.12E-02	12.630	2.05E-02	14.060	9.89E-02
5.430	4.80E 00	6.885	8.00E 01	8.989	2.93E-02	12.660	2.15E-02	14.100	1.03E-01
5.470	5.60E 00	6.932	6.57E 01	9.070	2.73E-02	12.690	2.25E-02	14.140	1.07E-01
5.500	8.39E 00	6.981	5.60E 01	9.130	2.60E-02	12.720	2.34E-02	14.180	1.11E-01
5.540	1.10E 01	7.030	4.90E 01	9.220	2.35E-02	12.760	2.46E-02	14.220	1.17E-01
5.580	1.44E 01	7.080	4.32E 01	9.310	2.10E-02	12.790	2.50E-02	14.270	1.26E-01
5.610	1.93E 01	7.130	3.81E 01	9.335	1.90E-02	12.820	2.55E-02	14.310	1.33E-01
5.650	2.59E 01	7.181	3.32E 01	9.398	1.49E-02	12.850	2.60E-02	14.350	1.41E-01
5.700	3.59E 01	7.233	2.79E 01	9.463	1.18E-02	12.890	2.69E-02	14.390	1.48E-01
5.800	9.00E 01	7.286	2.03E 01	9.494	1.05E-02	12.920	2.76E-02	14.430	1.54E-01
5.900	1.22E 02	7.339	1.31E 01	9.526	9.00E-03	12.950	2.83E-02	14.470	1.59E-01
5.908	1.26E 02	7.394	9.10E 00	9.590	7.20E-03	12.990	2.92E-02	14.510	1.64E-01
5.944	1.38E 02	7.449	6.59E 00	9.652	6.20E-03	13.020	3.01E-02	14.560	1.70E-01
5.979	1.47E 02	7.505	4.63E 00	9.713	5.20E-03	13.050	3.12E-02	14.600	1.75E-01
6.015	1.52E 02	7.533	3.91E 00	9.773	4.40E-03	13.090	3.26E-02	14.640	1.86E-01
6.051	1.53E 02	7.561	3.39E 00	9.834	3.75E-03	13.120	3.39E-02	14.680	1.98E-01
6.088	1.49E 02	7.619	2.68E 00	9.893	3.35E-03	13.160	3.58E-02	14.730	2.12E-01
		7.678	2.31E 00	9.953	2.95E-03	13.190	3.71E-02	14.770	2.23E-01
						13.230	3.95E-02	14.810	2.34E-01
						13.260	4.14E-02	14.860	2.44E-01
						13.300	4.37E-02	14.900	2.52E-01
						13.330	4.54E-02	14.950	2.63E-01
						13.370	4.78E-02	14.990	2.72E-01

Wavelength (μm)	S/d	$S/2\pi\alpha'_0$	Wavelength (μm)	S/d	$S/2\pi\alpha'_0$	Wavelength (μm)	S/d	$S/2\pi\alpha'_0$
15.038	0.3206E 01	0.2184E 05	17.123	0.3325E 02	0.1583E 06	19.841	0.7472E 02	0.3147E 06
15.088	0.3247E 01	0.2077E 05	17.182	0.2995E 02	0.1514E 06	19.920	0.6945E 02	0.3005E 06
15.129	0.3744E 01	0.2440E 05	17.241	0.3056E 02	0.1425E 06	20.068	0.6306E 02	0.2773E 06
15.175	0.3896E 01	0.2326E 05	17.301	0.3056E 02	0.1425E 06	20.272	0.6651E 02	0.3185E 06
15.221	0.4992E 01	0.2876E 05	17.361	0.2954E 02	0.1454E 06	20.479	0.8812E 02	0.4054E 06
15.267	0.5339E 01	0.2984E 05	17.422	0.2238E 02	0.1193E 06	20.691	0.7649E 02	0.3138E 06
15.314	0.5223E 01	0.2966E 05	17.483	0.2332E 02	0.1109E 06	20.907	0.8768E 02	0.3567E 06
15.361	0.7378E 01	0.5491E 05	17.544	0.2331E 02	0.1120E 06	20.128	0.1441E 03	0.5227E 06
15.408	0.8425E 01	0.5594E 05	17.606	0.2353E 02	0.1081E 06	21.354	0.1533E 03	0.5154E 06
15.456	0.8436E 01	0.5487E 05	17.668	0.2411E 02	0.1096E 06	21.584	0.1567E 03	0.5035E 06
15.504	0.8197E 01	0.5875E 05	17.730	0.2615E 02	0.1113E 06	21.820	0.1871E 03	0.5503E 06
15.552	0.8475E 01	0.5639E 05	17.794	0.2596E 02	0.1155E 06	22.060	0.1821E 03	0.6477E 06
15.601	0.9847E 01	0.7567E 05	17.857	0.2601E 02	0.1127E 06	22.306	0.1785E 03	0.6553E 06
15.649	0.9847E 01	0.7567E 05	17.921	0.1914E 02	0.7320E 05	22.658	0.1687E 03	0.6117E 06
15.699	0.1078E 02	0.7245E 05	17.986	0.1931E 02	0.7372E 05	22.815	0.1593E 03	0.6694E 06
15.748	0.1081E 02	0.7031E 05	18.051	0.1950E 02	0.6942E 05	23.079	0.3643E 03	0.1470E 07
15.798	0.1238E 02	0.7398E 05	18.116	0.1991E 02	0.6875E 05	23.348	0.3501E 03	0.1571E 07
15.848	0.1238E 02	0.7305E 05	18.182	0.1701E 02	0.5829E 05	23.624	0.3147E 03	0.1710E 07
15.898	0.1263E 02	0.6868E 05	18.248	0.1431E 02	0.5118E 05	23.908	0.2867E 03	0.1610E 07
15.949	0.1260E 02	0.6996E 05	18.315	0.1427E 02	0.5039E 05	24.195	0.5240E 03	0.2060E 07
16.000	0.1188E 02	0.7116E 05	18.382	0.1375E 02	0.5092E 05	24.492	0.6525E 03	0.2683E 07
16.051	0.1173E 02	0.7455E 05	18.450	0.3140E 02	0.1632E 06	24.795	0.5966E 03	0.2971E 07
16.129	0.1079E 02	0.7307E 05	18.519	0.3136E 02	0.1646E 06	25.107	0.4370E 03	0.2349E 07
16.181	0.1066E 02	0.7604E 05	18.587	0.3119E 02	0.1738E 06	25.426	0.5587E 03	0.2692E 07
16.234	0.1103E 02	0.7937E 05	18.657	0.3957E 02	0.2190E 06	25.753	0.8262E 03	0.3746E 07
16.287	0.9990E 01	0.7928E 05	18.727	0.5714E 02	0.2732E 06	26.089	0.8704E 03	0.3380E 07
16.340	0.1103E 02	0.7795E 05	18.797	0.5475E 02	0.2633E 06	26.434	0.6253E 03	0.3806E 07
16.393	0.1103E 02	0.7702E 05	18.868	0.5341E 02	0.2677E 06	26.788	0.6156E 03	0.3016E 07
16.447	0.1818E 02	0.1101E 06	18.939	0.5198E 02	0.2512E 06	27.152	0.1221E 04	0.4662E 07
16.502	0.1556E 02	0.1034E 06	19.011	0.5143E 02	0.2649E 06	27.525	0.1624E 04	0.7594E 07
16.556	0.1557E 02	0.1017E 06	19.084	0.6114E 02	0.2821E 06	27.910	0.1548E 04	0.7538E 07
16.611	0.1712E 02	0.1145E 06	19.157	0.6046E 02	0.3001E 06	28.305	0.1333E 04	0.6588E 07
16.667	0.1710E 02	0.1166E 06	19.231	0.6153E 02	0.2875E 06	28.711	0.1438E 04	0.6578E 07
16.722	0.1733E 02	0.1056E 06	19.305	0.8327E 02	0.4012E 06	29.129	0.2238E 04	0.9176E 07
16.779	0.1979E 02	0.1127E 06	19.380	0.8295E 02	0.4075E 06	29.560	0.2593E 04	0.9800E 07
16.835	0.1954E 02	0.1194E 06	19.455	0.8293E 02	0.4109E 06	30.003	0.1990E 04	0.1012E 08
16.892	0.2690E 02	0.1609E 06	19.531	0.8293E 02	0.4129E 06			
16.949	0.2690E 02	0.1614E 06	19.608	0.8379E 02	0.4095E 06			
17.007	0.2784E 02	0.1531E 06	19.685	0.7445E 02	0.3193E 06			
17.065	0.3056E 02	0.1600E 06	19.763	0.7472E 02	0.3129E 06			

TABLE 4. TRANSMISSION VERSUS THE PRODUCT W'·K(Δλ)
FOR CO₂

W'·K(Δλ)	τ[W'·K(Δλ)]	W'·K(Δλ)	τ[W'·K(Δλ)]
0.3980E-03	0.1000E+01	0.1500E+00	0.5600E+00
0.1780E-02	0.9800E+00	0.1620E+00	0.5400E+00
0.1990E-02	0.9700E+00	0.1780E+00	0.5250E+00
0.6300E-02	0.9550E+00	0.1820E+00	0.5000E+00
0.7070E-02	0.9400E+00	0.2000E+00	0.4800E+00
0.1000E-01	0.9300E+00	0.2510E+00	0.4500E+00
0.1260E-01	0.9200E+00	0.2820E+00	0.4250E+00
0.1590E-01	0.9100E+00	0.3180E+00	0.4000E+00
0.2000E-01	0.8900E+00	0.3550E+00	0.3750E+00
0.2520E-01	0.8750E+00	0.4260E+00	0.3500E+00
0.2820E-01	0.8670E+00	0.4460E+00	0.3200E+00
0.3160E-01	0.8500E+00	0.5260E+00	0.3000E+00
0.3550E-01	0.8400E+00	0.5620E+00	0.2750E+00
0.3900E-01	0.8300E+00	0.6030E+00	0.2700E+00
0.3980E-01	0.8200E+00	0.6200E+00	0.2600E+00
0.4470E-01	0.8100E+00	0.6300E+00	0.2400E+00
0.4790E-01	0.8000E+00	0.7080E+00	0.2250E+00
0.5260E-01	0.7800E+00	0.7950E+00	0.2000E+00
0.5650E-01	0.7500E+00	0.1000E+01	0.1750E+00
0.6310E-01	0.7400E+00	0.1110E+01	0.1500E+00
0.6400E-01	0.7250E+00	0.1590E+01	0.1250E+00
0.7500E-01	0.7000E+00	0.1780E+01	0.1000E+00
0.7950E-01	0.6750E+00	0.2510E+01	0.7500E-01
0.1000E+00	0.6500E+00	0.4260E+01	0.5000E-01
0.1120E+00	0.6250E+00	0.7410E+01	0.2500E-01
0.1260E+00	0.6000E+00	0.2240E+02	0.0000E+00
0.1410E+00	0.5750E+00	0.3000E+02	0.0000E+00

II.2.2. BAND MODEL FOR THE INTERVALS FROM 4.158 TO 4.454 μm AND 11.8 TO 20.0 μm

The second band model used for CO₂ is the Elsasser model and is applicable to the spectral region from 4.158 to 4.45 μm and from 11.8 to 20.0 μm. For this model, the transmission is given by

$$\tilde{T}(\Delta\lambda) = 1 - \sinh \beta \int_0^Y I_0(Y) \exp(-Y \cosh \beta) dY \quad (154)$$

where $Y = \frac{(S/d)W}{\sinh \beta}$

$$\beta = \frac{2\pi\alpha \bar{P}}{d}$$

and $I_0(Y)$ is a Bessel function with imaginary argument. W is the optical depth, and \bar{P} is the Curtis-Godson equivalent broadening pressure and are given, respectively, for a path of range

R by the expressions:

$$W = \int_0^R M \left(\frac{P}{P_0} \right) \left(\frac{T_0}{T} \right) dr \quad (155)$$

$$\bar{P} = \frac{P_0 \int_0^R M \left(\frac{P}{P_0} \right)^2 \left(\frac{T_0}{T} \right) dr}{W} \quad (156)$$

TABLE 5. SPECTRAL ABSORPTION COEFFICIENTS FOR CO₂

Wavelength (μm)	K($\Delta\lambda$) (cm^{-1})	Wavelength (μm)	K($\Delta\lambda$) (cm^{-1})
4.465	9.940E-03	5.220	5.660E-05
4.470	5.690E-03	5.260	3.940E-05
4.475	3.940E-03	5.290	2.340E-05
4.490	2.340E-03	5.320	1.500E-05
4.495	1.500E-03	5.355	5.590E-06
4.505	5.590E-02	9.130	1.24E-07
4.520	1.640E-02	9.220	2.05E-06
4.526	9.940E-05	9.310	6.25E-06
4.548	5.690E-05	9.335	6.25E-06
4.575	3.940E-05	9.398	4.00E-06
4.600	2.340E-05	9.463	2.16E-06
4.660	1.640E-05	9.494	4.00E-06
4.700	2.340E-05	9.526	5.00E-06
4.730	3.940E-05	9.590	5.00E-06
4.750	5.690E-05	9.652	2.18E-06
4.770	9.940E-05	9.713	6.22E-07
4.800	1.940E-04	9.773	2.67E-07
4.830	2.480E-04	9.834	1.00E-08
4.860	4.060E-04	9.893	1.00E-08
4.890	2.480E-04	9.953	1.00E-08
4.910	1.640E-04	10.070	3.40E-08
4.925	9.940E-05	10.190	2.05E-06
4.940	5.690E-05	10.290	6.06E-06
4.950	3.940E-05	10.440	1.94E-06
4.965	2.340E-05	10.550	6.03E-06
4.970	1.500E-05	10.900	1.24E-07
4.975	9.880E-06	11.500	3.13E-06
4.990	5.590E-06	11.670	4.36E-06
5.025	2.050E-06		
5.075	8.000E-07		
5.105	2.050E-06		
5.130	5.590E-06		
5.145	1.500E-05		
5.160	2.340E-05		
5.180	3.940E-05		

For a major portion of the 15.0- μm CO_2 absorption band, the band-model parameters S/d and $2\pi\alpha'/d$ are sensitive to temperature. Therefore, in order to correctly apply this model to the calculation of transmission for atmospheric paths, an effective absorbing temperature for the path must be calculated and the band-model parameters determined for that temperature. The effective temperature, T_h , for a path of range R can be approximated by solving the following equation:

$$\left(\frac{T_o}{T_h}\right)^{3/2} \left(\frac{\bar{P}}{\bar{P}_o}\right) \exp - \left(2000 \frac{T_o - T_h}{T_o T_h}\right) = \int_0^R M \left(\frac{T_o}{T}\right)^{5/2} \left(\frac{P}{P_o}\right)^2 \exp - 2000 \left(\frac{T_o - T}{T_o T}\right) dr \quad (157)$$

The band-model parameters for temperature T_h are determined by performing an interpolation between the parameters defined at 300 $^\circ\text{K}$ and 200 $^\circ\text{K}$, respectively. The interpolation equations, applicable for all wavelengths, are given by

$$\frac{S}{d} = \frac{K_1 \exp - (K_2/T_h)}{T_h^2} \quad (158)$$

$$\frac{2\pi\alpha'S}{d^2} = \frac{K_3 \exp - (K_4/T_h)}{T_h^2} \quad (159)$$

For the 4.3- μm CO_2 band, the values of S/d and $2\pi\alpha'/d$ are not particularly temperature sensitive, so only the values for $T = 300^\circ\text{K}$ are used. These coefficients are given in Table 6. K_1 , K_2 , K_3 , and K_4 are tabulated in Table 7 for the wavelength range from 11.79 to 20.0 μm .

II.3. OZONE

The band model used for ozone for the 9.6- μm spectral band is that developed by Zachor [12]. His method is based on an empirical fit of the Elsasser model to the laboratory data of Walshaw [13]. The resulting transmission function is given by Eq. (154) with

$$\beta = \left(\frac{2\pi\alpha_o}{d}\right) \left(\frac{\bar{P}}{\bar{P}_o}\right)^c \quad (160)$$

where c is a constant whose values are listed in Table 8 in conjunction with the values of S/d and $2\pi\alpha_o/d$. The values of W and \bar{P} are given by Eqs. (155) and (156), respectively, where M is the O_3 mixing ratio in percent by volume.

II.4. METHANE

The band model used to calculate the atmospheric transmittance for CH_4 is the Goody model given by Eq. (149). The equivalent path parameters W and \bar{P} are given by Eqs. (155) and (156),

TABLE 6. SPECTRAL ABSORPTION COEFFICIENTS FOR THE 4.3- μm CO₂ BAND

Wavelength (μm)	S/d	$2\pi\alpha'_0/d$
4.1580	0.2600E-03	0.1000E-05
4.1670	0.5900E-02	0.5000E-05
4.1750	0.2400E+00	0.8000E-04
4.1840	0.9940E-01	0.1815E-02
4.1930	0.9800E+00	0.7368E-03
4.2020	0.5046E+01	0.7632E-03
4.2110	0.1464E+02	0.8026E-03
4.2190	0.2728E+02	0.1158E-02
4.2280	0.3363E+02	0.1500E-02
4.2370	0.3363E+02	0.1553E-02
4.2460	0.2562E+02	0.1605E-02
4.2550	0.1344E+02	0.1684E-02
4.2640	0.2316E+02	0.1576E-02
4.2740	0.2592E+02	0.1421E-02
4.2830	0.2472E+02	0.1355E-02
4.2920	0.2070E+02	0.1211E-02
4.3010	0.1698E+02	0.1435E-02
4.3100	0.1219E+02	0.1263E-02
4.3190	0.7300E+01	0.1316E-02
4.3290	0.5000E+01	0.1316E-02
4.3380	0.2915E+01	0.1448E-02
4.3480	0.2020E+01	0.1342E-02
4.3570	0.1298E+01	0.1448E-02
4.3670	0.6860E+00	0.1290E-02
4.3760	0.3762E+00	0.1302E-02
4.3860	0.4599E+00	0.8289E-03
4.3960	0.6090E+00	0.5527E-03
4.4050	0.5890E+00	0.5000E-03
4.4150	0.5610E+00	0.4342E-03
4.4250	0.3833E+00	0.4800E-03
4.4350	0.2496E+00	0.6851E-03
4.4440	0.1855E+00	0.9218E-03
4.4540	0.8624E-01	0.1013E-02

TABLE 7. SPECTRAL ABSORPTION COEFFICIENTS FOR THE 15.0- μm CO₂ BAND

Wavelength (μm)	K ₁	K ₂	K ₃	K ₄	Wavelength (μm)	K ₁	K ₂	K ₃	K ₄
11.79	0.4960E 01	0.5120E 03	0.5210E-01	0.1371E 04	13.70	0.1719E 05	0.7776E 03	0.2590E 03	0.1262E 04
11.90	0.8680E 01	0.5120E 03	0.3049E 00	0.1418E 04	13.74	0.3462E 04	0.3097E 03	0.3093E 03	0.1304E 04
12.05	0.2281E 02	0.5120E 03	0.6201E 00	0.1631E 04	13.77	0.1281E 04	0.4217E 02	0.3339E 03	0.1350E 04
12.20	0.1040E 03	0.7055E 03	0.3694E 01	0.1646E 04	13.81	0.1229E 04	-0.3377E 00	0.4200E 03	0.1412E 04
12.35	0.2923E 03	0.8362E 03	0.4218E 01	0.1496E 04	13.85	0.3982E 03	-0.3496E 03	0.7854E 11	0.5328E 04
12.50	0.8354E 03	0.9921E 03	0.3968E 01	0.1418E 04	13.89	0.1847E 06	0.2947E 03	0.3052E 05	0.1857E 04
12.53	0.1134E 04	0.1063E 04	0.3932E 01	0.1406E 04	13.95	0.2866E 04	0.1781E 03	0.4001E 04	0.1699E 04
12.56	0.1581E 04	0.1131E 04	0.1134E 02	0.1629E 04	13.99	0.9503E 04	0.5409E 03	0.2722E 04	0.1626E 04
12.59	0.2657E 06	0.2131E 04	0.5443E 02	0.1753E 04	14.03	0.9309E 04	0.4656E 03	0.3134E 04	0.1616E 04
12.63	0.2886E 06	0.2127E 04	0.6953E 02	0.1769E 04	14.06	0.2199E 05	0.6026E 03	0.4106E 04	0.1624E 04
12.66	0.5547E 10	0.4303E 04	0.1056E 02	0.1372E 04	14.10	0.2451E 05	0.5670E 03	0.3670E 04	0.1551E 04
12.69	0.4121E 03	0.8242E 03	0.4582E 01	0.1422E 04	14.14	0.7930E 04	0.2646E 03	0.7788E 04	0.1686E 04
12.72	0.9680E 03	0.9952E 03	0.8368E 01	0.1520E 04	14.18	0.4181E 04	0.3927E 02	0.1300E 05	0.1744E 04
12.76	0.1208E 04	0.1034E 04	0.1004E 02	0.1543E 04	14.22	0.3320E 04	-0.1113E 03	0.1322E 05	0.1680E 04
12.79	0.1576E 04	0.1083E 04	0.1342E 02	0.1590E 04	14.27	0.7648E 04	0.7435E 02	0.1013E 05	0.1569E 04
12.82	0.2138E 04	0.1140E 04	0.2241E 02	0.1686E 04	14.31	0.2042E 04	-0.2913E 03	0.1056E 05	0.1526E 04
12.85	0.3828E 04	0.1258E 04	0.4513E 02	0.1819E 04	14.35	0.5341E 03	-0.6627E 03	0.1562E 05	0.1535E 04
12.89	0.4000E 04	0.1262E 04	0.4791E 02	0.1826E 04	14.39	0.4605E 03	-0.7497E 03	0.7459E 04	0.1299E 04
12.92	0.6420E 04	0.1356E 04	0.9884E 02	0.1966E 04	14.43	0.5586E 03	-0.7104E 03	0.8157E 04	0.1275E 04
12.95	0.1156E 05	0.1471E 04	0.1776E 03	0.2066E 04	14.47	0.6195E 03	-0.7126E 03	0.9928E 04	0.1246E 04
12.99	0.1779E 05	0.1554E 04	0.1533E 03	0.2013E 04	14.51	0.6513E 03	-0.7033E 03	0.8860E 04	0.1139E 04
13.02	0.2833E 05	0.1639E 04	0.1526E 03	0.1981E 04	14.56	0.5009E 03	-0.8024E 03	0.1799E 04	0.7323E 03
13.05	0.3799E 05	0.1685E 04	0.1220E 03	0.1902E 04	14.60	0.2645E 03	-0.9942E 03	0.2513E 04	0.7932E 03
13.09	0.1563E 06	0.1949E 04	0.1826E 03	0.1912E 04	14.64	0.3811E 03	-0.8926E 03	0.2483E 04	0.7391E 03
13.12	0.1121E 06	0.1852E 04	0.1225E 03	0.1801E 04	14.68	0.2964E 03	-0.9596E 03	0.3039E 04	0.7337E 03
13.16	0.1529E 06	0.1880E 04	0.1956E 03	0.1849E 04	14.73	0.3596E 03	-0.9178E 03	0.1042E 04	0.4670E 03
13.19	0.2323E 06	0.1887E 04	0.5823E 03	0.1983E 04	14.77	0.2856E 03	-0.9768E 03	0.1364E 04	0.5543E 03
13.23	0.1396E 06	0.1750E 04	0.4183E 03	0.1894E 04	14.81	0.7554E 03	-0.7286E 03	0.1794E 04	0.6056E 03
13.26	0.2016E 06	0.1777E 04	0.2805E 03	0.1742E 04	14.86	0.7240E 03	-0.7466E 03	0.1069E 05	0.9695E 03
13.30	0.2388E 06	0.1708E 04	0.2968E 03	0.1652E 04	14.90	0.2785E 04	-0.4781E 03	0.5989E 06	0.1726E 04
13.33	0.1046E 06	0.1504E 04	0.2820E 03	0.1647E 04	14.95	0.2061E 04	-0.6501E 03	0.1234E 07	0.1718E 04
13.37	0.5863E 05	0.1316E 04	0.4374E 03	0.1678E 04	14.99	0.4158E 04	-0.5511E 03	0.1326E 08	0.2253E 04
13.40	0.2818E 05	0.1023E 04	0.3298E 03	0.1522E 04	15.04	0.2406E 04	-0.3470E 03	0.2558E 04	0.6745E 03
13.44	0.7802E 05	0.1246E 04	0.2798E 03	0.1442E 04	15.08	0.7086E 03	-0.6943E 03	0.2048E 04	0.6550E 03
13.48	0.1341E 06	0.1360E 04	0.8617E 03	0.1571E 04	15.13	0.5428E 03	-0.7764E 03	0.6274E 03	0.3265E 03
13.51	0.3475E 06	0.1528E 04	0.1488E 04	0.1588E 04					
13.55	0.3454E 05	0.9799E 03	0.8273E 03	0.1568E 04					
13.59	0.1602E 05	0.7234E 03	0.4963E 03	0.1433E 04					
13.62	0.2796E 05	0.8623E 03	0.2765E 03	0.1241E 04					
13.66	0.1876E 05	0.7702E 03	0.2419E 03	0.1247E 04					

Wavelength (μm)	K_1	K_2	K_3	K_4	Wavelength (μm)	K_1	K_2	K_3	K_4
15.17	0.8198E 03	-0.7070E 03	0.1450E 04	0.6131E 03	17.30	0.9789E 05	0.1776E 04	0.1094E 03	0.1700E 04
15.22	0.9123E 03	-0.6771E 03	0.9524E 03	0.4844E 03	17.36	0.8987E 05	0.1790E 04	0.1124E 03	0.1749E 04
15.27	0.5597E 03	-0.7968E 03	0.7001E 03	0.4015E 03	17.42	0.7901E 05	0.1794E 04	0.9238E 02	0.1753E 04
15.31	0.7001E 03	-0.7238E 03	0.1610E 04	0.6188E 03	17.48	0.3691E 05	0.1662E 04	0.1141E 03	0.1856E 04
15.36	0.1007E 04	-0.6039E 03	0.2147E 05	0.1184E 04	17.54	0.1833E 05	0.1535E 04	0.1071E 03	0.1889E 04
15.41	0.1023E 04	-0.5910E 03	0.1086E 05	0.9644E 03	17.61	0.1127E 05	0.1449E 04	0.9019E 02	0.1890E 04
15.46	0.7357E 03	-0.6335E 03	0.1292E 05	0.1094E 04	17.67	0.7836E 04	0.1385E 04	0.9961E 02	0.1941E 04
15.50	0.6620E 03	-0.6161E 03	0.2224E 05	0.1507E 04	17.73	0.3778E 04	0.1243E 04	0.5891E 02	0.1861E 04
15.55	0.8717E 03	-0.5512E 03	0.1442E 04	0.8306E 03	17.79	0.1855E 04	0.1101E 04	0.3837E 02	0.1795E 04
15.60	0.8254E 03	-0.5590E 03	0.2645E 04	0.1012E 04	17.86	0.1400E 04	0.1049E 04	0.2995E 02	0.1759E 04
15.65	0.2784E 04	-0.1832E 03	0.1331E 05	0.1465E 04	17.92	0.8305E 03	0.9456E 03	0.1453E 02	0.1620E 04
15.70	0.1947E 04	-0.2642E 03	0.6661E 04	0.1332E 04	17.99	0.6014E 03	0.8841E 03	0.9487E 01	0.1543E 04
15.75	0.2217E 04	-0.1996E 03	0.4236E 04	0.1248E 04	18.05	0.4370E 03	0.8227E 03	0.6361E 01	0.1471E 04
15.80	0.4612E 04	0.4628E 02	0.1233E 05	0.1582E 04	18.12	0.3425E 03	0.7780E 03	0.5063E 01	0.1436E 04
15.85	0.4473E 04	0.6327E 02	0.3717E 04	0.1341E 04	18.18	0.2392E 03	0.7083E 03	0.3146E 01	0.1348E 04
15.90	0.6447E 04	0.2145E 03	0.3651E 04	0.1385E 04	18.25	0.5335E 03	0.8883E 03	0.1070E 02	0.1622E 04
15.95	0.2368E 04	0.1793E 02	0.2638E 04	0.1384E 04	18.32	0.4398E 04	0.1332E 04	0.8373E 02	0.2020E 04
16.00	0.1196E 04	-0.1171E 03	0.1823E 04	0.1372E 04	18.38	0.3669E 04	0.1300E 04	0.4536E 02	0.1901E 04
16.05	0.4167E 03	-0.3686E 03	0.2667E 03	0.8802E 03	18.45	0.3762E 03	0.8294E 03	0.1862E 01	0.1267E 04
16.13	0.1495E 07	0.1765E 04	0.4091E 03	0.1119E 04	18.52	0.1092E 03	0.5745E 03	0.1133E 01	0.1194E 04
16.18	0.1440E 12	0.4279E 04	0.1041E 04	0.1073E 04	18.59	0.1169E 03	0.5958E 03	0.1239E 01	0.1224E 04
16.23	0.1730E 12	0.4334E 04	0.1366E 04	0.1115E 04	18.66	0.1289E 03	0.6231E 03	0.1426E 01	0.1264E 04
16.29	0.1373E 06	0.1271E 04	0.9795E 03	0.1450E 04	18.73	0.1454E 03	0.6558E 03	0.1694E 01	0.1312E 04
16.34	0.3874E 05	0.9882E 03	0.4113E 03	0.1310E 04	18.80	0.1387E 03	0.6527E 03	0.1599E 01	0.1312E 04
16.39	0.3590E 05	0.9714E 03	0.3965E 03	0.1305E 04	18.87	0.1377E 03	0.6578E 03	0.1660E 01	0.1332E 04
16.45	0.2904E 05	0.9440E 02	0.4175E 03	0.1351E 04	18.94	0.1592E 03	0.6960E 03	0.2170E 01	0.1401E 04
16.50	0.2409E 05	0.8957E 03	0.3030E 03	0.1309E 04	19.01	0.1179E 03	0.6380E 03	0.1445E 01	0.1328E 04
16.56	0.2806E 05	0.9308E 03	0.2406E 03	0.1248E 04	19.08	0.1087E 03	0.6269E 03	0.1354E 01	0.1326E 04
16.61	0.2389E 05	0.9042E 03	0.2028E 03	0.1273E 04	19.16	0.1122E 03	0.6406E 03	0.1539E 01	0.1365E 04
16.67	0.5346E 05	0.1099E 04	0.1641E 03	0.1271E 04	19.23	0.8112E 02	0.5768E 03	0.1005E 01	0.1286E 04
16.72	0.1513E 06	0.1394E 04	0.6753E 03	0.1502E 04	19.31	0.7337E 02	0.5611E 03	0.9072E 00	0.1275E 04
16.78	0.8236E 05	0.1280E 04	0.1396E 04	0.1659E 04	19.38	0.7022E 02	0.5577E 03	0.8894E 00	0.1283E 04
16.84	0.6057E 05	0.1282E 04	0.6766E 03	0.1658E 04	19.46	0.5596E 02	0.5148E 03	0.6276E 00	0.1217E 04
16.89	0.9037E 05	0.1408E 04	0.2069E 03	0.1491E 04	19.53	0.5220E 02	0.5054E 03	0.6226E 00	0.1227E 04
16.95	0.1730E 06	0.1592E 04	0.1997E 03	0.1520E 04	19.61	0.4822E 02	0.4938E 03	0.5122E 00	0.1195E 04
17.01	0.1675E 06	0.1626E 04	0.2119E 03	0.1556E 04	19.69	0.4317E 02	0.4753E 03	0.4272E 00	0.1166E 04
17.06	0.1305E 06	0.1650E 04	0.1728E 03	0.1584E 04	19.76	0.4096E 02	0.4693E 03	0.4288E 00	0.1177E 04
17.12	0.1385E 06	0.1705E 04	0.1876E 03	0.1650E 04	19.84	0.3796E 02	0.4589E 03	0.3730E 00	0.1155E 04
17.18	0.1376E 06	0.1742E 04	0.2395E 03	0.1740E 04	19.92	0.3632E 02	0.4546E 03	0.3659E 00	0.1161E 04
17.24	0.1669E 06	0.1836E 04	0.2560E 03	0.1807E 04					

TABLE 8. EMPIRICAL CONSTANTS
FOR OZONE

Wavelength (μm)	S/d	$2\pi\alpha'_0/d$	c
9.398	0.476	0.712	0.477
9.463	10.0	1.70	0.654
9.494	14.3	1.48	0.648
9.526	9.43	2.07	0.699
9.590	4.58	1.36	0.602
9.652	7.15	2.03	0.602
9.713	8.34	1.49	0.648
9.773	8.00	1.67	0.699
9.834	7.14	1.86	0.756
9.893	5.20	1.74	0.725
9.953	3.22	1.82	0.748
10.07	0.944	2.27	0.745
10.19	0.318	0.554	0.301

respectively, where M is the mixing ratio for CH_4 expressed in percent by volume. The values of S/d and $S/2\pi\alpha'_0$ are given in Table 9.

II.5. NITROUS OXIDE

N_2O transmittance is calculated by the equation:

$$\tilde{T}(\Delta\lambda) = 1 - \text{erf} [W' \cdot K(\Delta\lambda)]$$

where W' is the equivalent sea-level path given by Eq. (148) with M the mixing ratio for N_2O in percent by volume and

$$\text{erf} (X) = \frac{2}{\sqrt{\pi}} \int_0^X e^{-x^2} dx$$

The values of $K(\Delta\lambda)$ are given in Table 10.

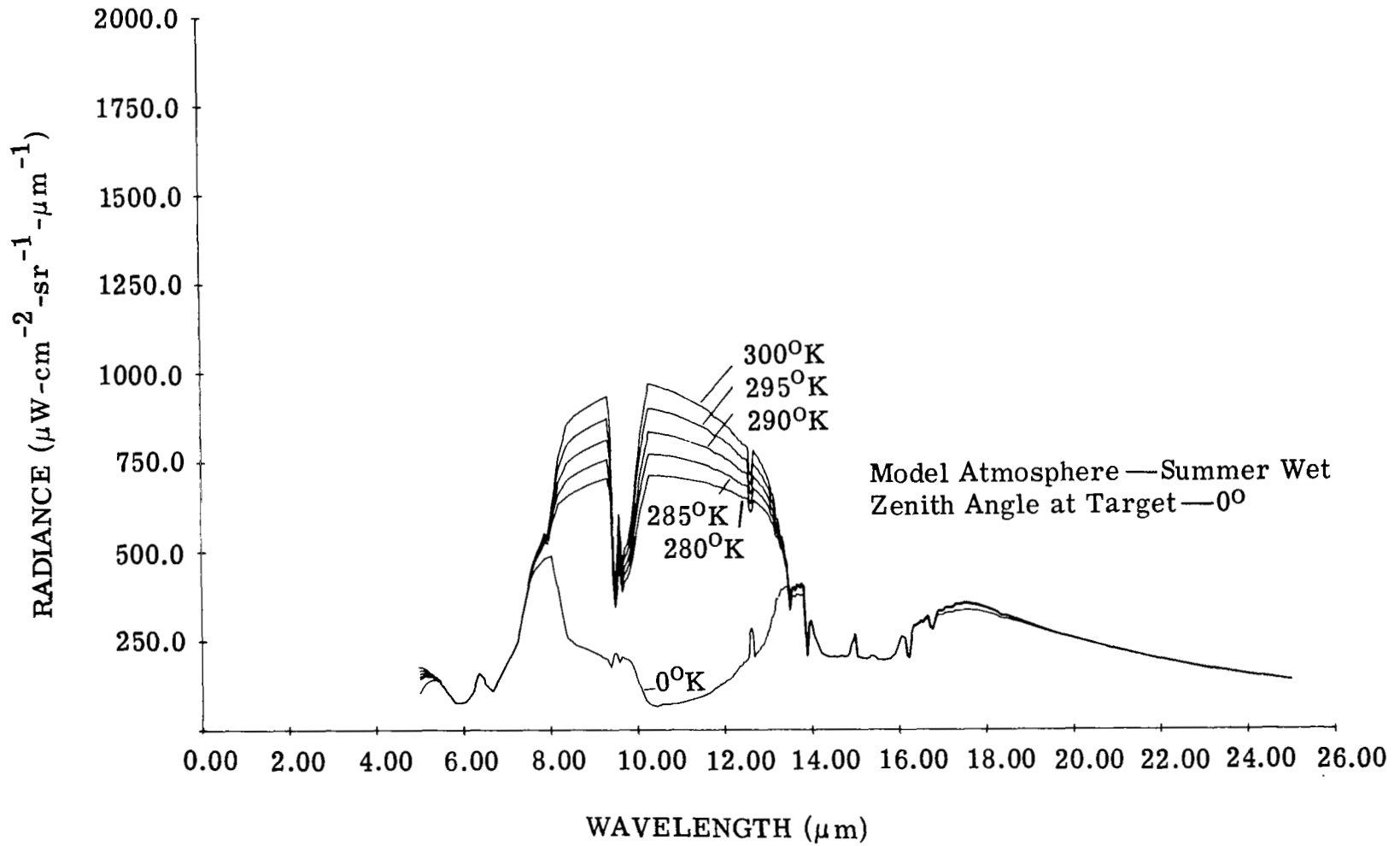
TABLE 9. SPECTRAL ABSORPTION COEFFICIENTS FOR CH₄

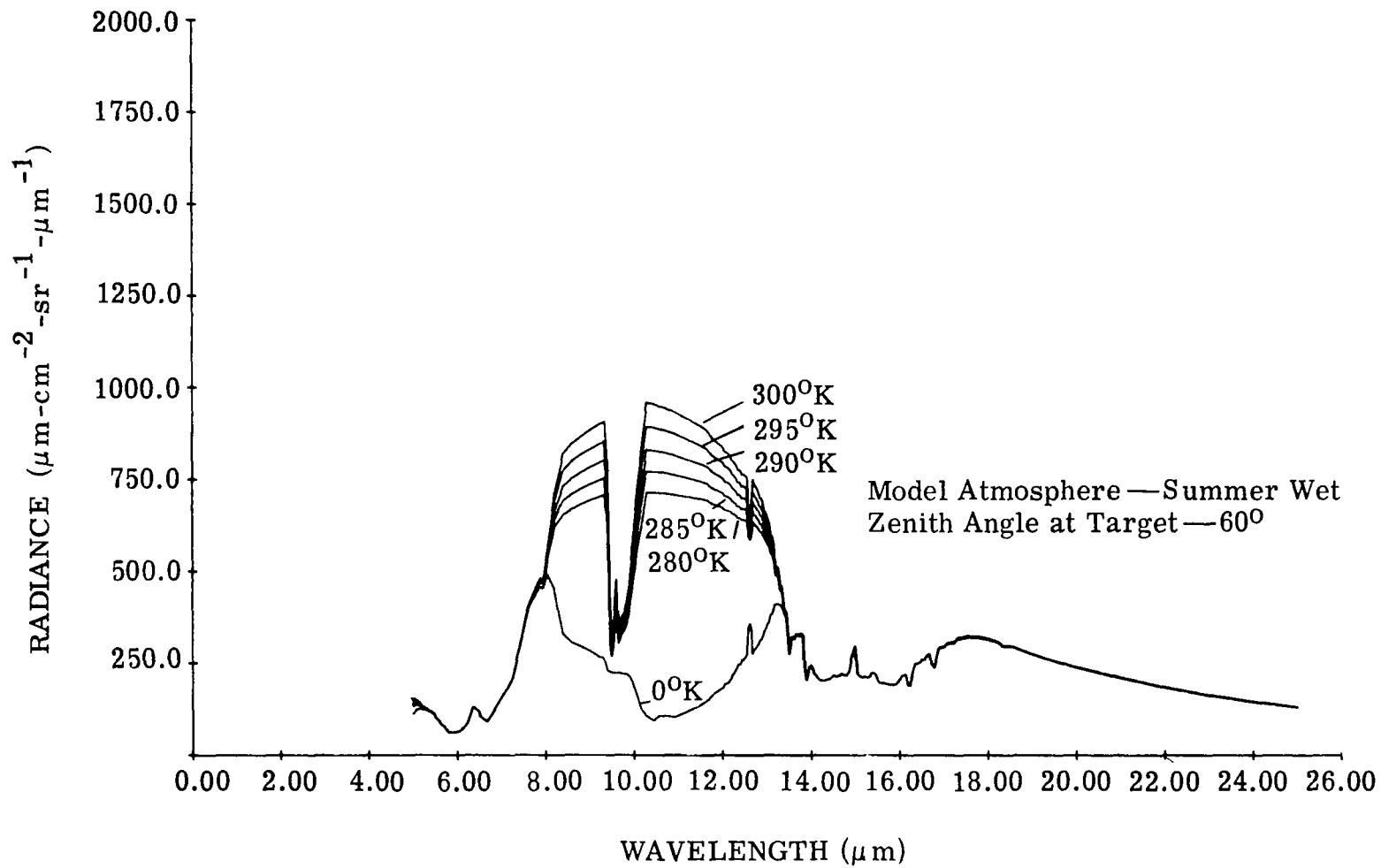
Wavelength (μm)	S/d	$S/2\pi\alpha'_0$	Wavelength (μm)	S/d	$S/2\pi\alpha'_0$
5.908	1.270E 00	8.493E-04	7.181	3.026E 01	4.604E-02
5.944	1.579E 00	1.287E-03	7.233	5.506E 01	1.058E-01
5.979	2.030E 00	1.621E-03	7.286	6.718E 01	1.927E-01
6.015	2.333E 00	1.965E-03	7.339	7.149E 01	2.803E-01
6.051	2.279E 00	2.411E-03	7.394	7.904E 01	3.328E-01
6.088	2.125E 00	2.820E-03	7.449	8.371E 01	2.933E-01
6.126	2.269E 00	3.001E-03	7.505	6.814E 01	1.815E-01
6.163	2.706E 00	3.031E-03	7.533	5.503E 01	1.472E-01
6.202	3.336E 00	2.758E-03	7.561	1.646E 02	3.013E-01
6.240	3.631E 00	2.246E-03	7.619	9.383E 01	4.427E-01
6.279	3.994E 00	1.740E-03	7.678	7.703E 01	5.420E-01
6.319	2.223E 00	1.461E-03	7.737	6.335E 01	3.009E-01
6.359	1.396E 00	2.222E-03	7.797	6.889E 01	2.554E-01
6.400	1.623E 00	5.437E-03	7.859	8.934E 01	2.679E-01
6.441	1.805E 00	9.401E-03	7.921	1.050E 02	2.582E-01
6.483	1.810E 00	8.250E-03	7.984	8.854E 01	1.913E-01
6.525	1.445E 00	3.352E-03	8.048	8.237E 01	1.462E-01
6.568	1.460E 00	1.219E-03	8.114	1.009E 02	1.139E-01
6.612	1.525E 00	1.551E-03	8.180	8.215E 01	7.593E-02
6.656	1.878E 00	2.477E-03	8.247	3.499E 01	3.492E-02
6.700	2.437E 00	3.548E-03	8.316	1.171E 01	1.717E-02
6.745	2.822E 00	4.497E-03	8.386	1.071E 01	1.229E-02
6.791	2.924E 00	5.358E-03	8.457	1.045E 01	8.246E-03
6.838	2.863E 00	6.086E-03	8.529	4.038E 00	4.308E-03
6.885	2.798E 00	6.675E-03	8.602	5.726E-01	2.267E-03
6.932	2.841E 00	7.130E-03	8.677	1.856E-01	1.478E-03
6.981	2.935E 00	7.449E-03	8.753	1.633E-01	9.756E-04
7.030	3.212E 00	7.771E-03	8.830	4.226E-01	7.455E-04
7.080	3.728E 00	8.835E-03	8.909	7.121E-01	5.811E-04
7.130	1.089E 01	1.759E-02	8.989	7.207E-01	4.008E-04
			9.070	6.525E-01	1.852E-04

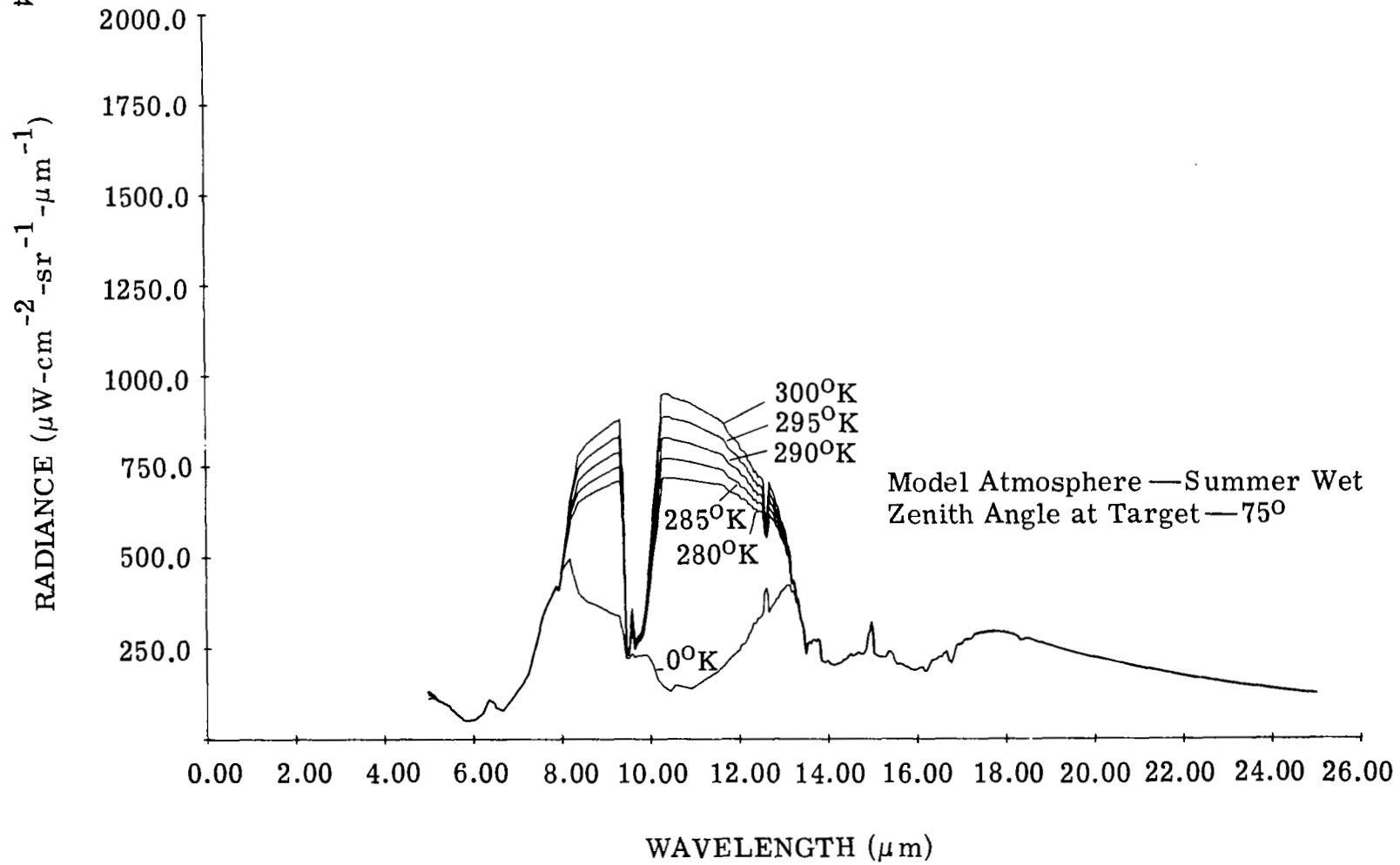
TABLE 10. SPECTRAL ABSORPTION COEFFICIENTS FOR N₂O

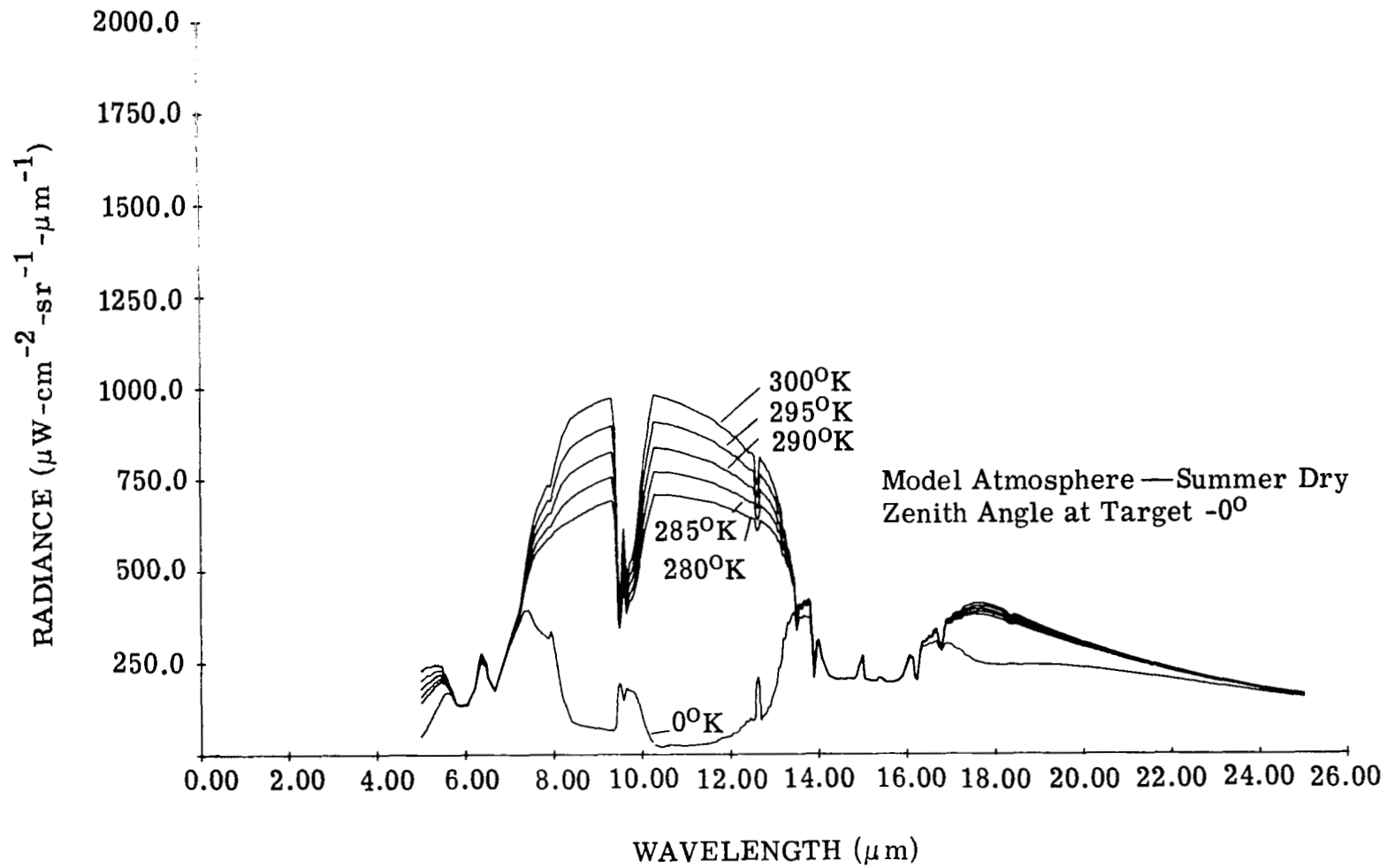
Wavelength	K($\Delta\lambda$) (cm ⁻¹)
4.14	0.0
4.22	0.0
4.25	1.17E-3
4.28	2.62E-3
4.30	1.32E-3
4.33	2.67E-3
4.37	8.06E-4
4.40	4.15E-3
4.45	6.59E-1
4.48	7.29E 0
4.50	5.23E 0
4.52	4.67E 0
4.54	5.70E 0
4.60	4.15E-1
4.70	9.29E-4
4.74	0.0

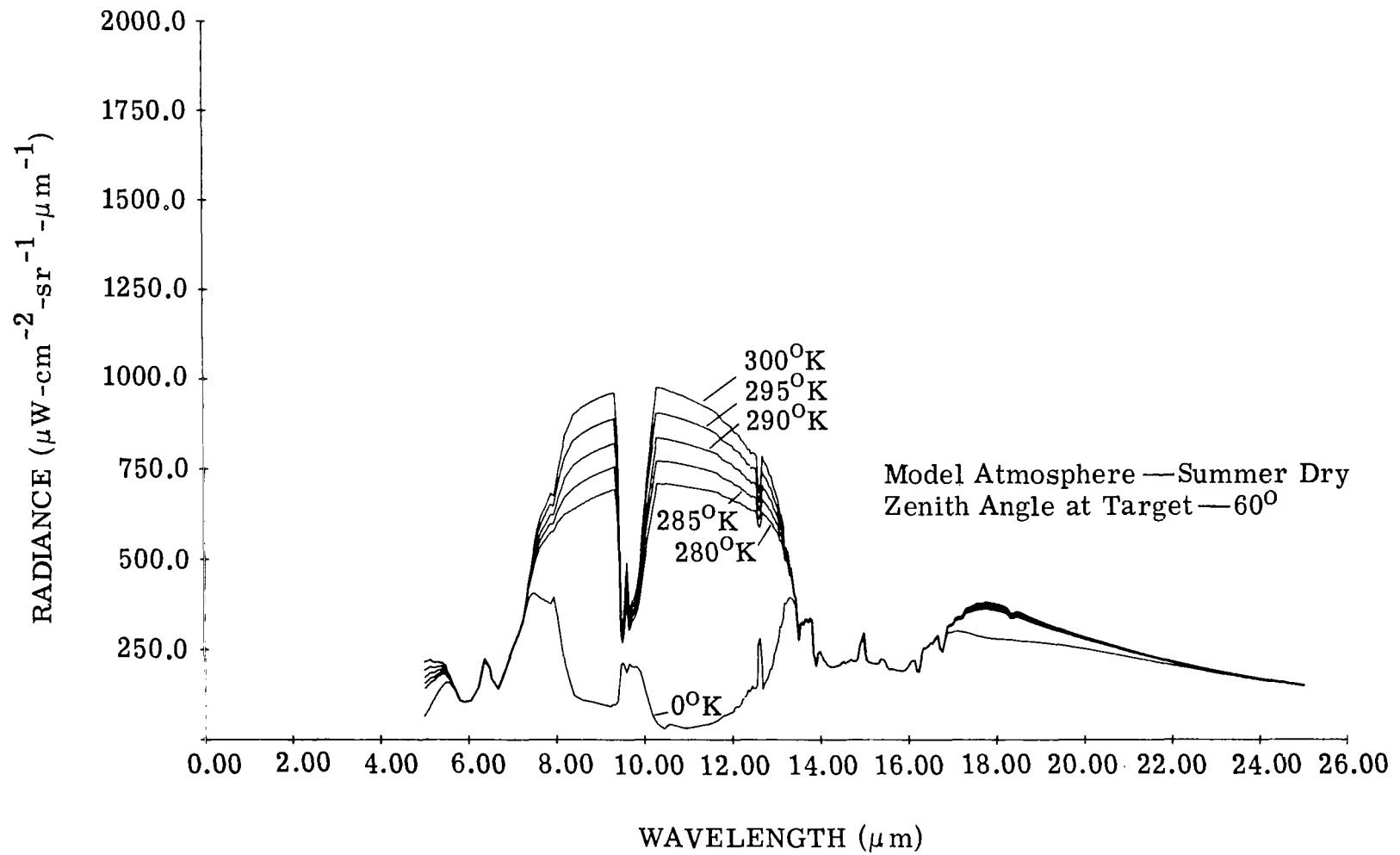
Appendix III
**PRESENTATION OF SPECTRAL RADIANCE FOR CLEAR ATMOSPHERES FOR VARIOUS MODEL
ATMOSPHERES, ZENITH OBSERVATION ANGLES, AND SEA TEMPERATURES**

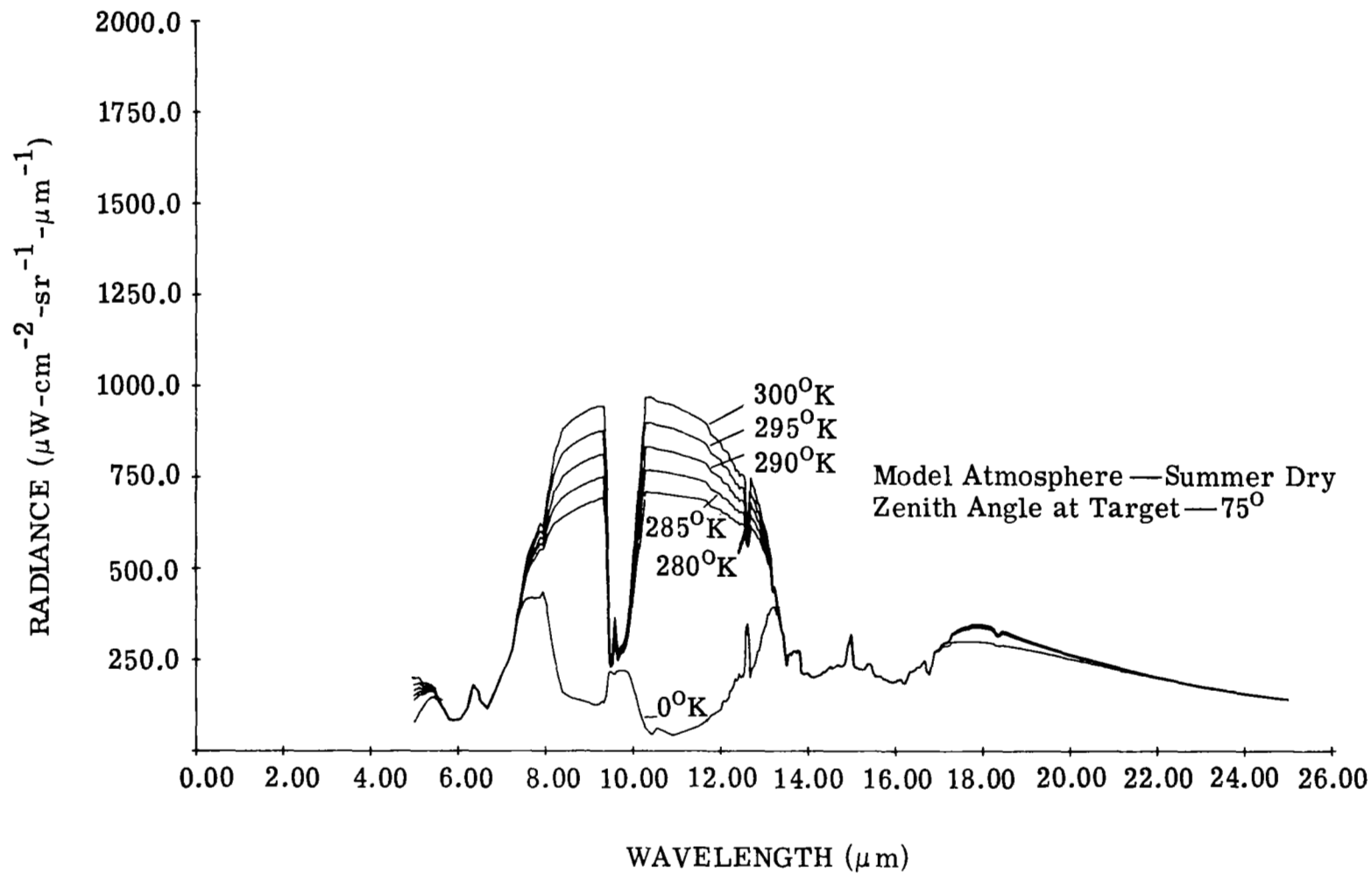


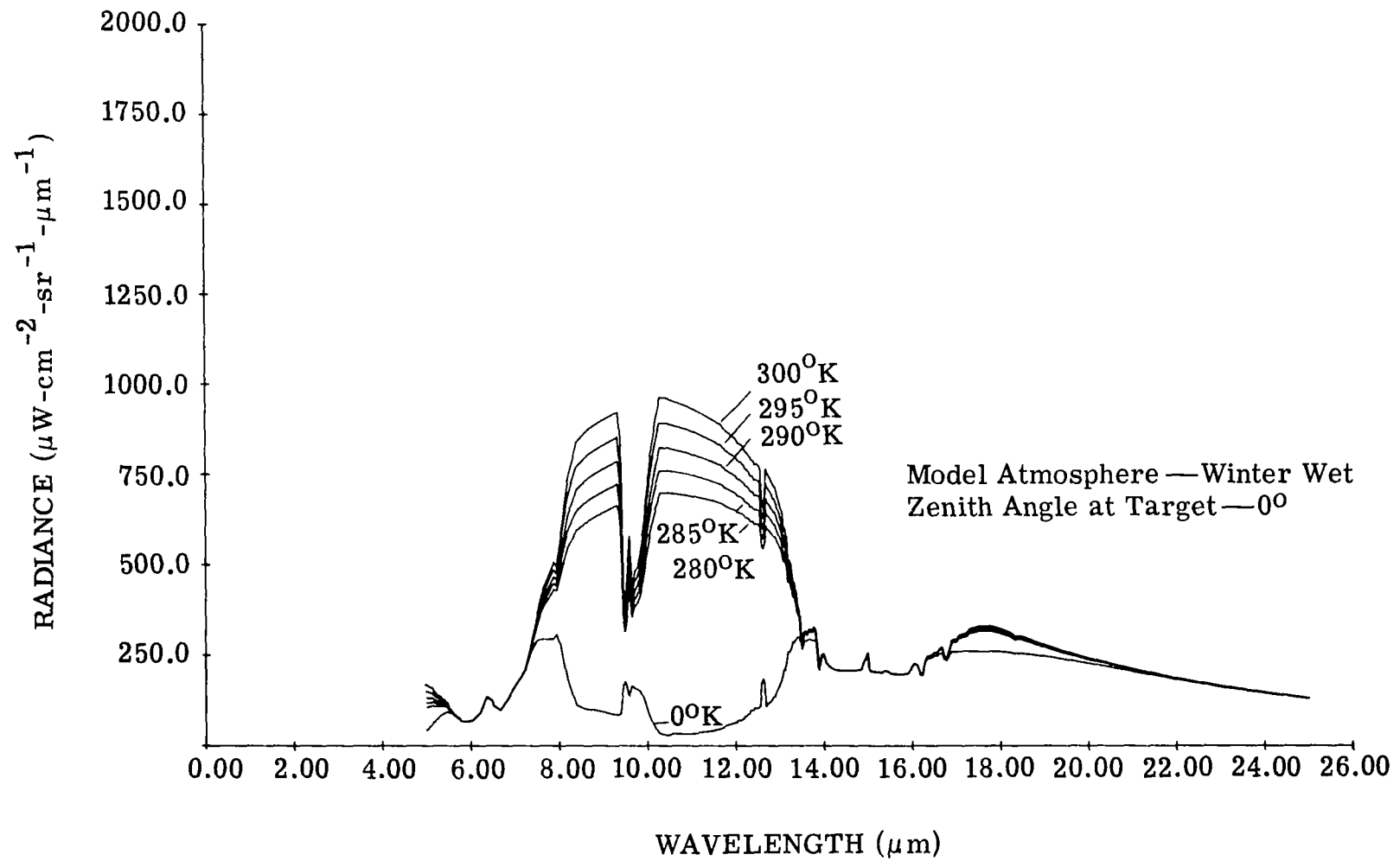


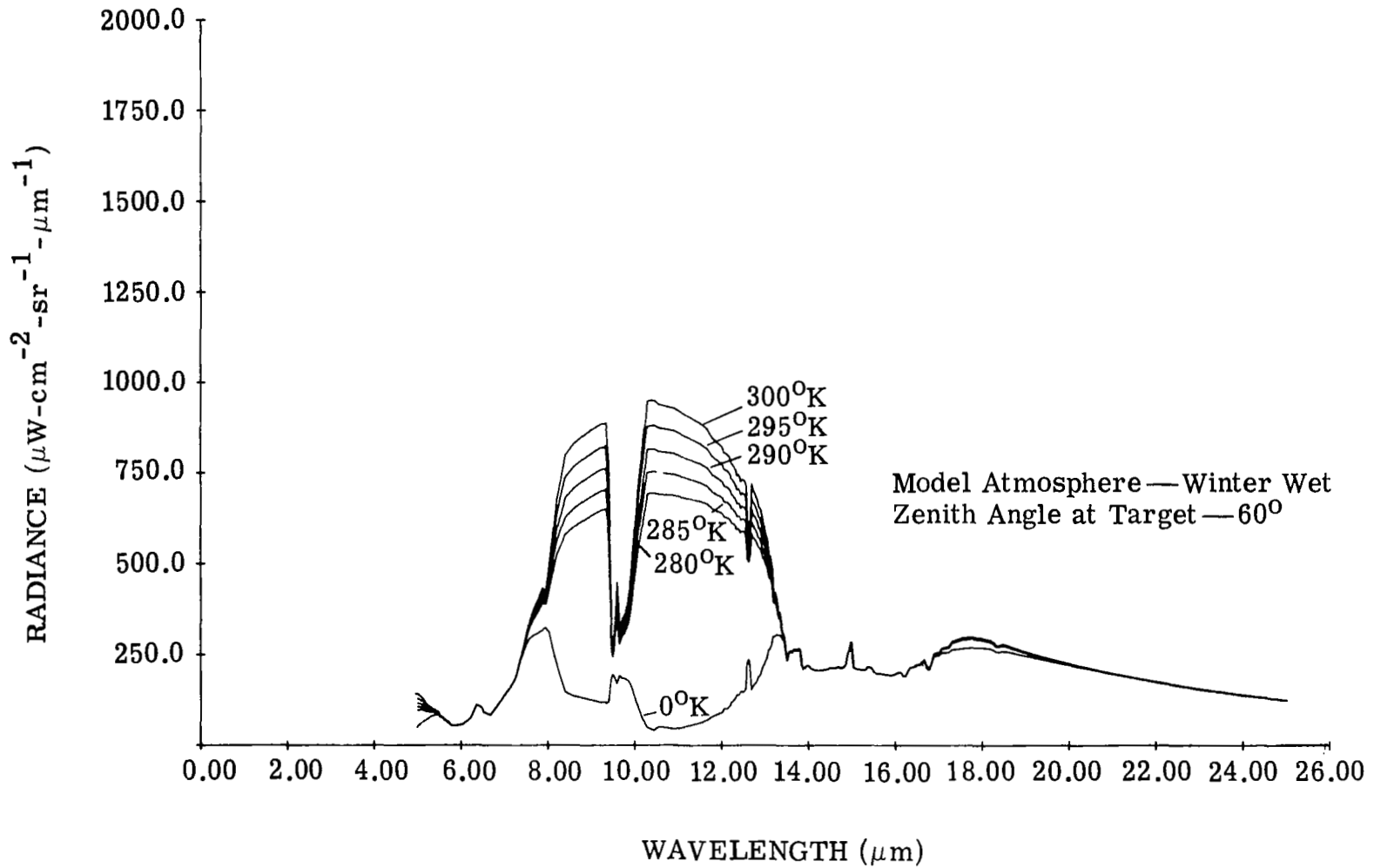


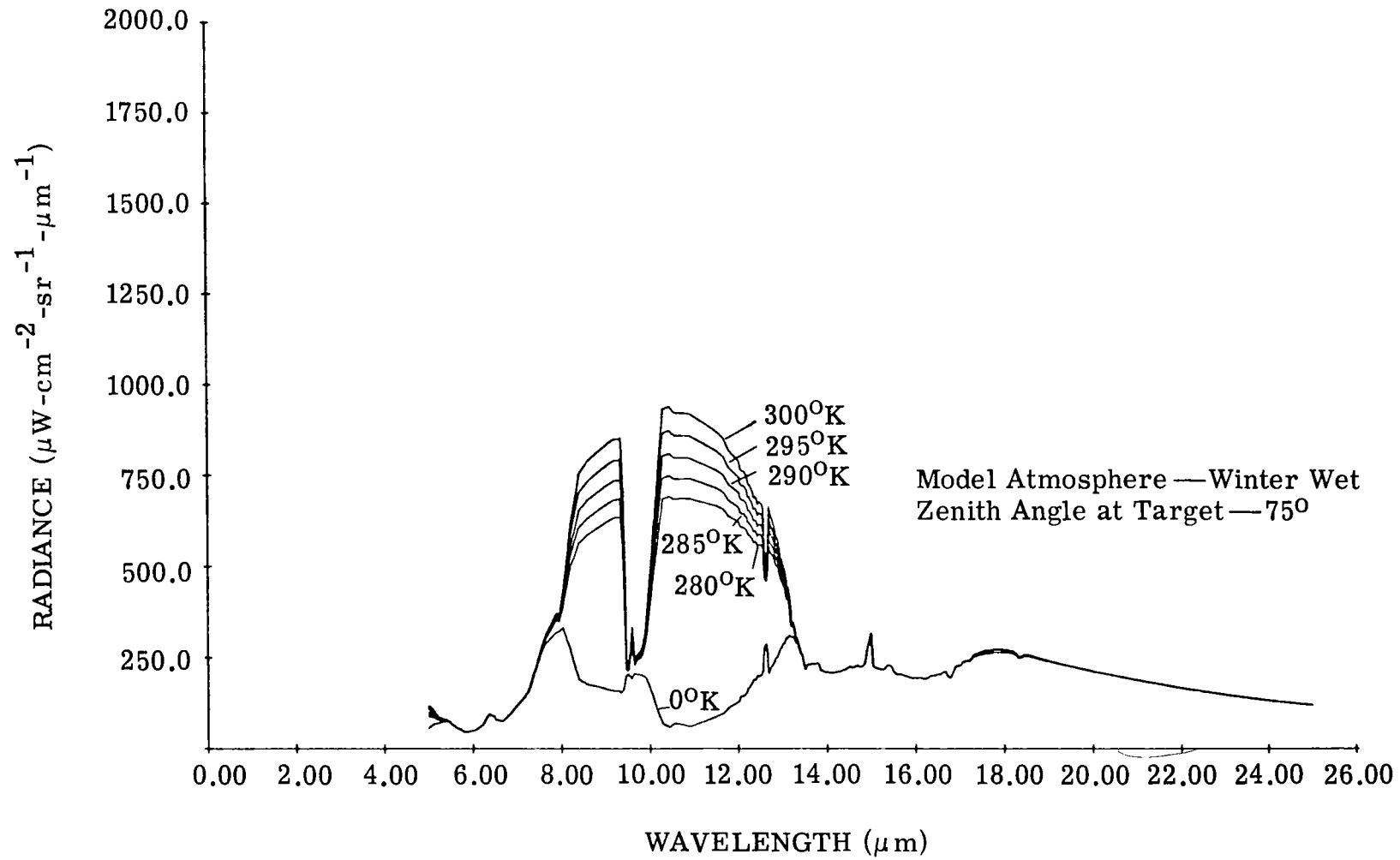


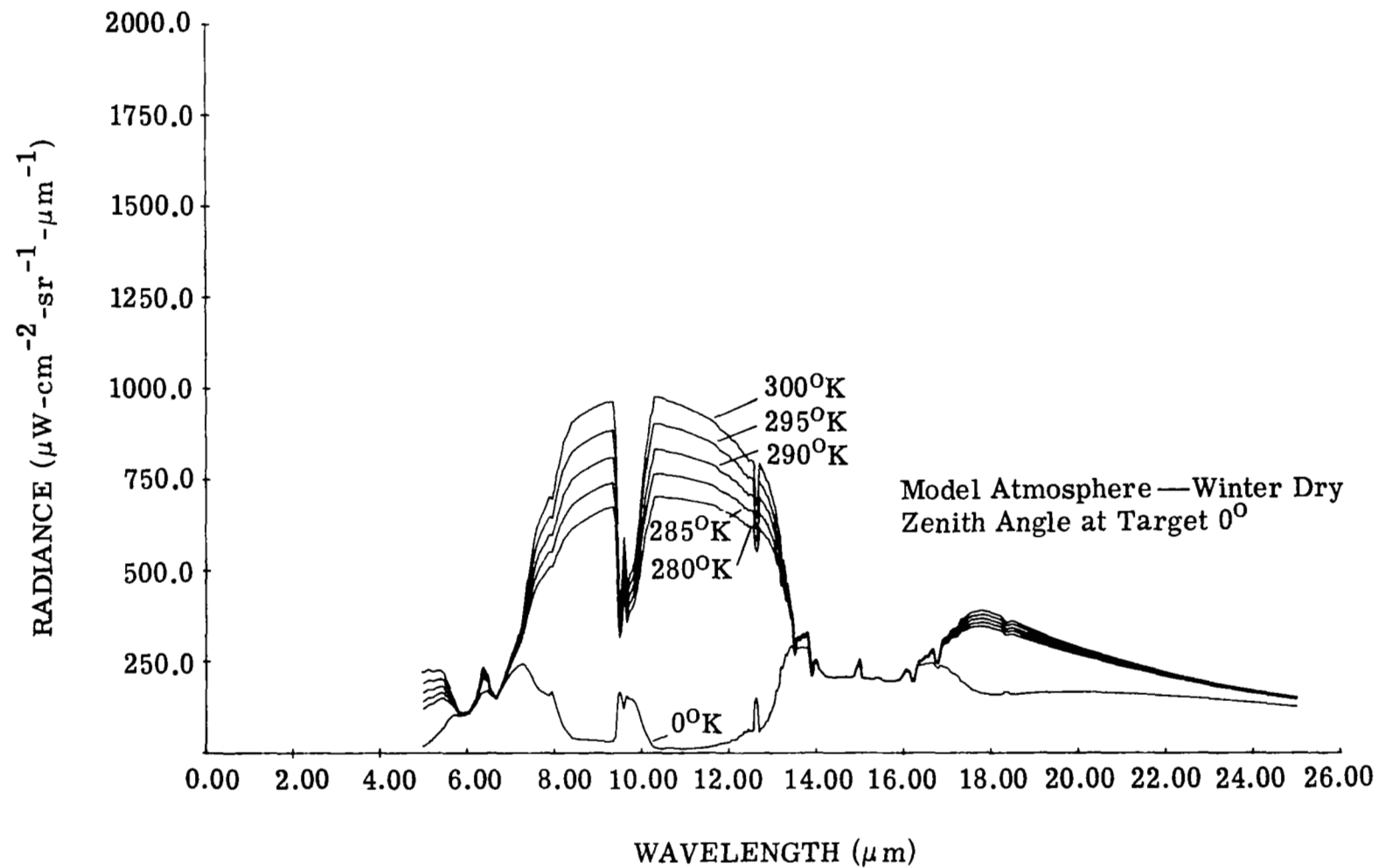


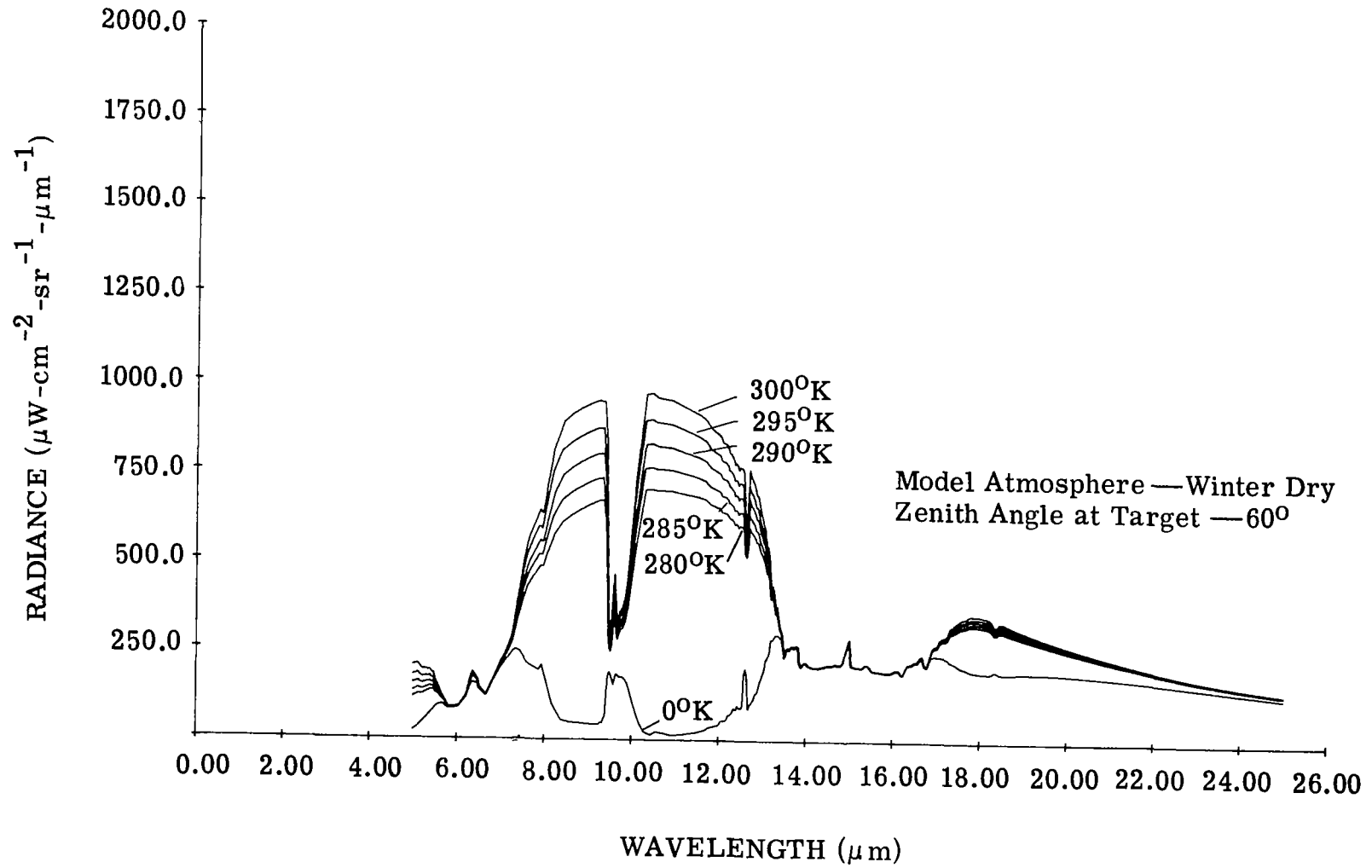


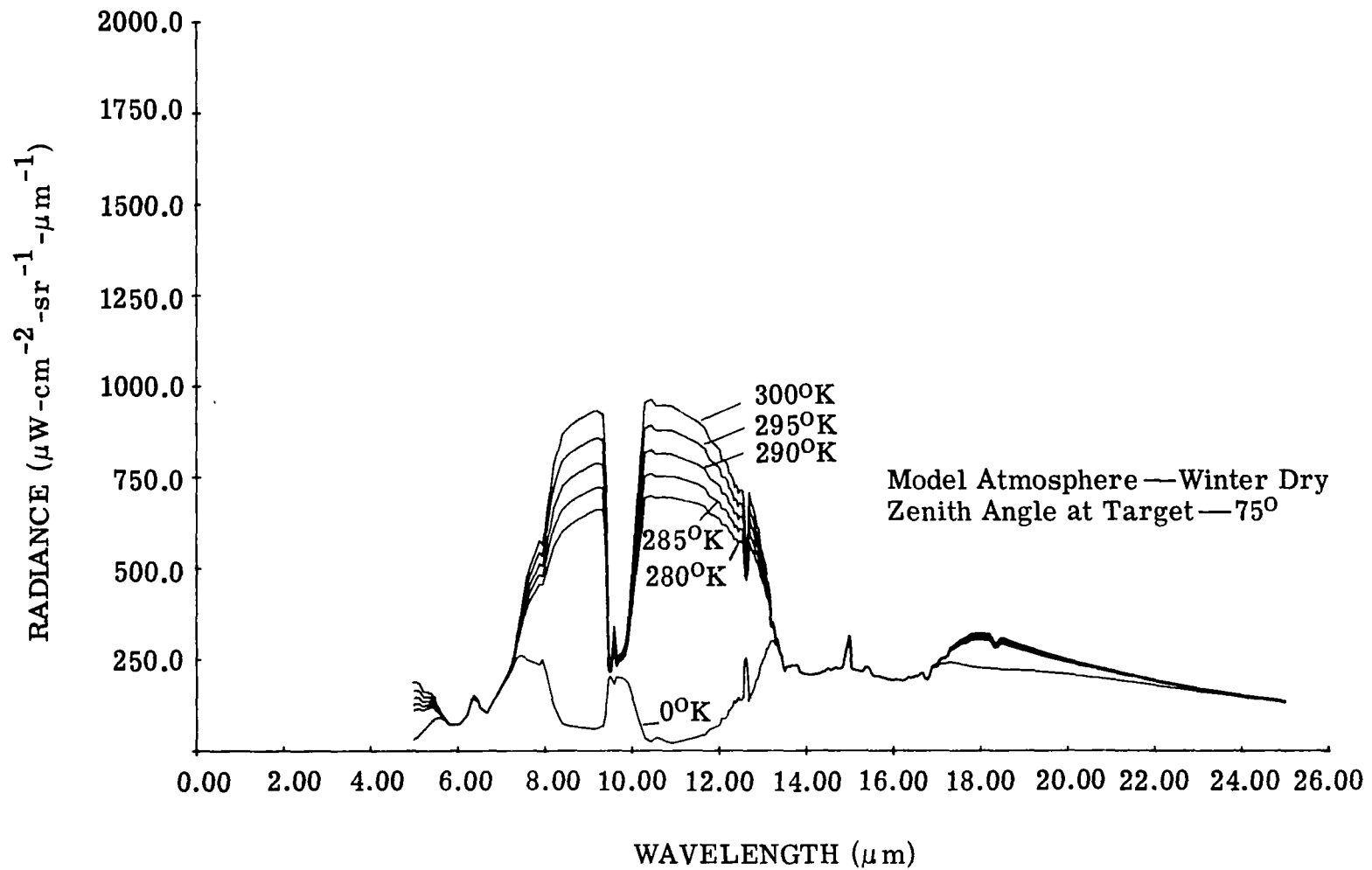


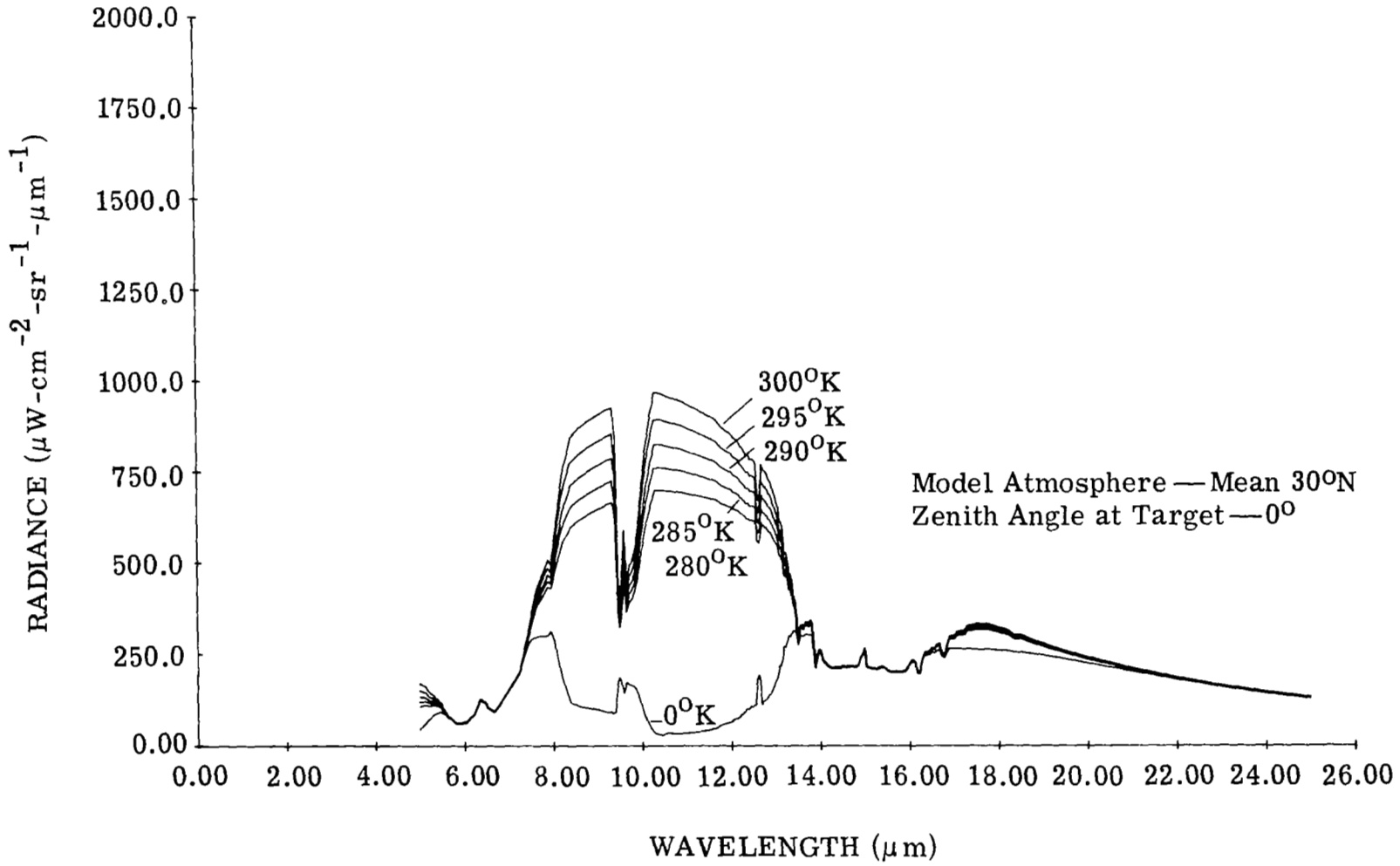


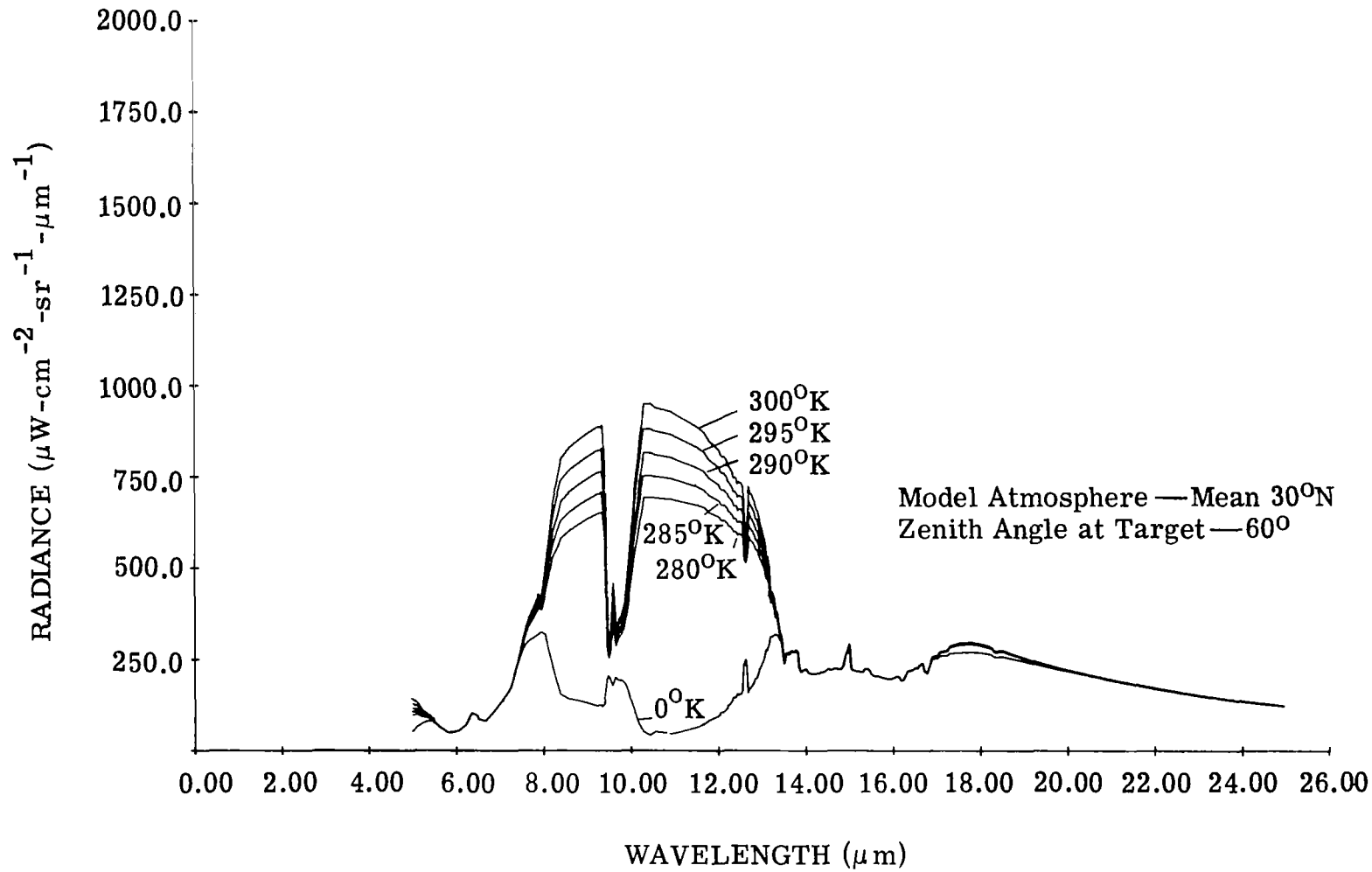


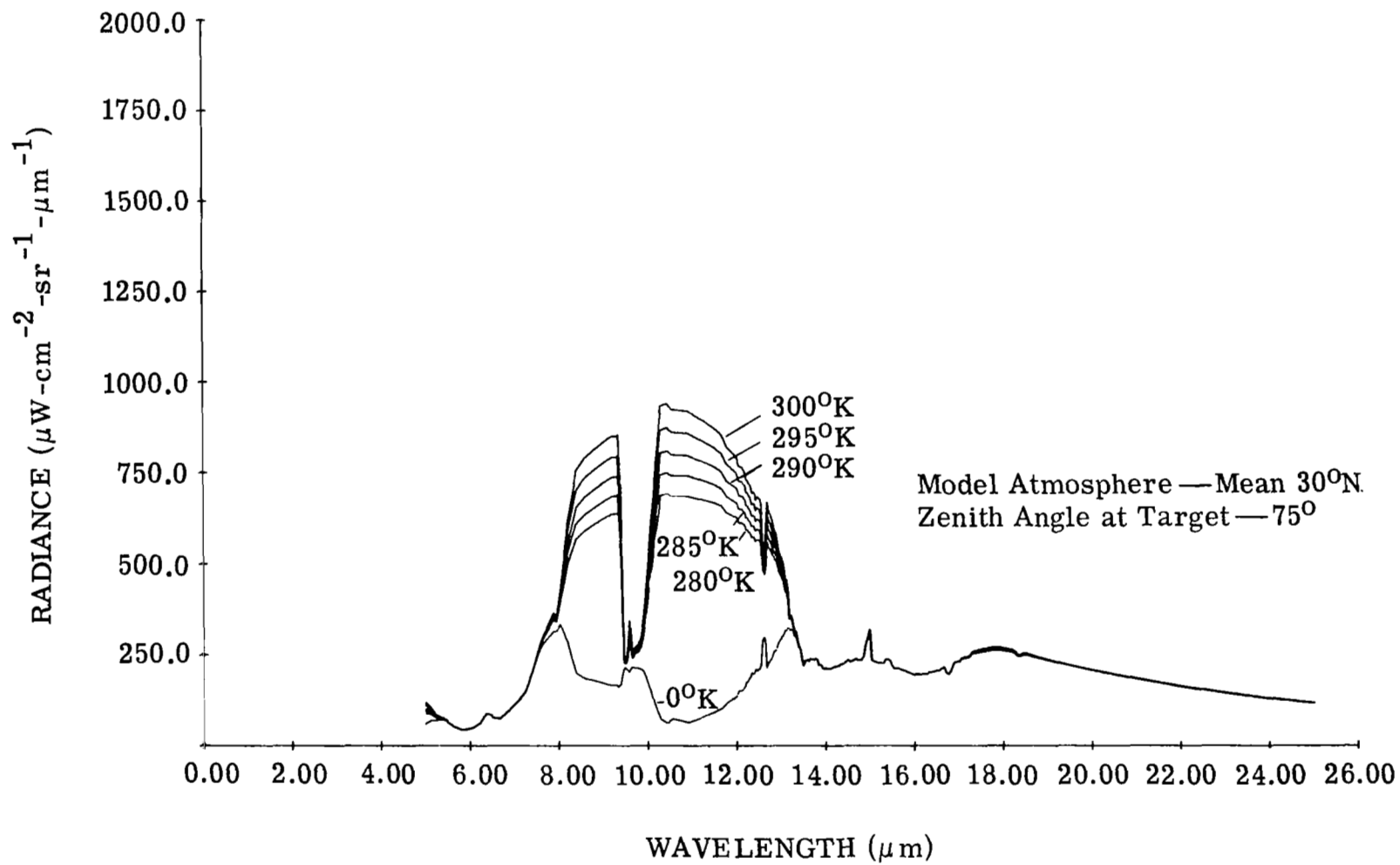












REFERENCES

1. D. Anding, IRIA State-of-the-Art Report: Band Model Methods for Computing Atmospheric Slant-Path Molecular Absorption, Report No. 7142-21-T, Willow Run Laboratories of the Institute of Science and Technology, The University of Michigan, Ann Arbor, February 1967.
2. M. Born and E. Wolf, Principles of Optics, Pergamon, 1964, Chap. 13.5.
3. H. C. Van DeHulst, Light Scattering by Small Particles, John Wiley and Sons, Inc., New York, 1964, Chap. 9.
4. M. Centeno, "The Refractive Index of Liquid Water in the Near Infrared Spectrum," J. Opt. Soc. Am., Vol. 31, March 1941, pp. 244-247.
5. L. Elterman, "Parameters for Attenuation in the Atmospheric Windows for Fifteen Wavelengths," Appl. Opt., Vol. 3, No. 6, 1964, p. 745.
6. J. B. Harvard, "On the Radiational Characteristics of Water Clouds of Infrared Wave Lengths," PhD Dissertation, The University of Washington, 1960.
7. M. Gutnick, Mean Moisture Profiles to 31 km for Middle Latitudes, Interim Notes on Atmospheric Properties No. 22, Geophysical Research Directorate, Air Force Cambridge Research Laboratories, Waltham, Mass., 1962.
8. K. J. K. Buettner and C. D. Kern, "The Determination of Infrared Emissivities of Terrestrial Surfaces," J. Geophys. Res., Vol. 70, No. 6, March 15, 1965, pp. 1329-37.
9. T. R. Crimmins and H. M. Horwitz, Multispectral Analysis and Estimation, Internal Memo, Infrared and Optics Laboratory, Willow Run Laboratories of the Institute of Science and Technology, The University of Michigan, Ann Arbor, 9 October 1969.
10. T. L. Altshuler, Infrared Transmission and Background Radiation by Clear Atmospheres, Report No. 6150199, General Electric Co., Philadelphia, Pennsylvania, December 1961.
11. J. N. Howard, D. E. Burch, and D. Williams, Near Infrared Transmission Through Synthetic Atmospheres, Geophysics Research Paper No. 40, Report No. AFCRC-TR-55-213, Ohio State University, Columbus, November 1955.
12. A. Zachor, Near Infrared Transmission over Atmospheric Slant Paths, Report No. R-328, Instrument Laboratory, Massachusetts Institute of Technology, Cambridge, July 1961.
13. C. D. Walshaw, "Integrated Absorption by the 9.6 Micron Band of Ozone," Quart. J. Roy. Meteorol. Soc., Vol. 83, 1957, pp. 315-321.